Copy No. 93

RM No. L6J01a

RM L6J01a

TECH LIBRARY KAFB, NM
0143895

7066

RESEARCH MEMORANDUM

AN INVESTIGATION OF THE EFFECTS OF SWEEP ON THE CHARACTERISTICS OF A HIGH-ASPECT-RATIO WING IN THE LANGLEY 8-FOOT HIGH-SPEED TUNNEL

By

Richard T. Whitcomb

Langley Memorial Aeronautical Laboratory
Langley Field, Va.

CLASSIFIED DOCUMENT

This document contains classified information affecting the National Defense of the United States within the meaning of the Espionage Act, USC 50:31 and 32. Its transmission or the revelation of its contents in any manner to an unauthorized person is prohibited by law. Information so classified may be imparted only to persons in the military and naval services of the United States, appropriate civilian officers and employees of the Federal Government who have a legitimate interest therein, and to United States citizens of known loyalty and discretion who of necessity must be informed thereof.

NATIONAL ADVISORY COMMITTEE FOR AERONAUTICS

WASHINGTON

February 14, 1947

3:9.98/13

TECH LIBRARY KAFB, NM
0143895

NACA RM No. L6J01a [redacted]L

NATIONAL ADVISORY COMMITTEE FOR AERONAUTICS

RESEARCH MEMORANDUM

AN INVESTIGATION OF THE EFFECTS OF SWEEP ON THE CHARACTERISTICS OF A HIGH-ASPECT-RATIO WING IN THE LANGLEY 8-FOOT HIGH-SPEED TUNNEL

By Richard T. Whitcomb

SUMMARY

An untwisted wing, which when unswept has an NACA 65-210 section, an aspect ratio of 9.0 and a taper ratio of 2.5:1.0, has been tested with no sweep, and 30° and 45° of sweepback and sweepforward in conjunction with a typical fuselage at Mach numbers from 0.60 to 0.96 at angles of attack generally between -2° and 10° in the Langley 8-foot high-speed tunnel. Sweep was obtained by rotating the wing semispans about a point in the plane of symmetry. The normal-force, pitching-moment, profile-drag, and loading characteristics for the wings have been obtained from pressure measurements and wake surveys. The results indicate that the wings with ±30° of sweep experienced the severe changes in characteristics associated with the presence of shock at higher Mach numbers than did the wing without sweep. The differences between the Mach numbers at which the changes occurred for the wings with ±30° sweep and no sweep were generally slightly less than the factor $\frac{1}{\cos \Lambda_r}$ times the Mach numbers at which the changes occurred for the unswept wing, Λ_r being the sweep angle. The wings with ±45° of sweep did not experience the changes in the characteristics associated with the presence of shock at an angle of attack of 2° at Mach numbers up to the highest test value. The magnitudes of changes in the normal-force and pitching-moment coefficients that occurred were less for the wing with 30° of sweep than for the unswept wing. The use of sweepforward was superior to sweepback in delaying and reducing the changes in the normal-force coefficients, but was inferior in delaying and reducing the changes in the profile-drag coefficients. Increasing the Mach number to the highest test values had little effect on the positions of the center of loads on the various configurations for the probable design load conditions.

INTRODUCTION

The results of investigations made in this country and in Germany (references 1 and 2) have shown that the use of sweepback

[redacted]

or sweepforward delays the onset of the radical changes in aerodynamic characteristics associated with the presence of shock on the wing. More recent investigations made in both countries have added considerable information on the characteristics of wings with sweep at supersonic as well as subsonic Mach numbers (reference 3) but little data is available for the transonic speed range. The data available, therefore, are insufficient for the proper design of aircraft with swept wings.

The NACA 65-210 wing model previously tested in the Langley 8-foot high-speed tunnel (reference 4) has been tested in conjunction with a typical fuselage with no sweep and 30° and 45° of sweepback and sweepforward of the quarter-chord line and several aileron deflections at Mach numbers from 0.60 to 0.96 at angles of attack generally between -2° and 10° to provide information on the following factors:

(1) The effects of sweep on aerodynamic characteristics of this particular wing in the Mach number range for which general information on the effects of sweep on aerodynamic characteristics is now available.

(2) The general effects of sweep on aerodynamic characteristics in the lower part of the transonic speed range for which little data are available.

(3) The effects of compressibility on the distributions of aerodynamic loads on swept wings at subsonic Mach numbers.

(4) The changes in the aerodynamic characteristics of a fuselage in the presence of swept wings at subsonic Mach numbers.

DEFINITIONS

The symbols are defined as follows:

b span of model

c section chord of wing, parallel to air stream

c_Λ section chord perpendicular to quarter-chord line of unswept wing

c_c chord of section perpendicular to the quarter-chord line of the unswept wing passing through the critical point, the intersection with the surface of the fuselage of the 70- or 20-percent-chord lines of the unswept wing for sweptback or sweptforward wings, respectively (see fig. 3)

configuration assuming wing rectangular through fuselage

$$X_a = \frac{X_w - c'_{w/4}}{c_f r + S_w} \text{ (reference 5)}$$

y distance from plane of symmetry along horizontal axis, inches

z distance from center line along vertical axis, inches

z' vertical distance from trailing edge of wing-fuselage-juncture chord, inches

α geometric angle of attack, degrees

ρ mass density in undisturbed stream, slugs per cubic foot

Λ_o sweep angle between line perpendicular to the plane of symmetry and leading edge of wing, degrees (positive values for sweepback, negative values for sweepforward)

Λ_r sweep angle between line perpendicular to the plane of symmetry and the quarter-chord line of the unswept wing, the principal reference line, degrees

The coefficients are defined as follows:

c_n' wing section normal-force coefficient (section perpendicular to quarter-chord line of the unswept wing)

$$c_n' = \frac{1}{c_\Lambda} \int_0^{c_\Lambda} (P_L - P_U)\, dl$$

c_t wing section twisting-moment coefficient about quarter-chord line of the unswept wing (section perpendicular to this line)

$$c_t = \frac{1}{(c_\Lambda)^2} \int_o^{c_\Lambda} (P_U - P_L) \left(l - \frac{c_\Lambda}{4} \right) dl$$

C_{N_w} wing normal-force coefficient

$$C_{N_w} = \frac{2}{S_w} \int_{a_1}^{a_2} c_\Lambda\, c_n'\, ds \text{ (see fig. 3)}$$

[redacted]

$C_{m_{c'/4_w}}$ wing pitching-moment coefficient about quarter-chord station of mean aerodynamic chord of wing

$$C_{m_{c'/4_w}} = \frac{2 \cos \Lambda}{S_w c'_w} \int_{a_1}^{a_2} c_\Lambda^2 \, c_t \, ds - \frac{2 \sin \Lambda}{S_w c'_w} \int_{a_1}^{a_2} c_\Lambda c_n' s \, ds + C_{N_w} X_w / c_w$$

c_{n_f} fuselage section normal-force coefficient (section parallel with air stream)

$$c_{n_f} = \frac{1}{c_f} \int_{6-g}^{25-g} (P_L - P_U) \, dx \text{ (see fig. 3)}$$

c_{m_f} fuselage section pitching moment coefficient about quarter chord station of wing section at fuselage surface

$$c_{m_f} = \frac{1}{c_f^2} \int_{6-g}^{25-g} (P_U - P_L) \, (x) \, dx$$

C_{N_a} over-all normal-force coefficient

$$C_{N_a} = \frac{S_w}{S_a} C_{N_w} + \frac{2 c_f r_f}{S_a} c_{n_f}$$

$C_{m_{c/4_a}}$ over-all pitching-moment coefficient about quarter-chord station of mean aerodynamic chord of over-all configuration

$$C_{m_{c'/4_a}} = \frac{c'_w S_w}{c'_a S_a} C_{m_{c'/4_w}} + \frac{S_w}{S_a} \left(\frac{X_a - X_w}{c'_a} \right) C_{N_w}$$

$$+ \frac{c_f 2 r_f}{c'_a S_a} c_{m_f} + \frac{c_f r_f}{S_a} \frac{X_a - X_w}{c'_a} c_{n_f}$$

C_{N_c} normal-force coefficient for wing outboard section through critical point

$$C_{N_c} = \frac{2}{S_w} \int_{s_c}^{a_2} c_\Lambda c_n \, ds$$

C_{B_c} bending-moment coefficient for section through critical point

$$C_{B_c} = \frac{2}{S_w d}\int_{s_c}^{a_2} c_\Lambda c_n' (s - s_c)\, ds$$

s'/d lateral position of center of load with reference to the section through critical point

$$s'/d = C_{B_c}/C_{N_c}$$

C_{t_e} twisting-moment coefficient about quarter chord of the unswept wing for wing outboard of critical section based on chord of section through critical point

$$C_{t_c} = \frac{2}{S_w c_c}\int_{s_c}^{a_2} c_\Lambda^2 c_t\, ds$$

l'/c_c chordwise position of center of load with reference to the quarter-chord line of the unswept wing

$$l'/c_c = \frac{C_{t_c}}{C_{N_c}}$$

c_t mean section twisting-moment coefficient

$$\bar{c}_t = \frac{2}{S_e \bar{c}_e}\int_{s_c}^{a_2} c_t c_\Lambda \cdot ds$$

c_{d_o} section profile-drag coefficient from wake survey measurements

$C_{D_{o_w}}$ wing profile-drag coefficient

$$C_{D_{o_w}} = \frac{2}{S_w}\int_{r_f}^{\infty} c c_{d_o}\, dy$$

[redacted]

APPARATUS

The Langley 8-foot high-speed tunnel, in which the tests were conducted, is of the single-return, closed-throat type.

The wing model tested as it appeared during previous tests is shown in figures 1 and 2. For the unswept condition with no fuselage, it has an NACA 65-210 airfoil section, an aspect ratio of 9.0, a taper ratio of 2.5:1.0, no twist or dihedral, and a 20-percent-chord aileron that extends from the 60-percent-semispan station to the end of the straight part of the trailing edge. The ordinates of the tip and the NACA 65-210 section of the unswept wing are presented in reference 4. Other dimensions of the unswept wing are presented in table I. Twenty static-pressure orifices were placed at each of eight stations along the wing span in lines perpendicular to the quarter-chord line of the unswept wing. The approximate chordwise locations of the orifices are given in reference 4 while the spanwise locations of the stations are presented in table II. The four inboard stations were placed on the left half of the wing and the four outboard stations were placed on the right half.

The model was supported in the tunnel by means of the vertical steel plate shown in figures 1 and 2. The plate, which is completely described in reference 4, has a chord of 50 inches, a thickness of 0.75 inch, and a modified ellipse profile.

Swept configurations were obtained by rotating the model with respect to the support plate about the main fastening screw, which is located at the midspan of the model and 0.4-root-chord length from the leading edge of the root chord. Wall pressure measurements indicate that the flow over the model on one side of the plate had very little effect on the flow on the other side even at the highest test Mach numbers. A given test configuration represents, therefore, not a yawed model but half of a swept-back model and half of a swept-forward model. Since the thickness of the boundary layer on the plate was small, the support had negligible effect on the data obtained.

Revised tips were added for each sweep. The shapes of the revised tips were similar to that of the unswept wing, the major axes of the tips were parallel to the stream direction, the minor axes were along the 40-percent-chord lines, and the widths were 0.47 inch (see fig. 3). The dimensions of the model with 30° and 45° of sweepback and sweepforward of the quarter-chord line are presented in table I and figure 3. The dimensions are based on the assumption that the surface of the plate at the root is the plane of symmetry. The locations of the pressure orifice stations with reference to the intersection of the quarter-chord line of the original wing and the center line for the swept configurations are presented in table II.

[redacted]

The effect of the addition of a fuselage to a complete wing was simulated by the addition of two half bodies of revolution to the test configuration at the surfaces of the support plate. The dimensions of the half bodies of revolution, the center lines of which coincided with the chord plane of the wing, are shown in figure 3. The chordwise positions of the fuselage with respect to the wing for the various sweep angles are presented in table I. Twenty-eight pressure orifices were placed in one of the halves in two planes at 45° to the plane of symmetry through the center line as shown in figure 3.

Wake surveys were made behind the wing by means of the rake described in reference 4 and shown in figure 2.

METHODS AND PROCEDURES

Tests

Pressure measurements were made at the eight stations on the wing and on the fuselage at the Mach numbers and angles of attack listed in table IV. All pressure measurements were made with the revised tips described in the section on Apparatus. Since the pressure stations are on both sides of the wing model, pressure data for a given sweep were necessarily obtained during tests of two configurations. Wake-survey measurements were made at the stations listed in table III at the Mach numbers and angles of attack listed in table IV. Wake-survey measurements were made with and without the revised tips for sweep angles of 30° and 45° at the three stations nearest the tip. All other wake surveys were made with the revised tips.

Corrections for Tunnel-Wall Interference

The expressions available for the calculation of the effects of tunnel-wall interference are inadequate for the accurate determination of those effects for swept wings at high subsonic Mach numbers. No corrections for these effects have been applied, therefore, to the results of the present tests of swept wings. To make the data presented consistent, no corrections have been applied to the data obtained for the unswept condition. Estimations of the order of magnitude of the effects of tunnel-wall interferences, using the expressions presented in reference 4, indicate that the corrections to be applied to dynamic pressures and Mach numbers for all conditions except that of no sweep at a Mach number of 0.925 are less, and in most cases much less, than 1 percent. The corrections to be applied to the results obtained for no sweep at a Mach number of 0.925 may be as large as 3 percent.

[redacted]

Limiting Test Mach Numbers

The tunnel choked at Mach numbers of approximately 0.945, 0.975, and 0.985 for sweep angles of 0°, 30°, and 45°, respectively. The data obtained when the tunnel is choked are not applicable to the prediction of wing characteristics for free air (reference 6) and therefore they are not presented.

Static pressure measurements made on the tunnel wall indicate that there are perceptible tendencies toward choke at the plane of the model at a Mach number of 0.925 and 0.960 for unswept and swept conditions, respectively. The results obtained at these Mach numbers, even if completely corrected for the usual effects of tunnel-wall interference, may not, therefore, indicate the exact flight characteristics. The general trends, however, are believed to be illustrated by the results obtained at these Mach numbers.

With the support strut for the wake-survey rake in place (fig. 2) the tunnel choked at this strut when the uncorrected Mach number at the plane of the model was 0.882. As explained in reference 4, choking at the survey strut simply imposes a limitation on the maximum test Mach number and does not affect the applicability of the results. The data obtained for the model with the wake-survey strut in place can thus be assumed to be correct up to the choking Mach number of the wake-survey strut and data up to this Mach number have been presented.

Reynolds Number Range

When the Mach number was increased from 0.60 to 0.96, the Reynolds numbers for the unswept wing based on the mean chord varied from 1.05×10^6 to 1.25×10^6. The Reynolds numbers for the swept wings were greater than these values by the ratios of the mean chords of these wings to the mean chord of the unswept wing (table I).

REDUCTION OF DATA AND RESULTS

Aerodynamic Characteristics

Section normal-force coefficient c_n' and section twisting-moment coefficients about the quarter-chord line of the unswept wing c_t have been obtained by integrating the pressure-distribution diagrams for the eight wing-orifice stations.

The wing normal-force coefficient has been obtained by integrating a curve of $c_n' c_A$ versus the distance along the quarter-chord line of the

unswept wing, and dividing the results by the area of the wing outboard of the fuselage. Variations of the resulting wing normal-force coefficients with angle of attack for the various sweep angles are presented in figure 4 while variations of this coefficient with Mach number are presented in figure 5. Variations of the slopes of the wing normal-force-coefficient curves, $dC_{N_w}/d\alpha$, with Mach number at an angle of attack of 2° are presented in figure 6.

The wing twisting-moment coefficient about the quarter-chord line of the unswept wing has been obtained by integrating a curve of $c_t c^2$ versus distance along this line and dividing the result by the area and mean aerodynamic chord of the wing outboard of the fuselage. The wing bending-moment coefficient about a line perpendicular to the quarter-chord line of the unswept wing at its intersection with the plane of symmetry in terms of the mean aerodynamic chord of the wing was calculated from data obtained during the integration of a curve of $c' n^2 \Lambda$ versus the distance along this line. The wing pitching-moment coefficient about a lateral axis through the intersection of the quarter-chord line of the unswept wing and the plane of symmetry has been obtained by adding the components of the wing twisting and bending-moment coefficients about this axis. By adding to this pitching-moment coefficient the product of the wing normal-force coefficient and the distance from this axis to the quarter-chord station of the mean aerodynamic chord, the pitching-moment coefficients about this station has been obtained. The variations of the wing pitching-moment coefficient about the quarter chord of the mean aerodynamic chord of the wing with wing normal-force coefficient for various Mach numbers are presented in figure 7. Variations of this coefficient with Mach number for wing normal-force coefficients of 0.1, 0.3, and 0.5 are presented in figure 8.

The total-pressure and static-pressure measurements made during the wake surveys have been reduced to section profile-drag coefficients by use of the expressions presented in reference 7. The total wing profile-drag coefficient has been obtained by integrating a curve of $c_{d_o} c$ versus the semispan from the plane through the wing-fuselage junctures to beyond the tip and dividing the result by the area of the wing outboard of the fuselage. The result obtained indicates the exact wing profile-drag coefficient only if the measurements made near the fuselage do not include part of the total pressure losses for the fuselage. The results of a preliminary investigation indicate that these measurements include only a small part of these losses. It may be assumed for all practical purposes, therefore, that the result obtained does indicate the total wing-drag coefficient. The total wing profile drag coefficient for the wing with 45° of sweepback was obtained from measurements made at the two chordwise positions given in table III. The results of measurements made at both of these chordwise positions but at one spanwise position

[redacted]

indicate that there was very little cross flow behind the wing even at the highest test angles. It may be assumed, therefore, that the measurement made indicates the true total wing-profile-drag coefficients for the wing with 45° of sweep.

Variations of the wing-profile-drag coefficient with wing normal-force coefficient are presented in figure 9 while variations of this coefficient with Mach number for wing normal-force coefficients of 0.2 and 0.5 are presented in figure 10. To indicate the effect of sweep alone on the profile-drag characteristics of the wing, the variations of wing profile-drag coefficient with Mach number for the various sweeps and an angle of attack of 2° are presented in figure 11.

The fuselage-section normal-force coefficient and fuselage-section pitching-moment coefficient about the quarter-chord station of the chord at the wing-fuselage juncture in terms of this chord have been obtained by integrating a pressure-distribution diagram for the fuselage orifice station. Since the pressure measurements were made along the central portion of the fuselage only, the normal and pitching-moment coefficients obtained are not for a complete fuselage section in the presence of the wing. However, these coefficients do have significance. The difference of the pressures on the upper and lower surfaces of the fuselage with no wing produced by changing the angle of attack are concentrated near the nose and tail, while differences in the pressures on these surfaces produced by the presence of the wing are concentrated on the central portion of the fuselage (reference 8). The coefficients obtained from pressures measured along the central portion of the fuselage, are therefore, very nearly equal to the changes in the fuselage-section coefficients produced by the presence of the wing. The ratios of the fuselage-section normal-force coefficient to the wing normal-force coefficient are presented in figure 12. Variations of the fuselage-section pitching-moment coefficient with fuselage-section normal-force coefficient are presented in figure 13.

The results of previous theoretical and experimental work (reference 8) indicate that for an unswept wing at low Mach numbers the effect of the wing on the total fuselage coefficients are probably nearly the same as the effects of the wing on the section coefficients for the fuselage planes for which measurements were made. To obtain approximations of the over-all effects of the wing it has been assumed that the effects of the wing on the total fuselage coefficients are the same as the effects of the wing on the section coefficients for all the test conditions. The over-all normal-force coefficient for the wing has been determined by adding the fuselage normal-force coefficient in terms of the over-all wing area to the wing normal-force coefficient in terms of the same area. The over-all wing area has been assumed to be the area of wing outboard of the area of wing outboard of the fuselage plus the area of a rectangular portion of a wing with a chord equal to the chord of the section at the juncture of the wing and fuselage, and

a span equal to the diameter of the fuselage. The over-all pitching-moment coefficient for the wing has been determined by adding the pitching-moment coefficient of the fuselage about the quarter chord of the mean aerodynamic chord of the over-all wing area in terms of this chord and area to the pitching-moment coefficient outboard the fuselage of the wing about this same point in terms of the same area and chord. Variations of the over-all pitching-moment coefficient for the wing with the over-all normal-force coefficient are presented in figure 14. Variations of the over-all pitching-moment coefficient with Mach number for over-all normal-force coefficients of 0.1, 0.3, and 0.5 are presented in figure 15.

Variations of the spanwise distribution of section normal-force and section profile-drag coefficient with angle of attack for a Mach number of 0.600 are presented in figures 16 and 17, respectively. The section profile-drag coefficients are based on the chord of the model directly in front of the measurement stations.

Vertical variations of the total-pressure losses for 30° sweepback and sweepforward at stations approximately 2.0 wing-fuselage-juncture chords behind the trailing edge of this juncture and 0.18 semispans from the planes of symmetry are presented in figure 18.

Aerodynamic Loads

An analysis of the structure and the aerodynamic loadings of swept wings indicates that the maximum bending and shear loads produced by the air forces on a swept wing will probably occur at the principal wing-fuselage joint nearest the center of load. For swept-back wings this joint will be near the trailing edge while for swept-forward wings it will be near the leading edge. To show the magnitude of the effects of changes in Mach number on the distribution of load with respect to these joints on wings similar to those tested, the distributions of load with respect to the critical point, the intersections of the 70- and 20-percent-chord lines of the original wing with the surface of the fuselage have been determined for the swept-back and swept-forward wings, respectively. To provide a basis of comparison the distribution of load with respect to the wing-fuselage juncture of the unswept wing have also been determined.

The distance along the swept semispan from the section through the critical point to the section including the center of load outboard the intersection in terms of the swept semispan has been determined by integrating a curve of section load versus the distance along the swept semispan. The distance from the quarter-chord line of the unswept wing to the center of load in terms of the chord of the section through the critical point of intersection has been determined by integrating the curves of section twisting moment versus the distance along the swept semispan. The ratios of the loads outboard the sections through critical points to the total

[redacted]

loads on the wings have also been determined. The load centers and ratios for angles of attack from 2° to 10° are presented in figure 19.

The effects of changes in Mach number on the load distributions for a wing loading of 200 pounds per square foot at an altitude of 30,000 feet are shown in figure 20.

To allow the determination of the effects of changes in Mach number on the distributions of load with reference to other points on the wing, the spanwise distributions of load on the full wing and the distribution of twisting moment outboard the sections through the assumed critical points for various angles and Mach numbers are presented in figures 21 through 30. The unusual shapes of the loading distributions near the root are due to the fact that the section loadings in this region are not for complete sections (fig. 3).

DISCUSSION

Variables

Since the aspect ratio, wing section, taper ratio, and Reynolds number range changed when sweep angle was changed, the results presented do not indicate the exact effects of sweep alone. However, the effects of the present changes in these other variables on most of the variations of characteristics with Mach number are small with respect to the effects of the corresponding sweeps (references 9, 10, and 11).

Wing Normal-Force Characteristics

The wing with 0° sweep at angles of attack of 0°, 2°, 4°, and 7° experienced reductions in the normal-force coefficients when the Mach number was increased beyond values of approximately 0.79, 0.77, 0.74, and 0.73, respectively (fig. 5). The wing with 30° of sweepback at the same angles of attack experienced similar reductions at Mach numbers approximately 0.10 greater than these values. This difference is slightly less than the increment of 0.12 obtained by use of the factor, $\frac{1}{\cos \Lambda_r} - 1$ times the Mach numbers at which reductions in normal-force coefficients occur. The wing with 30° of sweepforward at angles of attack of 0°, 2°, 4°, and 7° experienced reductions in the wing normal-force coefficients at Mach numbers approximately 0.10, 0.12, 0.14, and 0.15 greater, respectively, than for those at which reduction occurred on the wing with no sweep for the same angles of attack. These differences are generally slightly greater than the Mach number increments obtained using the factor described above.

There are no major reductions in the normal-force coefficients for the wings with 45° of sweepback and sweepforward at an angle of attack of 2° at Mach numbers up to 0.96, the highest test value (fig. 5). For 7° angles of attack these configurations experience reductions in normal-force coefficients at Mach numbers of 0.92 and 0.94, values which are approximately 0.17 and 0.19 greater than the Mach number at which the wing with no sweep experiences a reduction in this coefficient at this angle of attack. These differences are considerably less than the calculated Mach number increment of approximately 0.30 for these configurations for 7° angles of attack.

The results obtained for the wings with ±30° of sweep indicate not only that the reductions in normal-force coefficients occur at higher Mach numbers on swept wings than on similar unswept wings but, more importantly, that the percent reductions that occur are generally less, in some cases much less, for swept wings than for a similar unswept wing (fig. 5). Insufficient data are available to show the exact effect of progressively increasing the sweep angles beyond 30° on the magnitude of the reductions of normal-force coefficients but the data obtained for the wing with 45° of sweep indicate that the magnitudes of these reductions are probably further reduced by increasing the sweep angle beyond 30°. The magnitudes of reductions for swept-forward wings are considerably less than those for swept-back wings with similar sweep angles even when the sweep angles are measured to the half chord line.

As would be expected the slopes of the wing normal-force curves, $dC_{N_w}/d\alpha$, for the configurations with sweep are considerably less than the slopes of these curves for the model without sweep at the subcritical Mach numbers at an angle of attack of 2° (fig. 6). These differences are due primarily to variations of the sweep angle but variations on the aspect ratio and to a lesser extend variations in the section, and Reynolds number (reference 10) produce part of the differences. The slope of normal-force curve for the model with no sweep starts to decrease when the Mach number is increased beyond approximately 0.74. It starts to increase again, however, at a Mach number of 0.83. At this Mach number the slope is approximately 85 percent of the maximum value obtained at a Mach number of 0.74. The slopes of these curves for the models with 30°, -30°, 45°, and -45° of sweep started to decrease at Mach numbers of 0.08, 0.16, 0.19, and 0.20 greater, respectively, than the value at which the slope of the curve for the model with no sweep started to decrease. The slope for the model with 30° sweepback ceases to decrease when the Mach number is increased beyond approximately 0.90. The percent reduction of the slope for this configuration is greater than that for the model with no sweep,

[redacted]

the slope at a Mach number of 0.90 being 80 percent of the slope at 0.82. The percent reduction in slope for the model with 30° sweepforward appears to be much less than that for the model with 30° of sweepback. The slope for this configuration at the highest test Mach number, 0.96, is approximately 5 percent less than the maximum at 0.90.

Wing Pitching-Moment Characteristics

There are large variations of the wing pitching-moment coefficients at given wing normal-force coefficients for the wing with no sweep when the Mach number is increased from approximately 0.75 to the highest test value, 0.925 (fig. 8). Similar changes occur for the wings with sweep, but they occur at a higher Mach number than do the corresponding changes for the wing with no sweep. The magnitudes of the changes for 30° and 45° of sweepback and 45° of sweepforward are generally less than the corresponding changes for the wing with no sweep, but the magnitudes of the changes for 30° of sweepforward are greater than the corresponding changes for this wing.

Wing Profile-Drag Characteristics

The wing profile-drag coefficient for the wing with no sweep at an angle of attack of 2° starts to increase rapidly when the Mach number is increased beyond approximately 0.74 (fig. 11). A similar increase occurs on the wing with 30° sweepback at a Mach number of approximately 0.09 greater than this value. This increment is approximately 75 percent of the factor $\frac{1}{\cos \Lambda_x} - 1$ times the Mach number at which the drag rise occurs on the wing with no sweep. The rate of increase of the wing profile-drag coefficient with Mach number on the wing with 30° sweepback is approximately the same as that for the wing with no sweep. The wing profile-drag coefficient for the wing with 30° sweepforward starts to rise very gradually at a Mach number of approximately 0.75. When the Mach number is increased beyond approximately 0.86 the rate of increase is about the same as that for the wing with 30° of sweepback. There is only a slight increase in the wing profile-drag coefficient for the wing with 45° of sweepback with 2° angle of attack when the Mach number is increased to the highest test value.

The wake-survey measurements indicate that the increase in the profile-drag coefficient for the wing with 30° of sweepforward at at Mach number of approximately 0.75 is due to separation near the wing-fuselage juncture. It is quite probable, therefore, that separation also occurs on portions of the fuselage at this Mach

number and that the increase in the profile-drag coefficient for the over-all configuration is greater than that for the wing alone.

The use of tips perpendicular to the quarter-chord line instead of the revised tip described in the section on Apparatus increased slightly the drag coefficients for the swept-back wings at all angles of attack and Mach numbers.

Effect of Wing on Fuselage Characteristics

The changes in the fuselage section normal-force coefficients produced by the wing are approximately 75 percent of the wing normal-force coefficients for the configurations with no sweep and sweepback at angles of attack of 2°, 4°, 7°, and 10° and at all Mach numbers up to the highest test values (fig. 12). For the wing with sweepforward at these same angles of attack and at the lower Mach numbers, the ratios of these coefficients are approximately 0.90. For 45° of sweepforward the ratios do not change appreciably when the Mach number is increased up to the highest test values; however, for 30° of sweepforward at some angles of attack the ratios change radically when the Mach number is increased to this value. At an angle of attack of 2° it increases by approximately 75 percent.

Over-all Characteristics for Wing

Since the changes in the fuselage normal-force coefficients produced by the wing are approximately equal to the wing normal-force coefficients for most conditions, the over-all normal-force coefficients for the wing are nearly same as the wing normal-force coefficients. In most cases the difference between the two coefficients is less than 4 percent of the wing normal-force coefficient.

The variations of the over-all pitching-moment coefficients with Mach number for various values of the over-all normal-force coefficients are approximately the same as the variations of the wing pitching-moment coefficients with Mach number for the same values of the wing normal-force coefficients (fig. 15).

Stalling Characteristics

Since the Reynolds numbers, airfoil sections in flow direction, and aspect ratios for the various configurations differed, the results obtained at the highest angles of attack at a Mach number of 0.60 do not indicate the [redacted] sweep alone on the angle

of attack and normal-force coefficient at which stall occurs. Since the Reynolds numbers for the tests were considerably lower and the Mach numbers considerably higher than those for the usual landing conditions, the results cannot be used to estimate the stalling characteristics for the landing conditions. It is believed, however, that the results do indicate for some maneuvering conditions the locations of initial flow separation due to increasing the angle of attack to relatively high values. At a Mach number of 0.60 this initial separation occurred first on the inboard sections of the wings with no sweep and sweepforward and on the outboard sections of the wings with sweepback (figs. 16 and 17).

Load Distributions

The center of load on the wing with no sweep for a wing loading of 200 pounds per square foot an an altitude of 30,000 feet shifts inboard very slightly and rearward by a considerable amount when the Mach number is increased from approximately 0.75 to the highest test value (fig. 20). The center of load on the wing with 30° of sweepback for the same conditions does not shift along the swept-back semispan but shifts rearward with reference to this line approximately the same distances as the center of load on the wing with no sweep shifts chordwise. The center of load on the wing with 45° of sweepback shifts slightly outboard along the swept-back semispan and rearward with reference to this line for the particular over-all loading selected. The centers of load on the wings with sweepforward shift slightly inboard along the swept-forward semispan but do not shift by a significant amount with reference to this line.

CONCLUDING REMARKS

The results of tests of wings with no sweep and 30° and 45° of sweepback and sweepforward in conjunction with a typical fuselage at Mach numbers up to 0.96 indicated the following:

1. The wings with ±30° of sweep experienced the severe changes in characteristics associated with the presence of shock at higher Mach numbers than did the wing without sweep. The differences between the Mach numbers at which the changes occurred for the wings with ±30° sweep and no sweep were generally slightly less than the factor $\frac{1}{\cos \Lambda_r} - 1$ times the Mach numbers at which the changes occurred for the unswept wing, Λ_r, being the sweep angle.

2. The wings with $\pm 45^{\circ}$ of sweep did not experience the changes in the characteristics associated with the presence of shock at an angle of attack of 2° at Mach numbers up to the highest test values.

3. The magnitudes of changes in the normal-force coefficients that occur were less for the wing with $\pm 30^{\circ}$ of sweep than for the unswept wing.

4. The use of sweepforward was superior to sweepback in delaying and reducing the changes in the normal-force coefficients but was inferior in delaying and reducing the changes in the profile-drag coefficients.

5. Increasing the Mach number to the highest test values had little effect on the positions of the center of loads on the various configurations for the probable design load conditions.

Langley Memorial Aeronautical Laboratory
National Advisory Committee for Aeronautics
Langley Field, Va.

[redacted]

REFERENCES

1. Matthews, Charles W., and Thompson, Jim Rogers: Comparative Drag Measurements at Transonic Speeds of Rectangular and Swept-Back NACA 65_1-009 Airfoils Mounted on a Freely Falling Body. NACA ACR No. L5G30, 1945.

2. Ludwieg, H.: Versuchsergebnisse. Pfeilflügel bei hohen Geschwindigkeiten. Bericht 127 der Lilienthal-Gesellschaft, 1940, pp. 44-52.

3. Ellis, Macon C., Jr., and Hasel, Lowell E.: Preliminary Tests at Supersonic Speeds of Triangular and Swept-Back Wings. NACA RM No. L6L17, 1946.

4. Whitcomb, Richard T.: Investigation of the Characteristics of a High-Aspect-Ratio Wing in the Langley 8-foot High-Speed Tunnel. NACA RM No. L6H28a, 1946.

5. Warner, Edward P., and Johnston, Paul S.: Aviation Handbook. McGraw-Hill Book Co., Inc., 1931.

6. Byrne, Robert W.: Experimental Constriction Effects in High-Speed Wind Tunnels. NACA ACR No. L4L07a, 1944.

7. Baals, Donald D., and Mourhess, Mary J.: Numerical Evaluation of the Wake-Survey Equations for Subsonic Flow Including the Effect of Energy Addition. NACA ARR No. L5H27, 1945.

8. Multhopp, H.: Aerodynamics of the Fuselage. NACA TM No. 1036, 1942.

9. Stack, John, and Lindsey, W. F.: Characteristics of Low-Aspect-Ratio Wings at Supercritical Mach Numbers. NACA ACR No. L5J16, 1945.

10. Abbott, Ira H., von Doenhoff, Albert E., and Stivers, Louis S., Jr.: Summary of Airfoil Data. NACA ACR No. L5C05, 1945.

11. Ferri, Antonio: Completed Tabulation in the United States of Tests of 24 Airfoils at High Mach Numbers (Derived from Interrupted Work at Guidonia, Italy, in the 1.31- by 1.74-Foot High-Speed Tunnel). NACA ACR No. L5E21, 1945.

TABLE I

GENERAL DIMENSIONS

Symbol	Description	Dimensions				
Λ_r	Sweep of 25-percent-chord line of original wing, degrees	0	30.0	45.0	-30.0	-45.0
Λ_c	Sweep of leading edges of actual wings, degrees	2.7	32.7	47.7	-27.3	-42.3
$\Lambda_{c/2}$	Sweep of 50-percent-chord line of actual wings, degrees	-2.7	27.6	42.8	-33.0	-48.2
b	Span, inches	37.8	34.2	28.2	33.8	27.4
d	Span along 25-percent-chord line of original wing, $b/2 \cos \Lambda_r$, inches	18.9	19.7	19.9	19.5	19.4
c_r	Root chord, inches	6.00	6.64	7.97	7.23	9.03
c_g	Tip chord, inches	2.40	2.53	3.07	2.66	3.33
c_f	Chord at intersection of wing and fuselage, inches	5.64	6.20	7.27	6.73	8.20
$\bar{c}_e$	Mean chord of wing extended through fuselage, inches	4.20	4.59	5.52	4.95	6.18
$\bar{c}_w$	Mean chord of wing outboard of fuselage, inches	4.02	4.26	5.17	4.80	5.76
S_e	Area of wing extended through fuselage, inches^2	158.6	157.0	155.6	167.4	169.2
S_w	Area of wing outboard of fuselage, inches^2	137.4	133.0	127.0	141.2	137.0
S_a	Area of wing assuming wing straight through fuselage, inches^2	158.6	156.2	154.4	166.4	167.8
A_e	Aspect ratio assuming wing extended through fuselage, b^2/S_e	9.0	7.4	5.1	6.8	4.4
A_w	Aspect ratio of wing outboard fuselage, $(b - 2r)^2/S_w$	8.5	7.0	4.7	6.3	4.1

[redacted]

[redacted]

TABLE I.- Concluded

GENERAL DIMENSIONS - Concluded

Symbol	Description	Dimensions				
A_a	Aspect ratio assuming wing straight through fuselage, b^2/S_a	9.0	7.5	5.2	6.9	4.5
	Taper ratio of wing outboard of fuselage, c_f/c_g	2.35	2.45	2.37	2.53	2.46
	Taper ratio assuming wing extended through fuselage, c_r/c_g	2.50	2.63	2.60	2.72	2.70
c'_w	Mean aerodynamic chord of wing outboard of fuselage, inches	4.24	4.62	5.45	4.99	6.10
c''_w	Mean aerodynamic chord of over-all configuration assuming wing rectangular through fuselage, inches	4.43	4.86	5.77	5.25	6.48
X_f	Inches	0	.94	1.65	-1.22	-2.20
X_w	Inches	0	4.74	6.93	-4.67	-6.67
X_a	Inches	0	4.19	6.00	-4.09	-5.68
X_e	Inches	0	-.14	-.28	.15	.35
g	Distance from nose of fuselage to intersection of quarter-chord line of original wing and plane of symmetry, inches	14.10	13.20	12.10	14.75	15.30
	Ratio of $2c_f r$ to S_w	.15	.18	.22	.18	.22
c_c	Chord at critical section, inches	5.64	5.41	5.19	5.45	5.24
	Position of critical chord with respect to intersection of c/4 line of original wing (percent "d")	10.0	16	22.4	15.5	21.1
	Ratio of thickness to chord for sections parallel to airstream	10.0	9.0	7.5	8.2	6.6
	Position of maximum thickness, percent chord	42	43	43	41	41

[redacted]

TABLE II

Locations of pressure orifice stations with reference to the intersection of the 25 percent chord line of the original wing and the center line (percent of swept-back semispan)

Sweep angle, Λ_r				
0°	30°	45°	-30°	-45°
11.0	12.7	14.4	7.6	5.2
20.0	21.3	22.9	16.3	14.0
30.0	30.9	32.4	26.0	23.7
43.0	43.4	44.7	38.6	36.4
56.0	55.8	57.0	51.1	49.1
64.0	63.5	64.7	58.9	56.9
80.0	78.8	79.8	74.4	72.5
95.0	93.2	94.0	88.9	87.1

NATIONAL ADVISORY
COMMITTEE FOR AERONAUTICS

[redacted]

TABLE III

LOCATION OF RAKE FOR WAKE SURVEYS

[Sweep angles]

0°		30°		45°		-30°	
x (in.)	2y/b	x (in.)	2y/b	x (in.)	2y/b	x (in.)	2y/b
8.4	0.127	16.8	0.175	17.1	0.210	9.8	0.180
8.4	.180	16.8	.292	17.1	.384	9.8	.300
8.4	.250	16.8	.490	17.1	.508	9.8	.500
8.4	.500	16.8	.725	17.1	.740	9.8	.750
8.4	.750	16.8	.910	25.1	.740	9.8	.950
8.4	.950	16.8	1.000	25.1	.925	17.3	.180
				25.1	1.000		

NATIONAL ADVISORY
COMMITTEE FOR AERONAUTICS

[redacted]

TABLE IV

TEST POINTS

Pressure measurements		Wake survey measurements	
$\Lambda_r = 0°$		$\Lambda_r = 0°$	
M	α (deg)	M	α (deg)
0.600	-2,0,2,4,7,10	0.600	0,2,4,7
.750	-2,0,2,4,7,10	.700	-2,0,2,4,7
.800	-2,0,2,4,7,10	.750	-2,0,2,4,7
.850	0,2,4,7	.800	-2,0,2,4,7
.890	0,2,4,7	.850	0,2,4
.925	0,2,4,7	.890	0,2,4
$\Lambda_r = 30°$		$\Lambda_r = 30°$	
M	α (deg)	M	α (deg)
0.800	-2,0,2,4,7,10	0.600	0,2,5,8
.800	-2,0,2,4,7,10	.750	-2,0,2,5,8
.850	-2,0,2,4,7	.800	-2,0,2,5,8
.890	0,2,4,7	.850	-2,0,2,5
.925	0,2,4,7	.890	0,2,5
.960	0,2,4,7		
$\Lambda_r = 45°$		$\Lambda_r = 45°$	
M	α (deg)	M	α (deg)
0.600	-2,2,7,10,13	0.600	0,3,6,9
.800	-2,2,7,10	.800	-2,0,3,6
.890	-2,2,7,10	.850	-2,0,3,6
.925	-2,2,7,10	.890	0,3,6
.960	-2,2,7,10		

NATIONAL ADVISORY
COMMITTEE FOR AERONAUTICS

[redacted]

TABLE IV. - Concluded

TEST POINTS - Concluded

$\Lambda_r = -30°$		$\Lambda_r = -30°$	
M	α (deg)	M	α (deg)
0.600	-2,0,2,4,7,10	0.600	0,2,5,8
.800	-2,0,2,4,7,10	.750	-2,0,2,5,8
.850	-2,0,2,4,7	.800	-2,0,2,5,8
.890	0,2,4,7	.850	-2,0,2,5
.925	0,2,4,7	.890	0,2,5
.960	0,2,4,7		

$\Lambda_r = -45°$	
M	α (deg)
0.600	-2,2,7,10,13
.800	-2,2,7,10
.890	-2,2,7,10
.925	-2,2,7,10
.960	-2,2,7,10

NATIONAL ADVISORY
COMMITTEE FOR AERONAUTICS

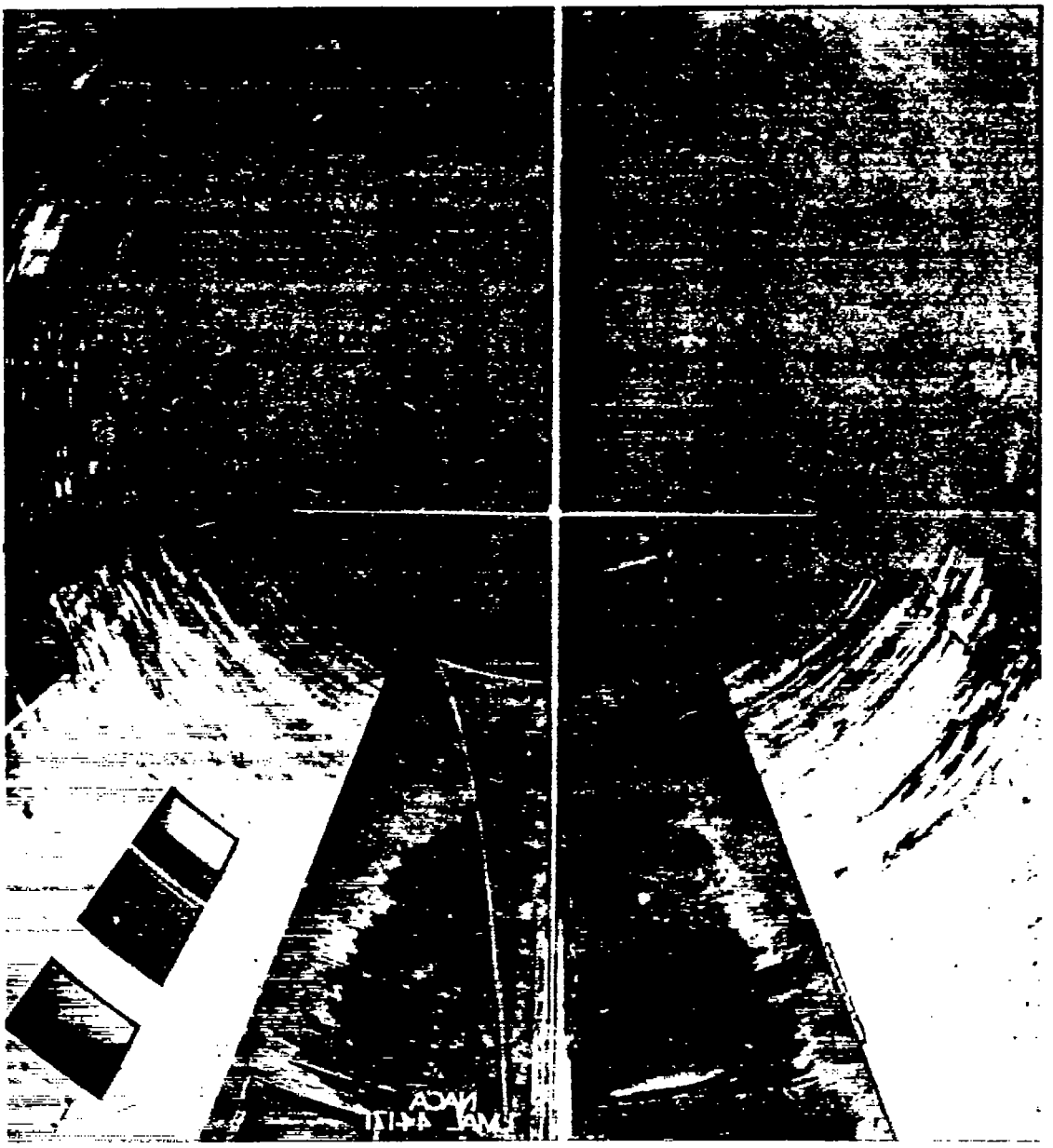

Figure 1.- Unswept wing without fuselage on plate.

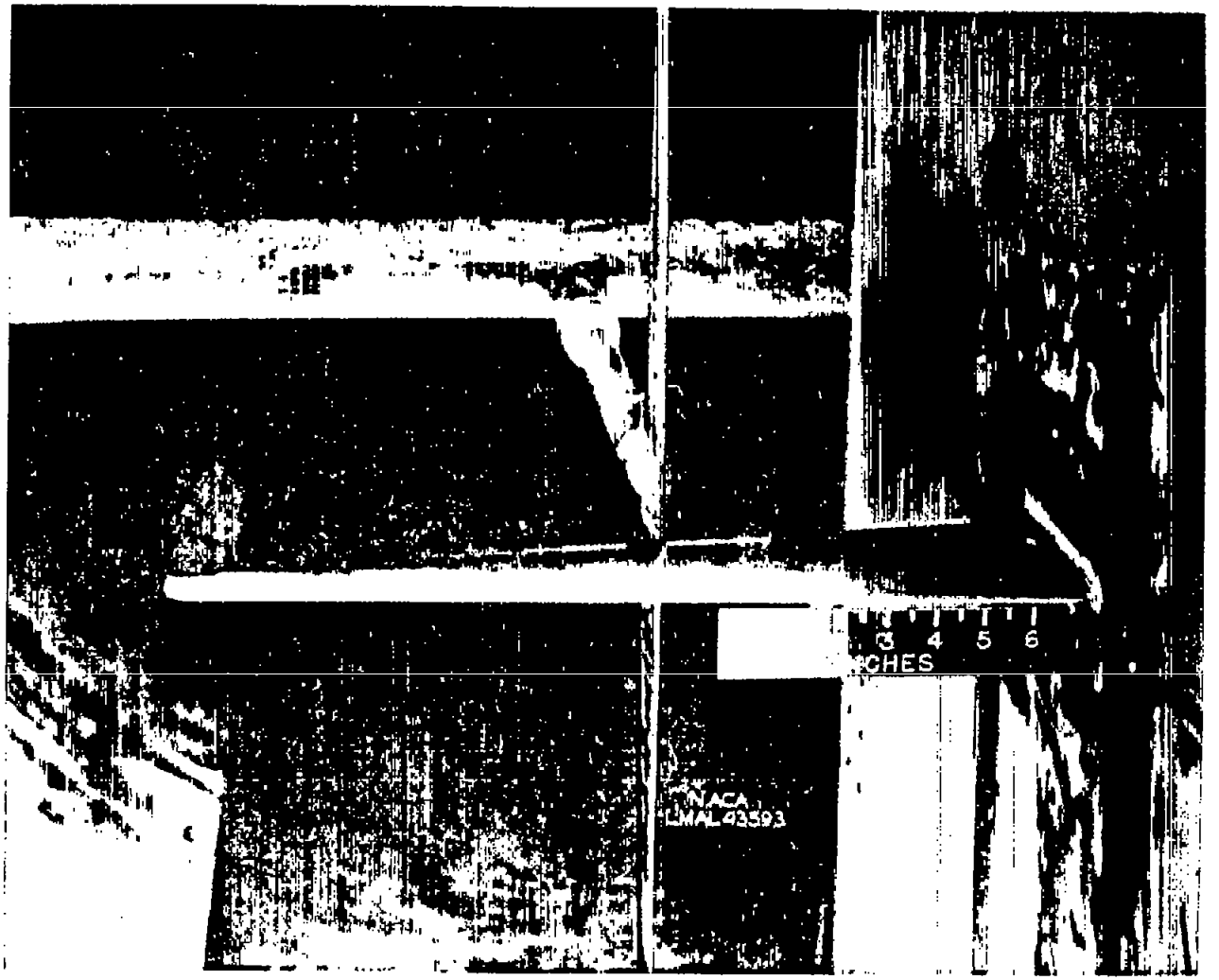

Figure 2.- Close-up of unswept wing showing wake-survey rake.

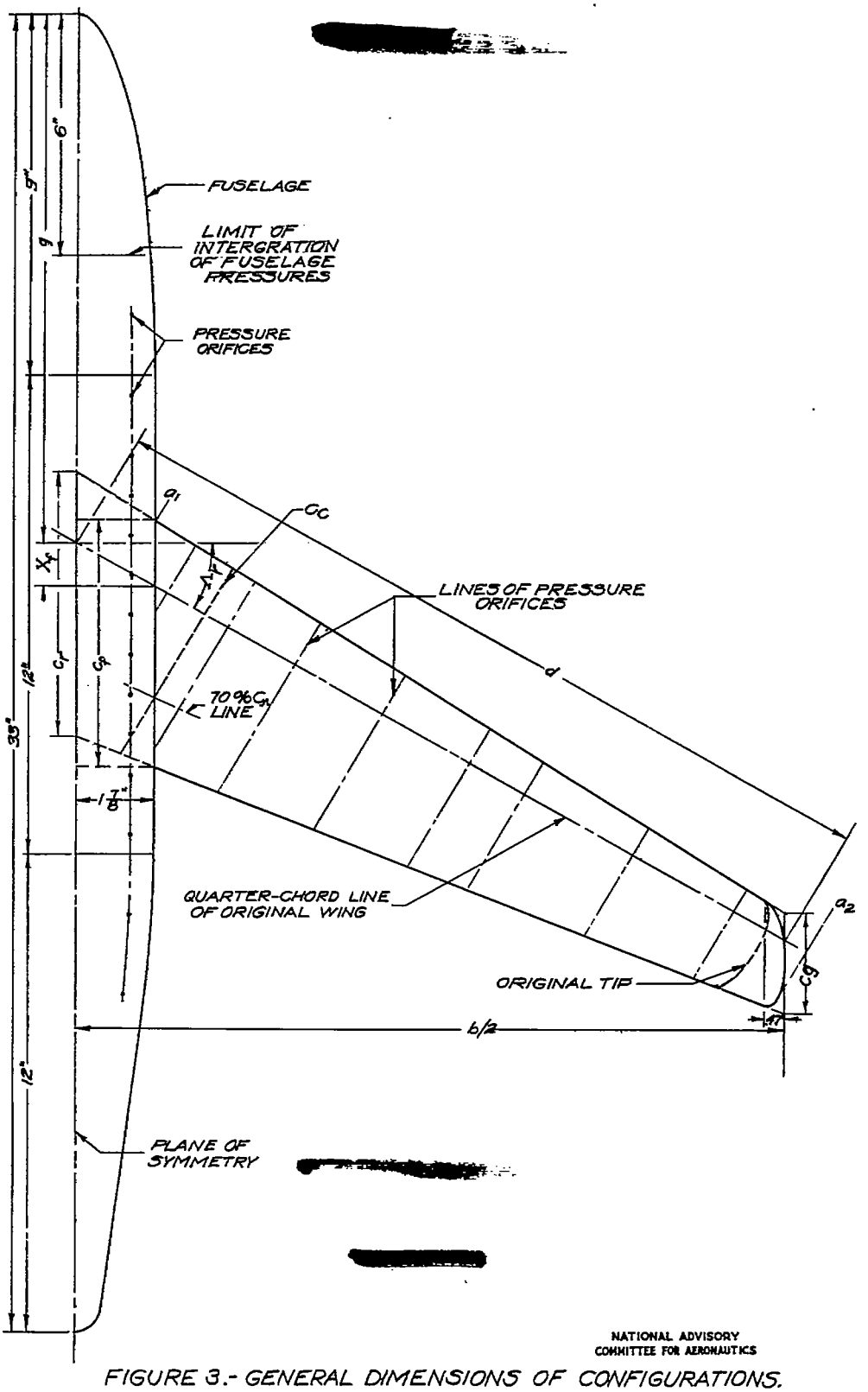

FIGURE 3.- GENERAL DIMENSIONS OF CONFIGURATIONS.

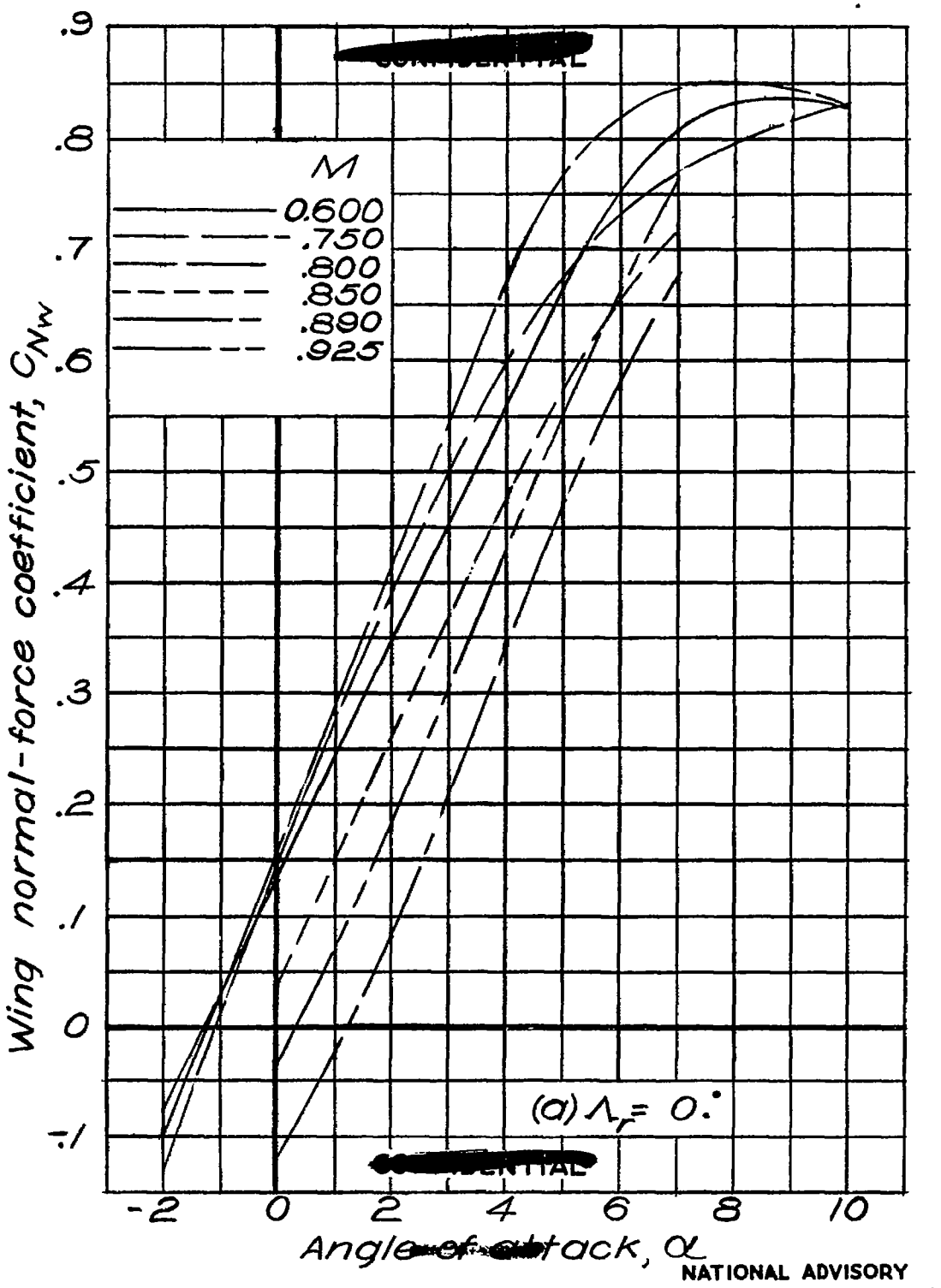

Figure 4 .— Variation of wing normal-force coefficient with angle of attack.

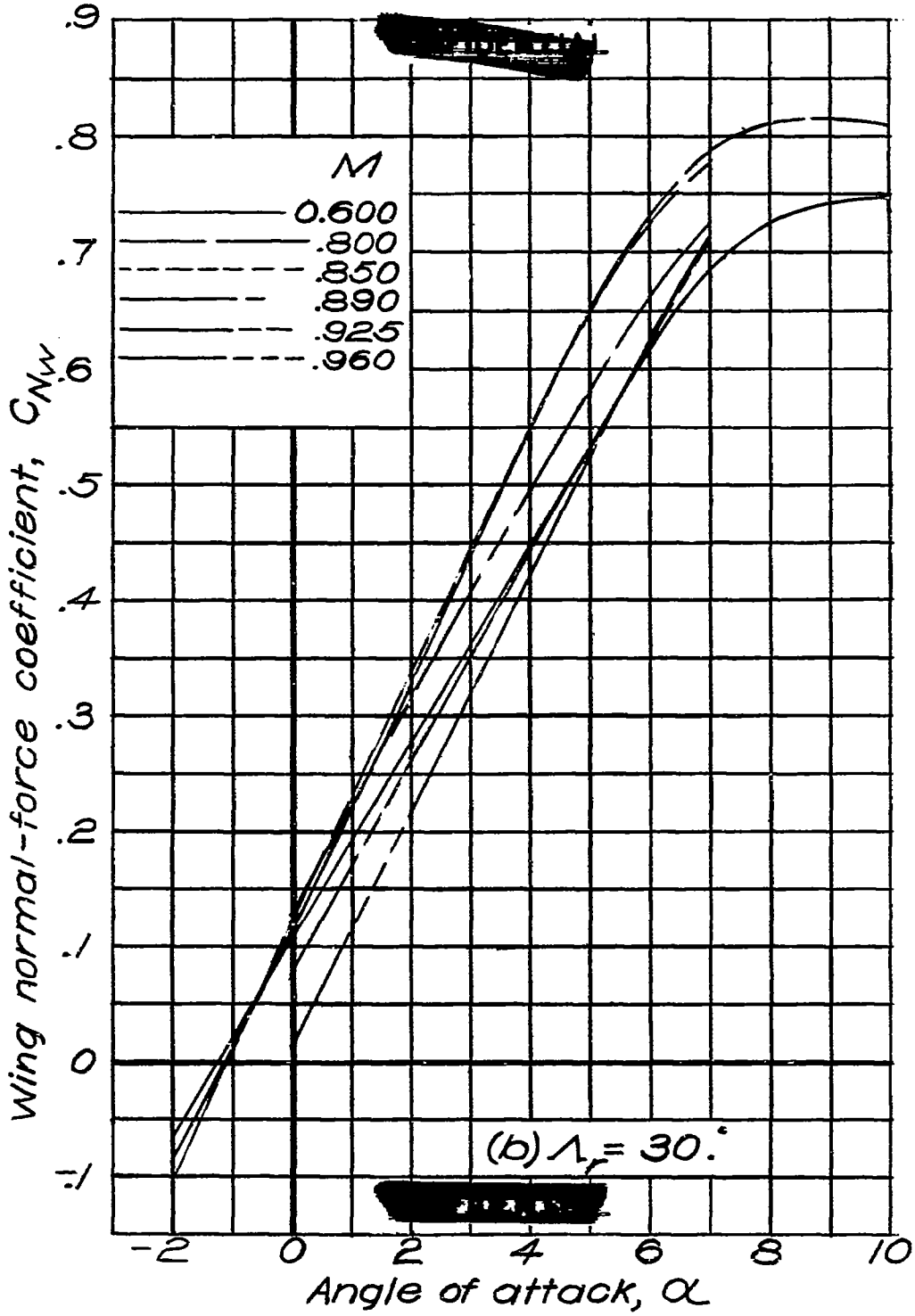

Figure 4 .- Continued.

NATIONAL ADVISORY
COMMITTEE FOR AERONAUTICS

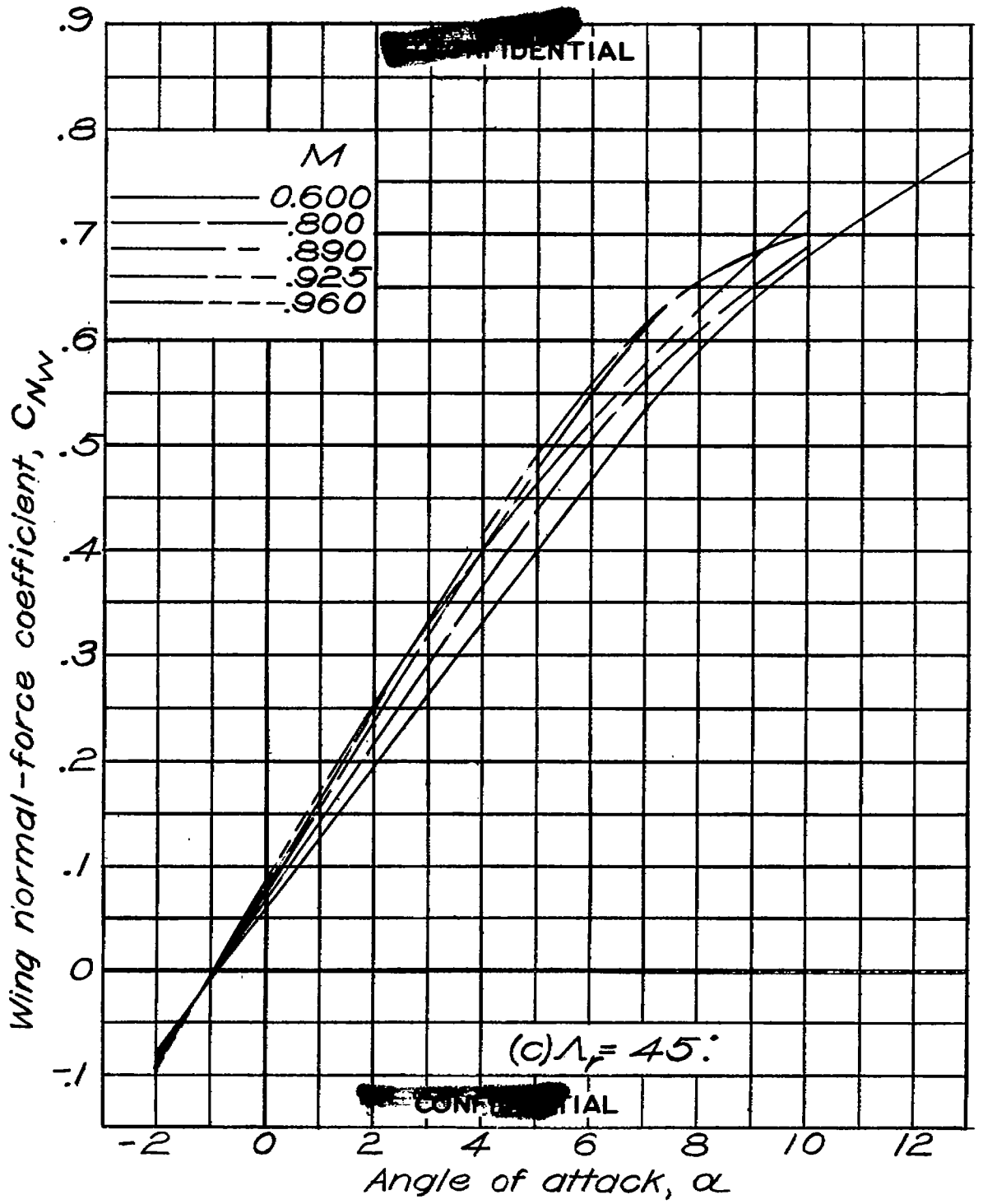

Figure 4.- Continued.

NATIONAL ADVISORY
COMMITTEE FOR AERONAUTICS

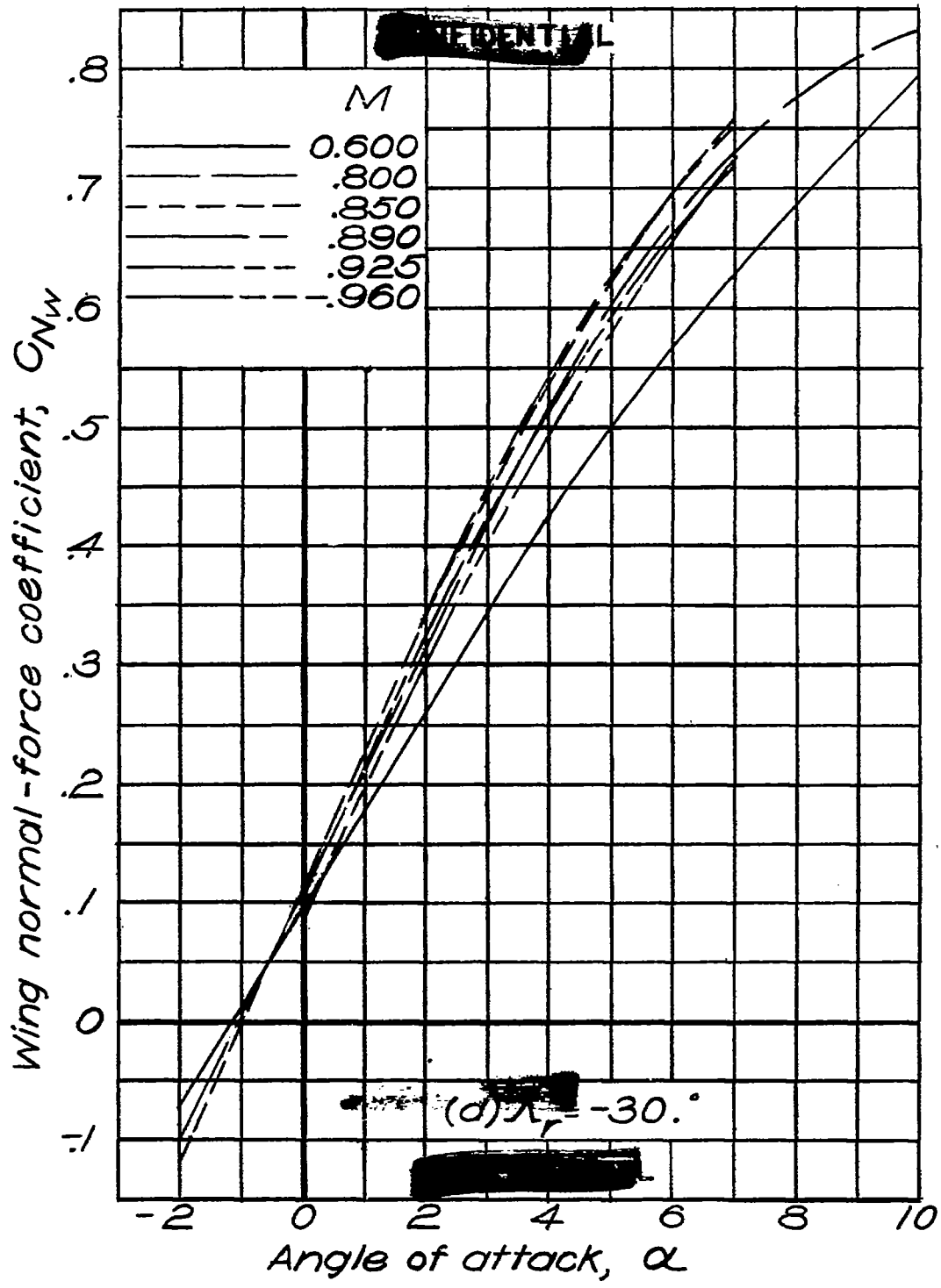

Figure 4 .- Continued.

NATIONAL ADVISORY
COMMITTEE FOR AERONAUTICS

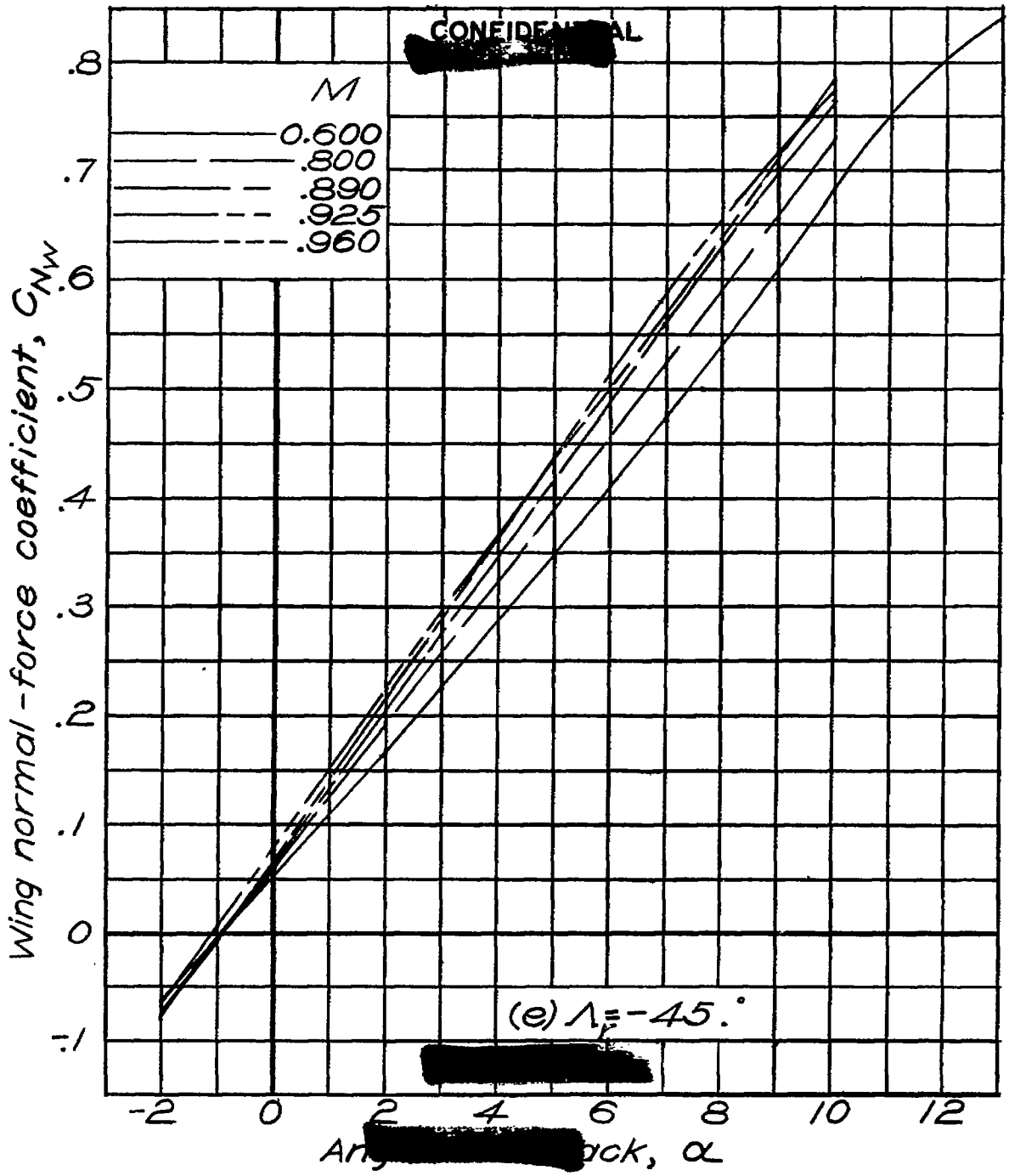

Figure 4 .- Concluded.

NATIONAL ADVISORY
COMMITTEE FOR AERONAUTICS

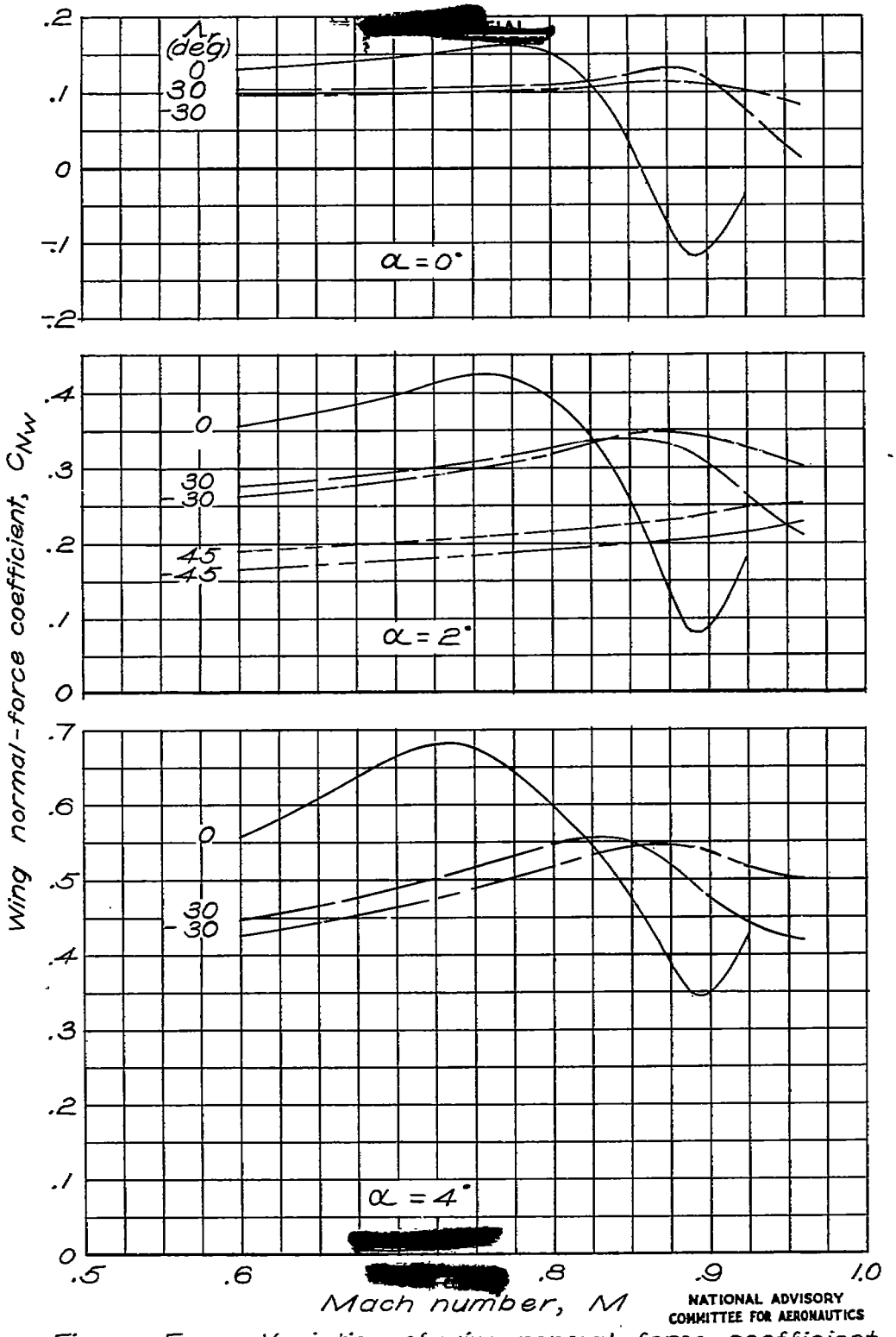

Figure 5 .- Variation of wing normal-force coefficient with Mach number.

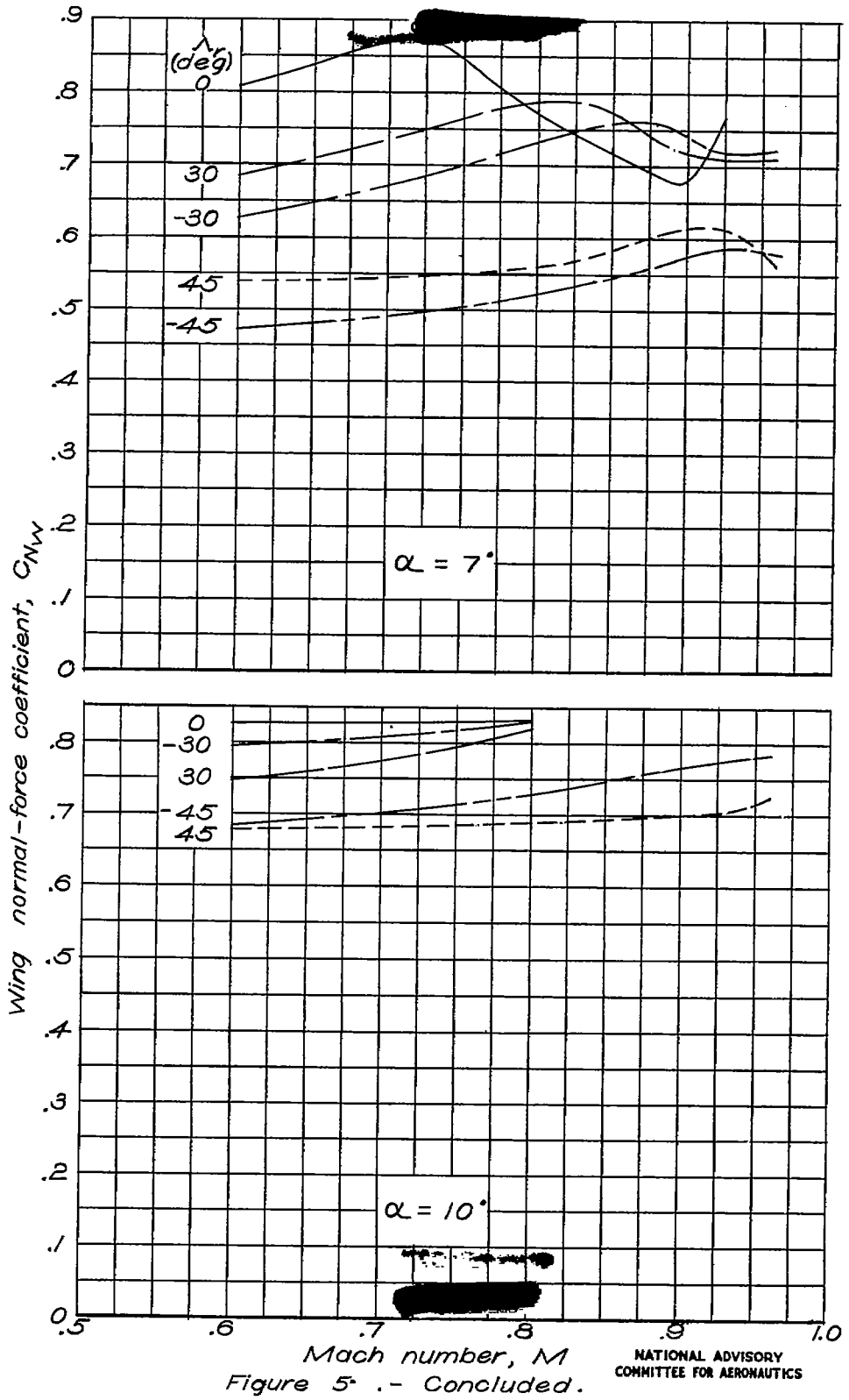

Figure 5. - Concluded.

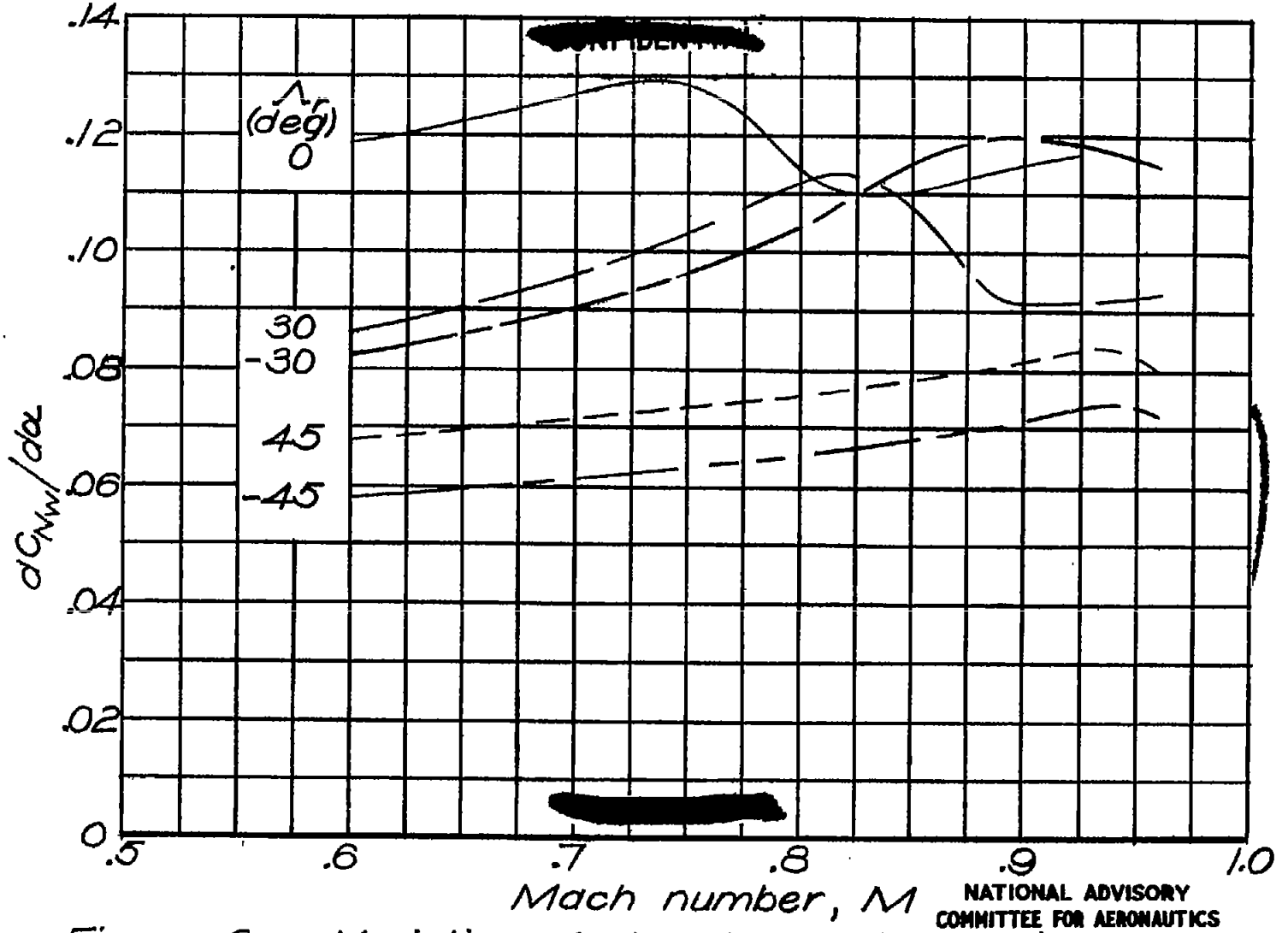

Figure 6.- Variation of the slopes of the wing normal-force curves with Mach number. $\alpha = 2°$.

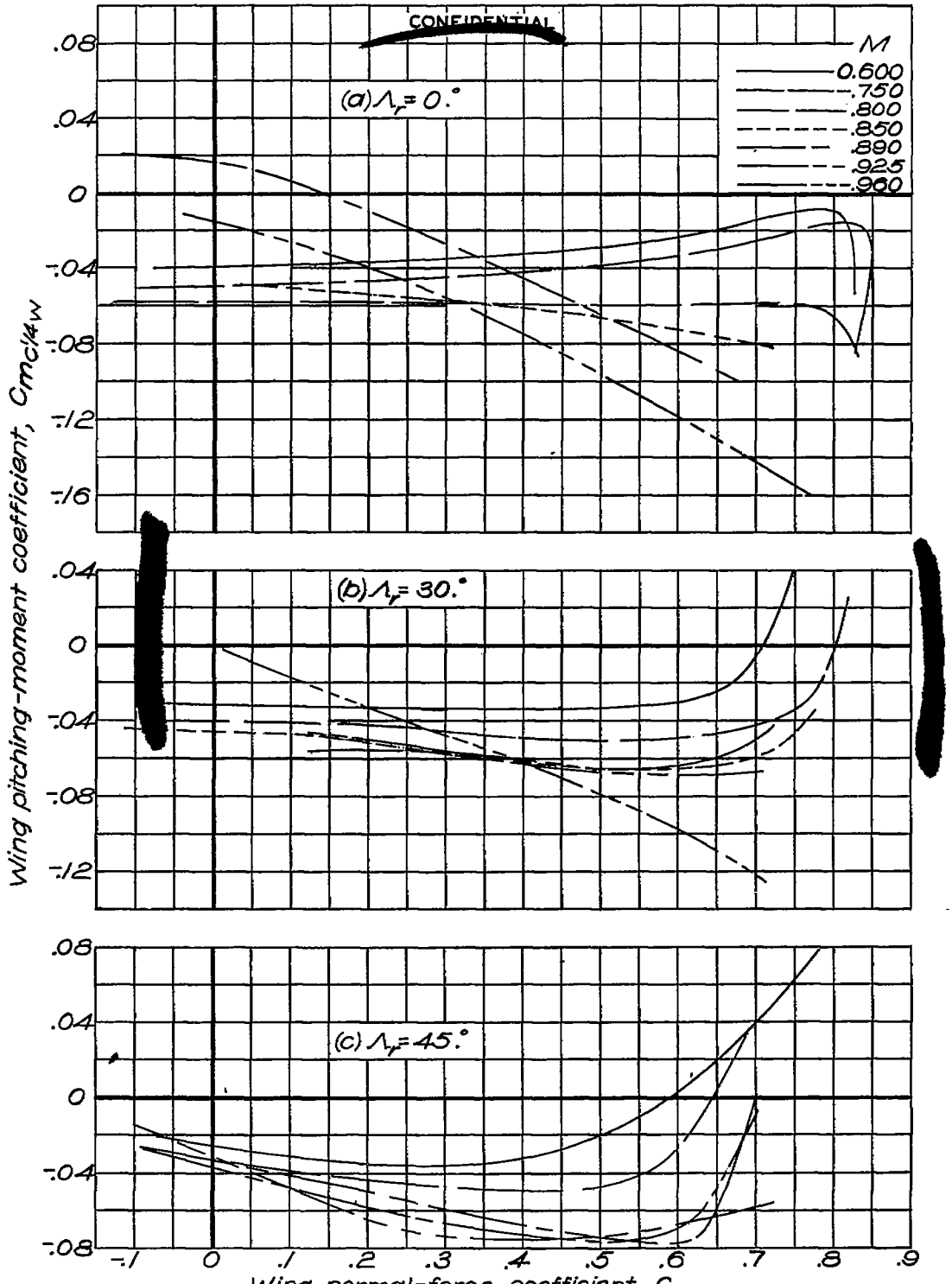

Figure 7 .- Variation of wing pitching-moment coefficient with wing normal-force coefficient.

NATIONAL ADVISORY COMMITTEE FOR AERONAUTICS.

CONFIDENTIAL

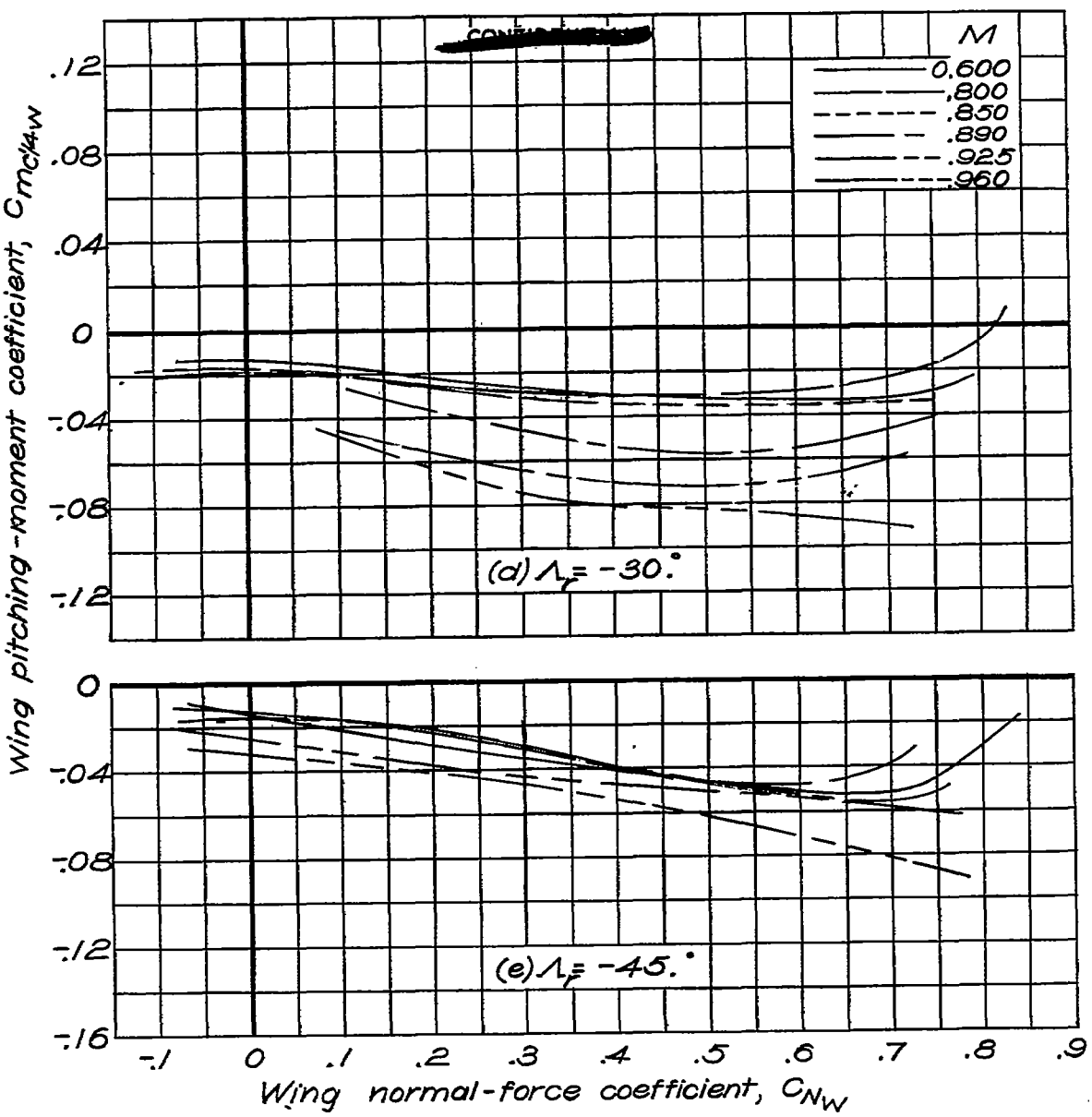

Figure 7.- Concluded.

NATIONAL ADVISORY COMMITTEE FOR AERONAUTICS

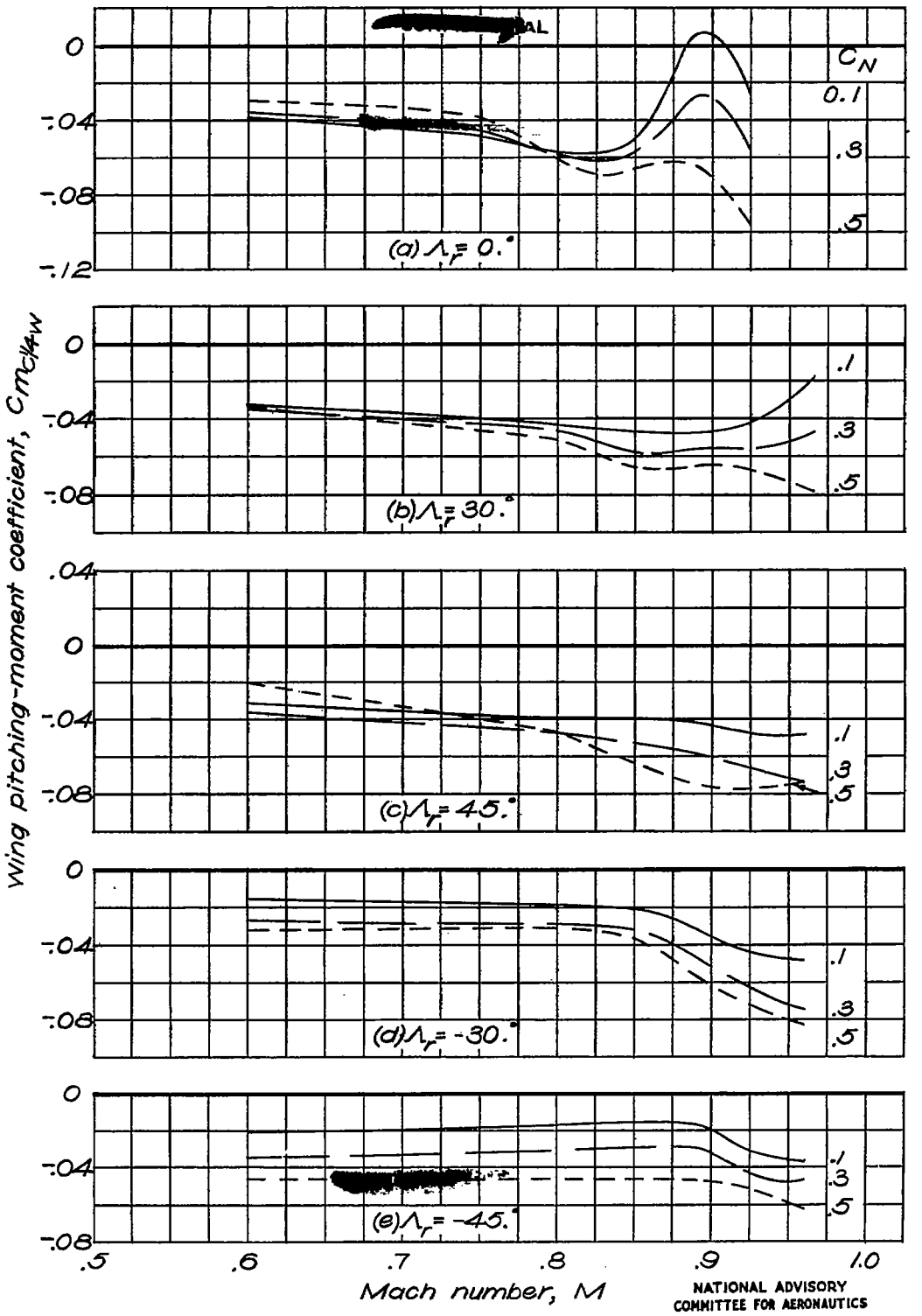

Figure 8.— Variation of wing pitching-moment coefficient with Mach number for constant wing normal-force coefficients.

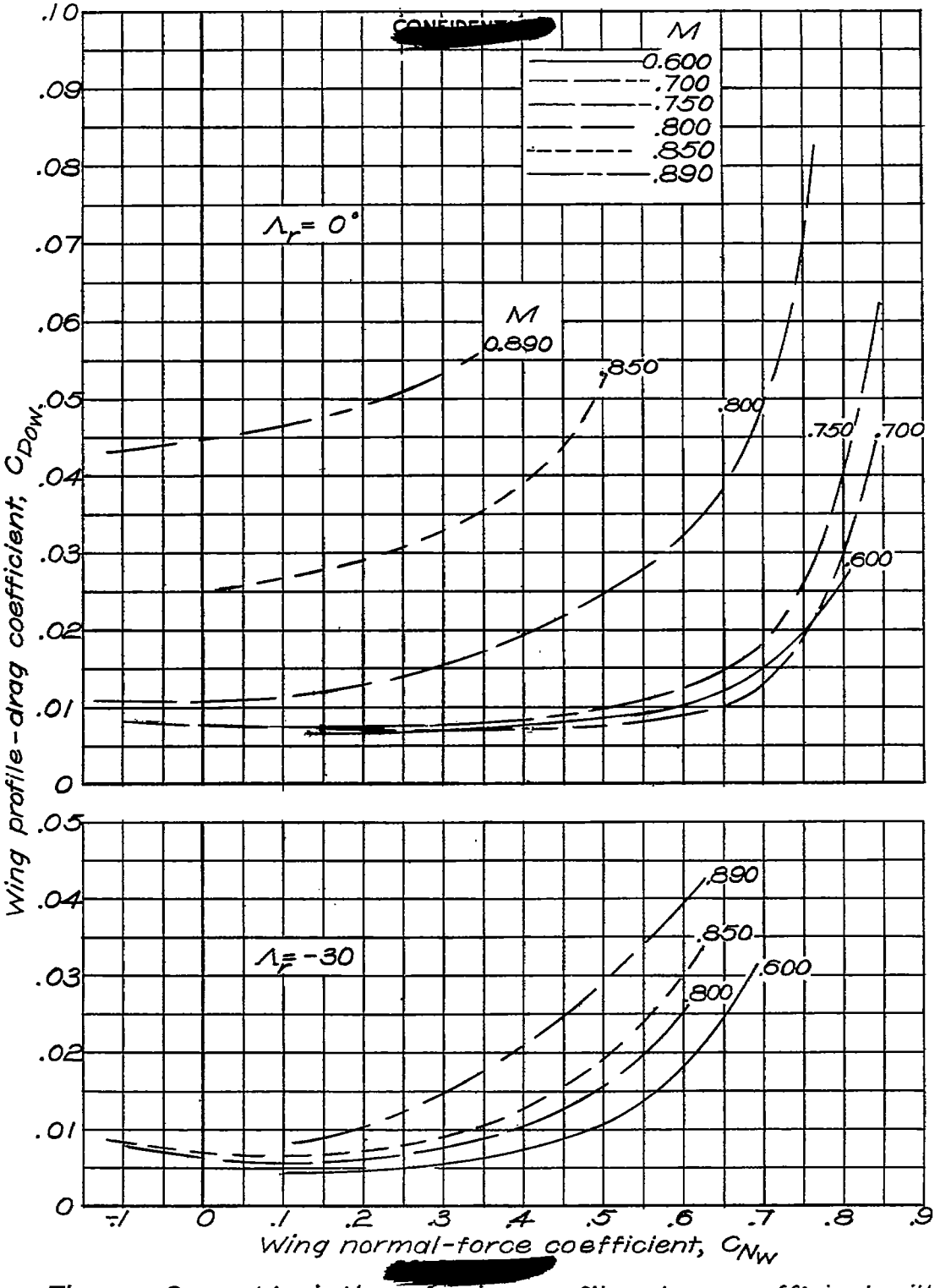

Figure 9 .- Variation of wing profile-drag coefficient with wing normal-force coefficient.

NATIONAL ADVISORY COMMITTEE FOR AERONAUTICS

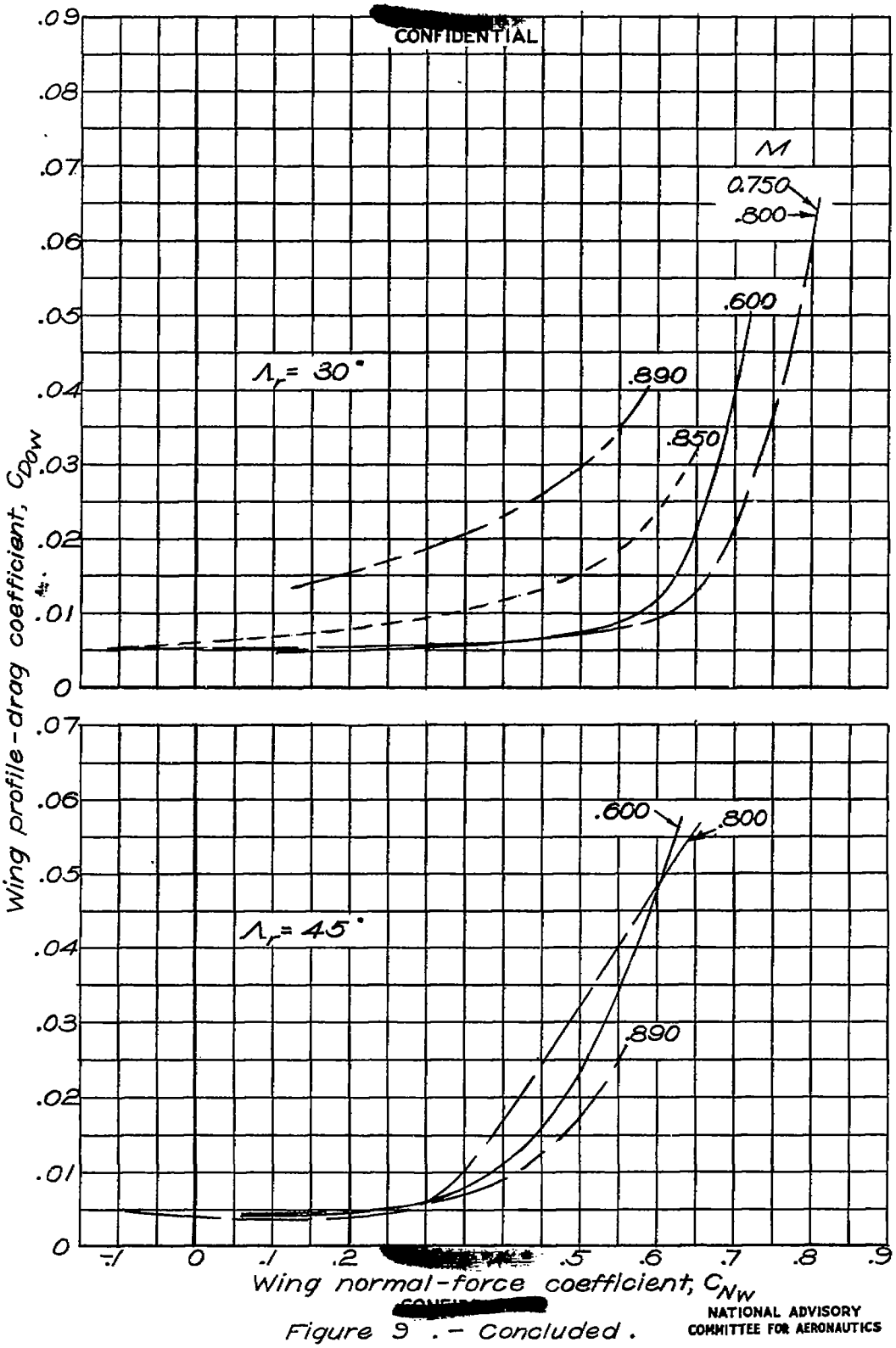

Figure 9 .- Concluded.

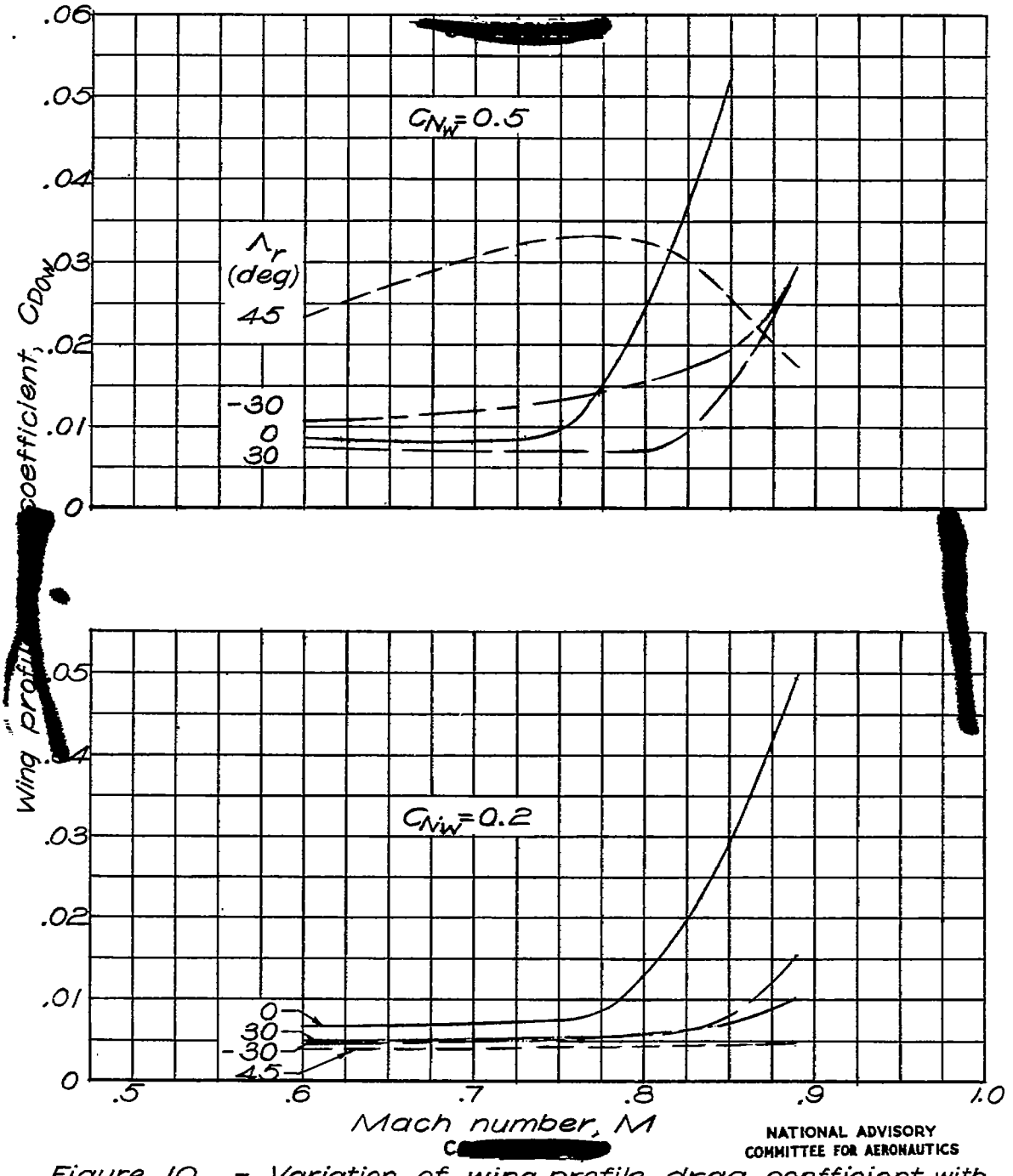

Figure 10 .- Variation of wing profile-drag coefficient with Mach number for constant wing normal-force coefficient.

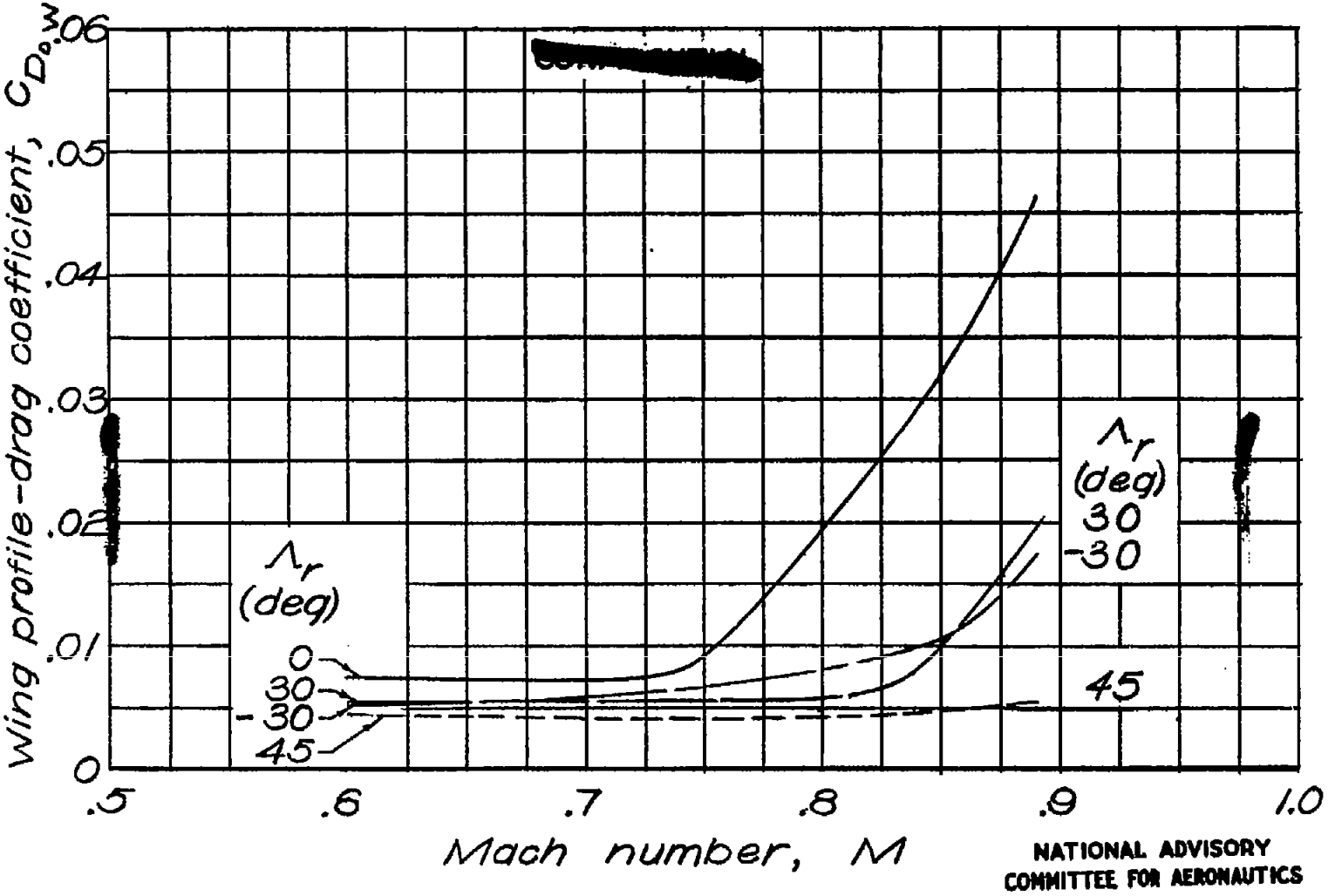

Figure 11 .— Variation of wing profile-drag coefficient with Mach number. $\alpha = 2°$.

[redacted]

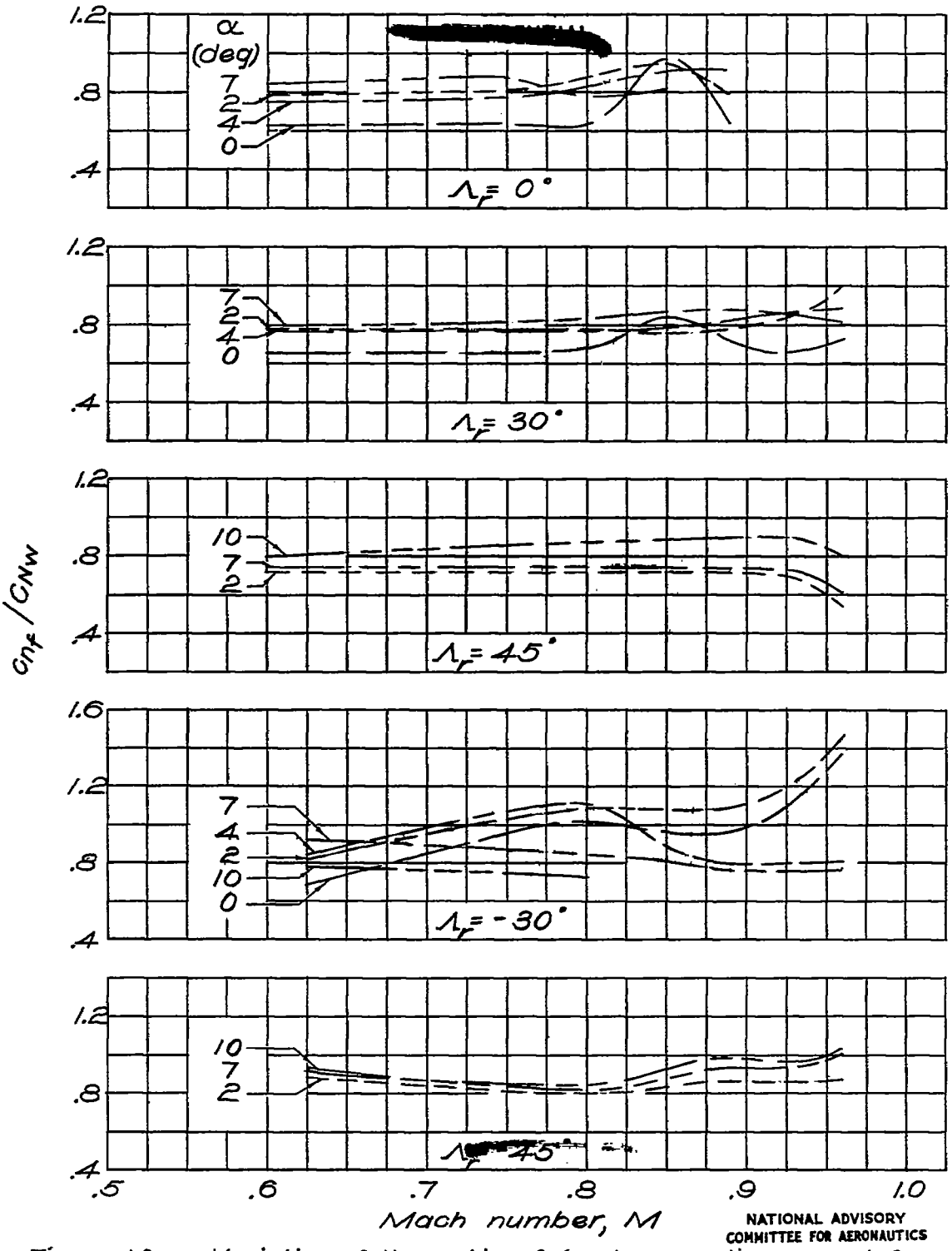

Figure 12.- Variation of the ratio of fuselage section normal-force coefficient to wing normal-force coefficient with Mach number.

[redacted]

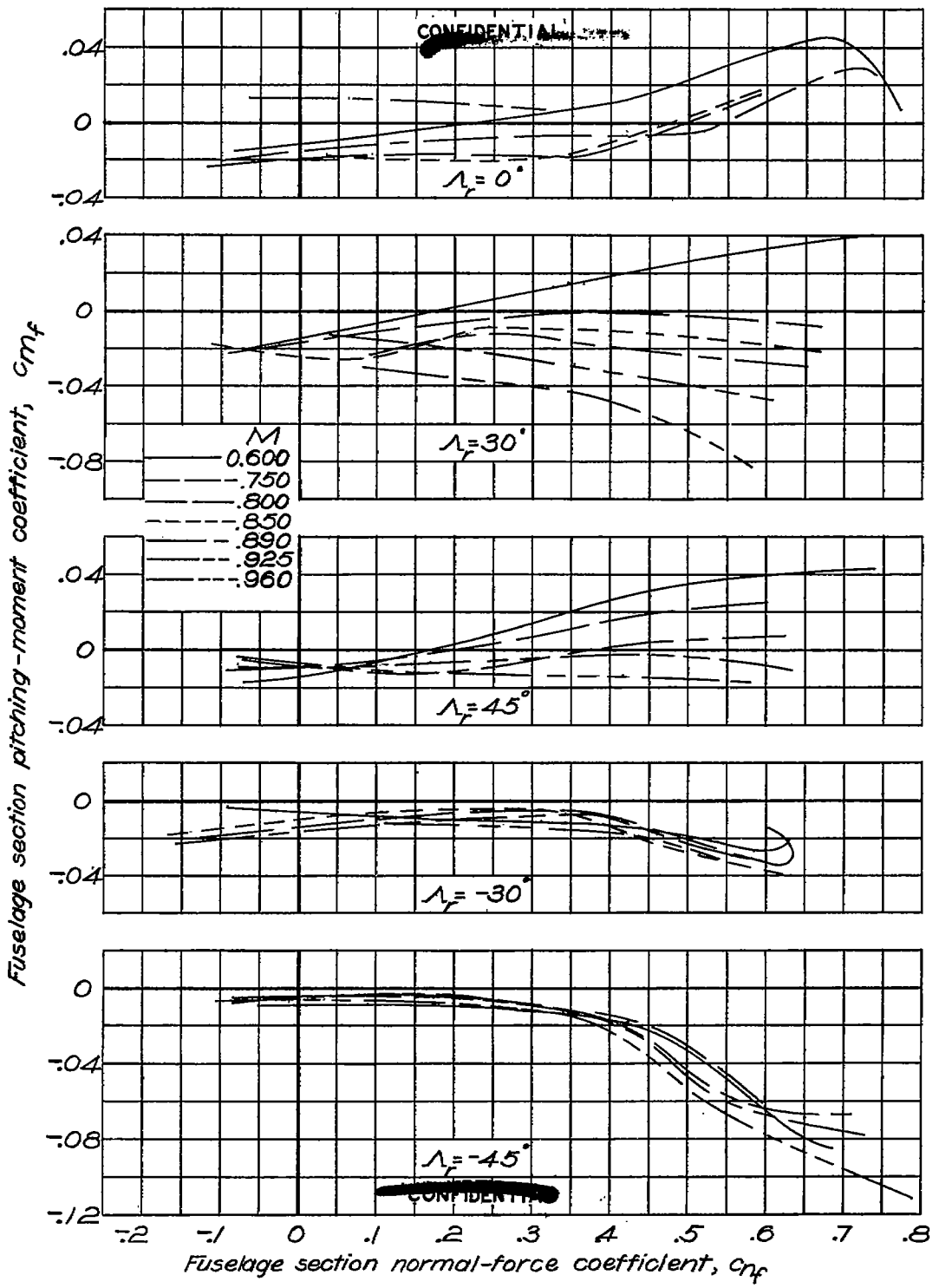

Figure 13.— Variation of fuselage section pitching-moment coefficient with fuselage section normal-force coefficient.

NATIONAL ADVISORY COMMITTEE FOR AERONAUTICS

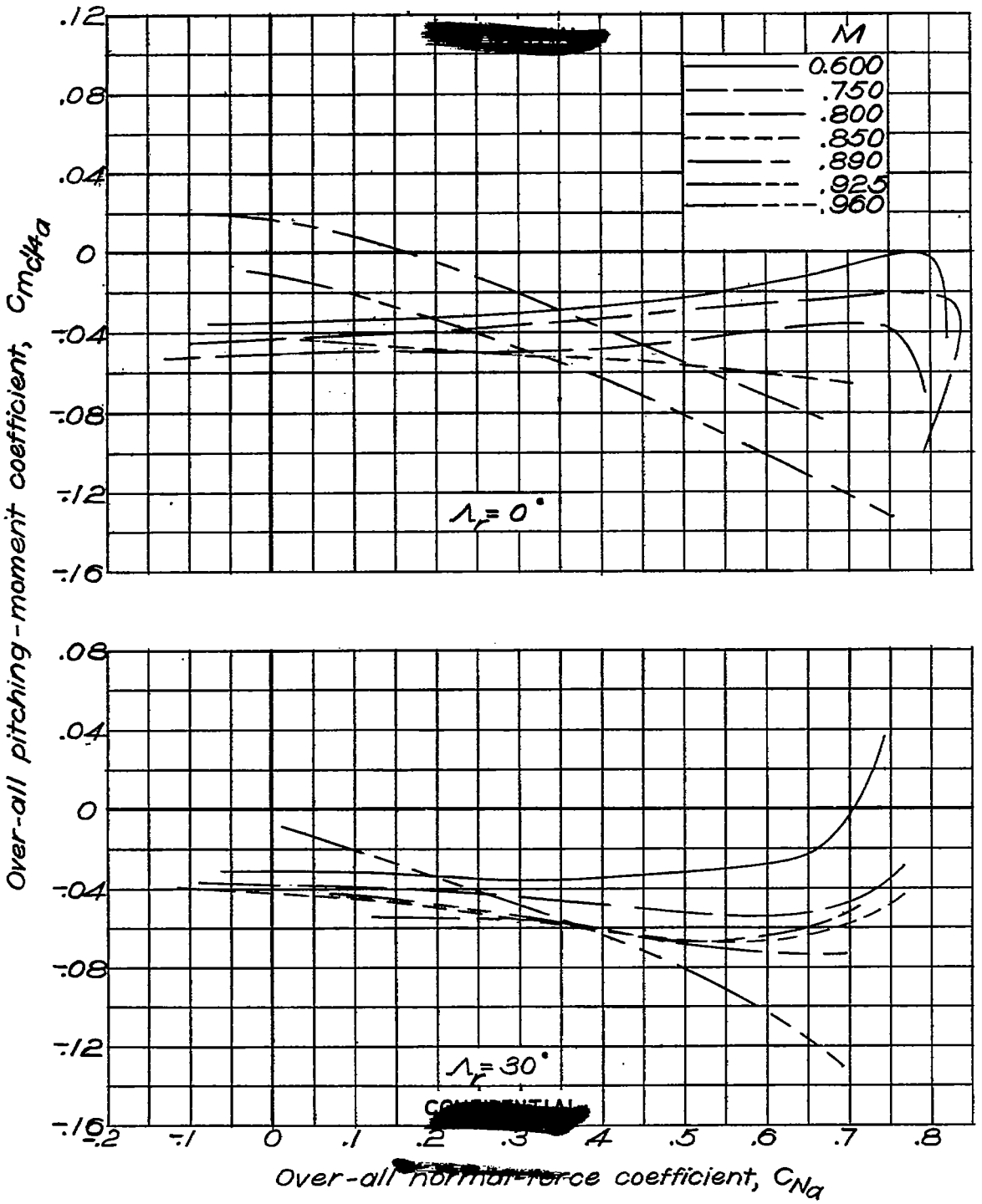

Figure 14.- Variation of over-all pitching-moment coefficient with over-all normal-force coefficient.

NATIONAL ADVISORY COMMITTEE FOR AERONAUTICS

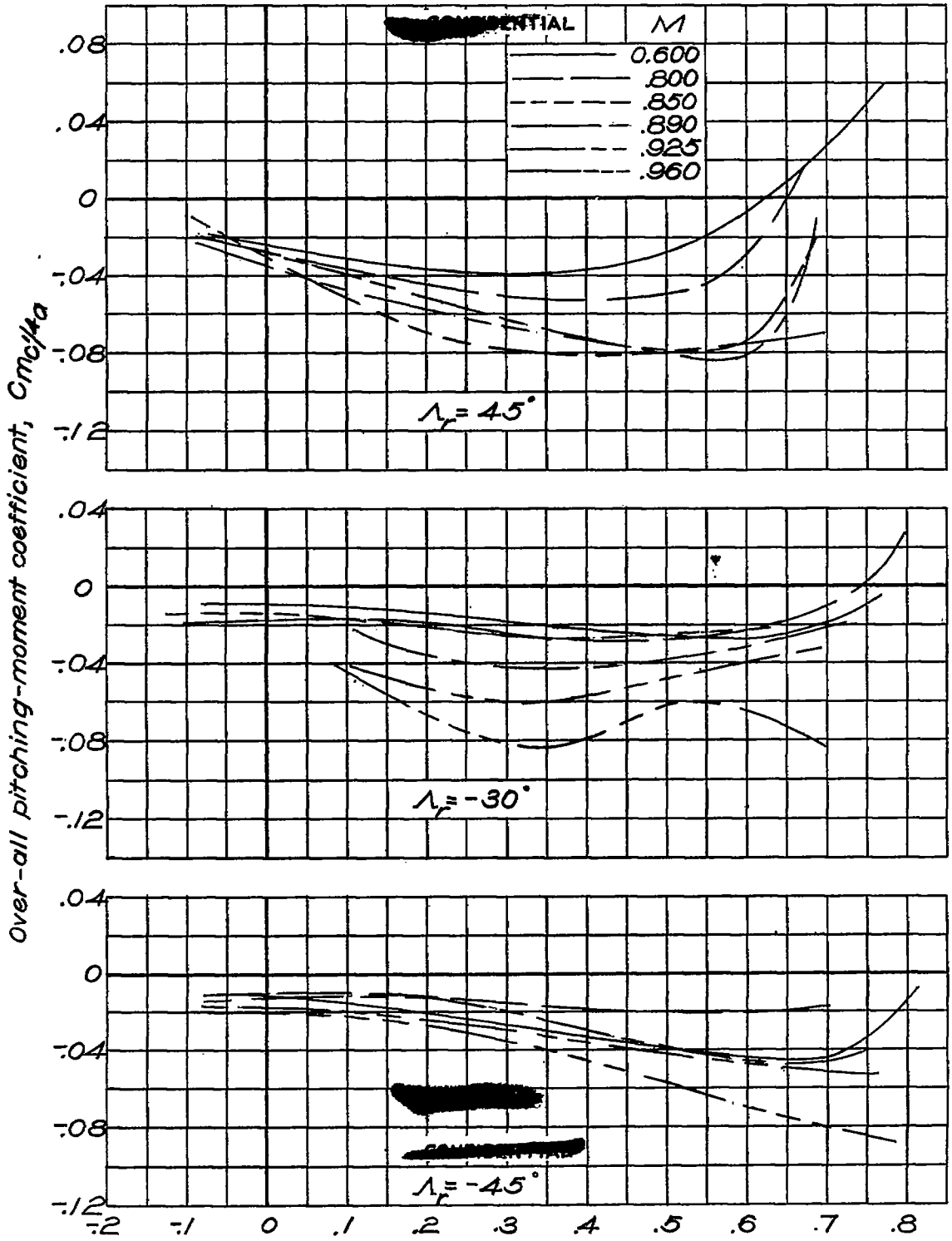

Figure 14.- Concluded.

NATIONAL ADVISORY COMMITTEE FOR AERONAUTICS

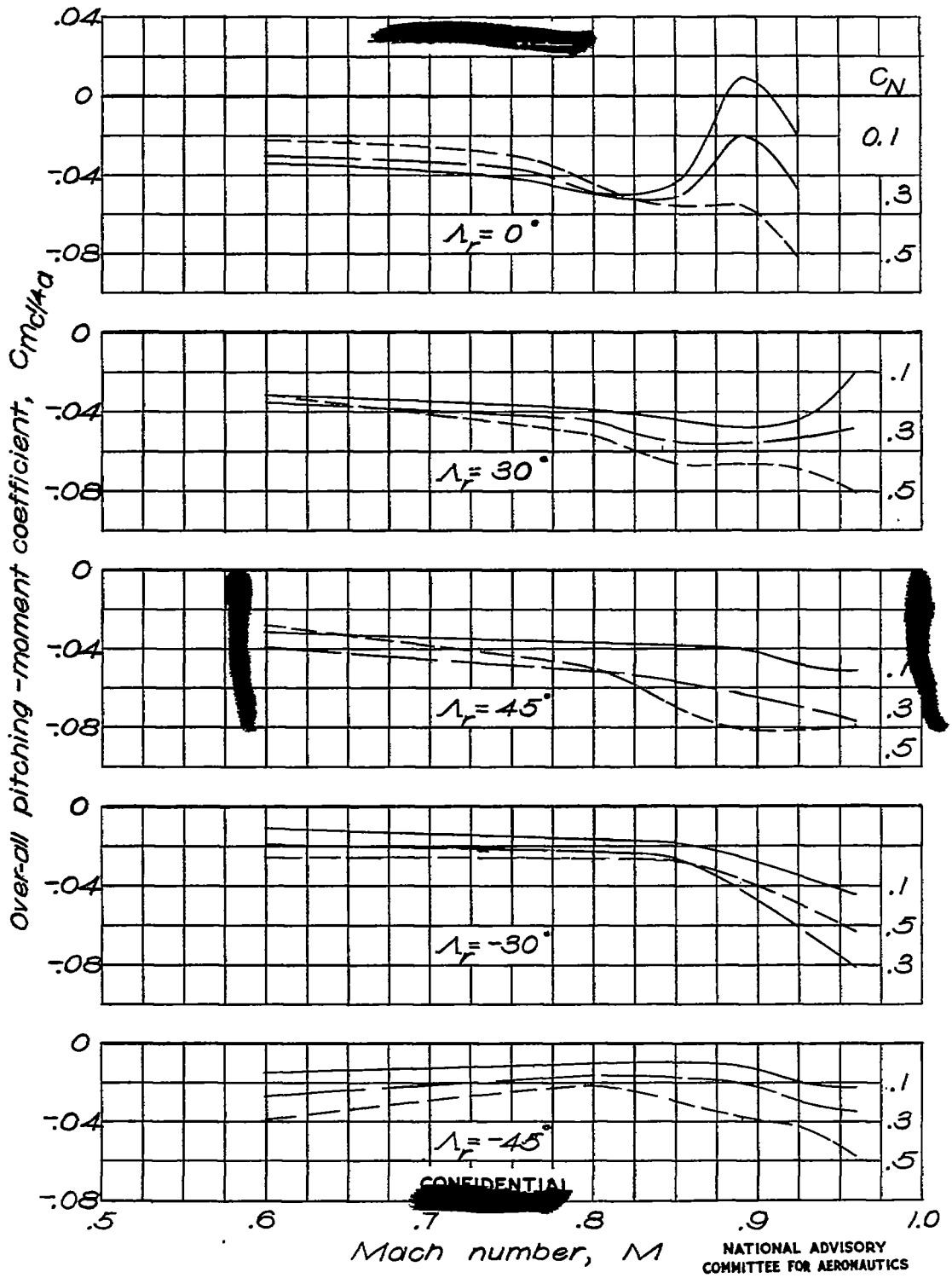

Figure 15.- Variation of over-all pitching-moment coefficient with Mach number for constant normal-force coefficients.

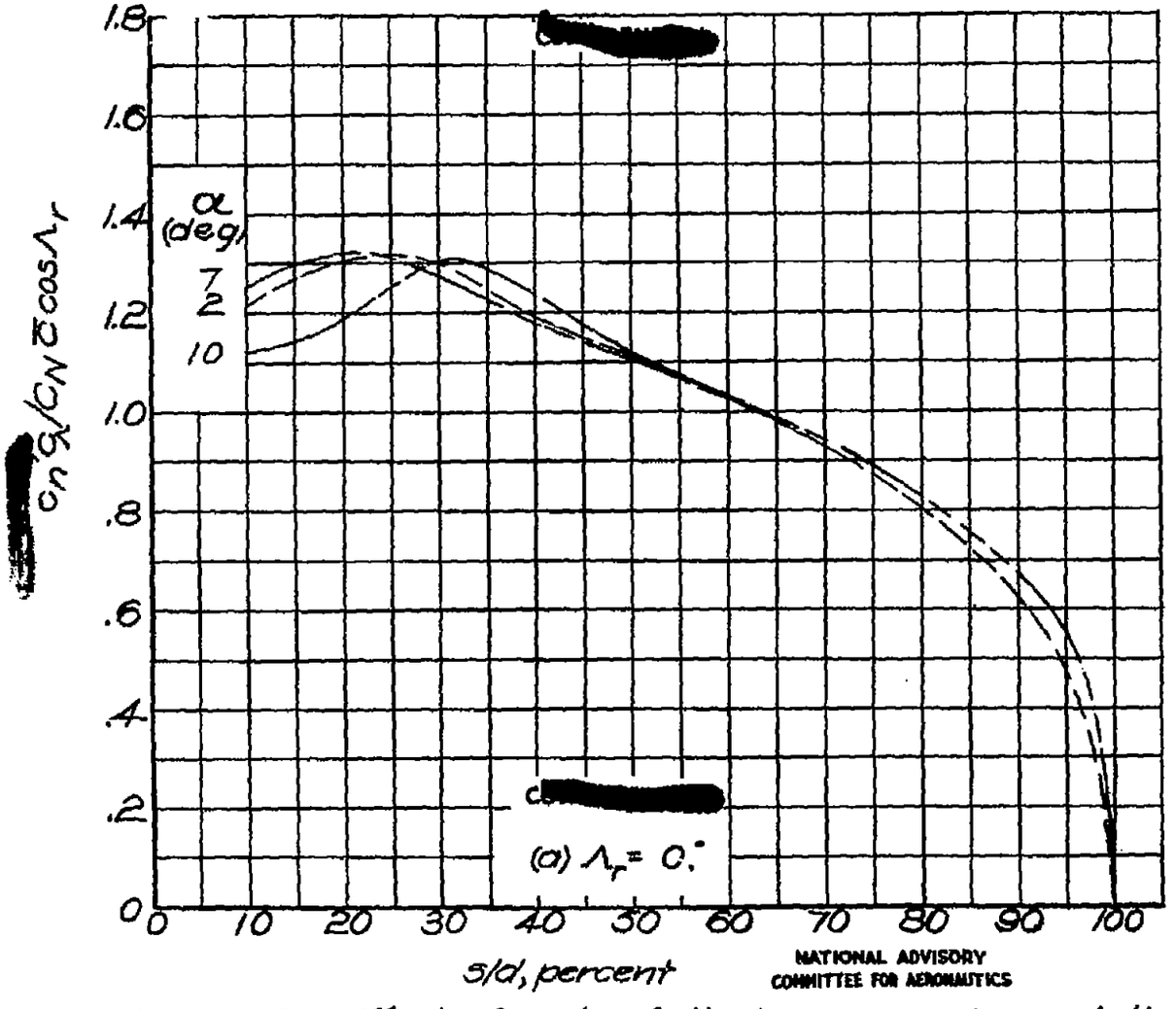

Figure 16.- Effect of angle of attack on spanwise variation of section loading. M = 0.600.

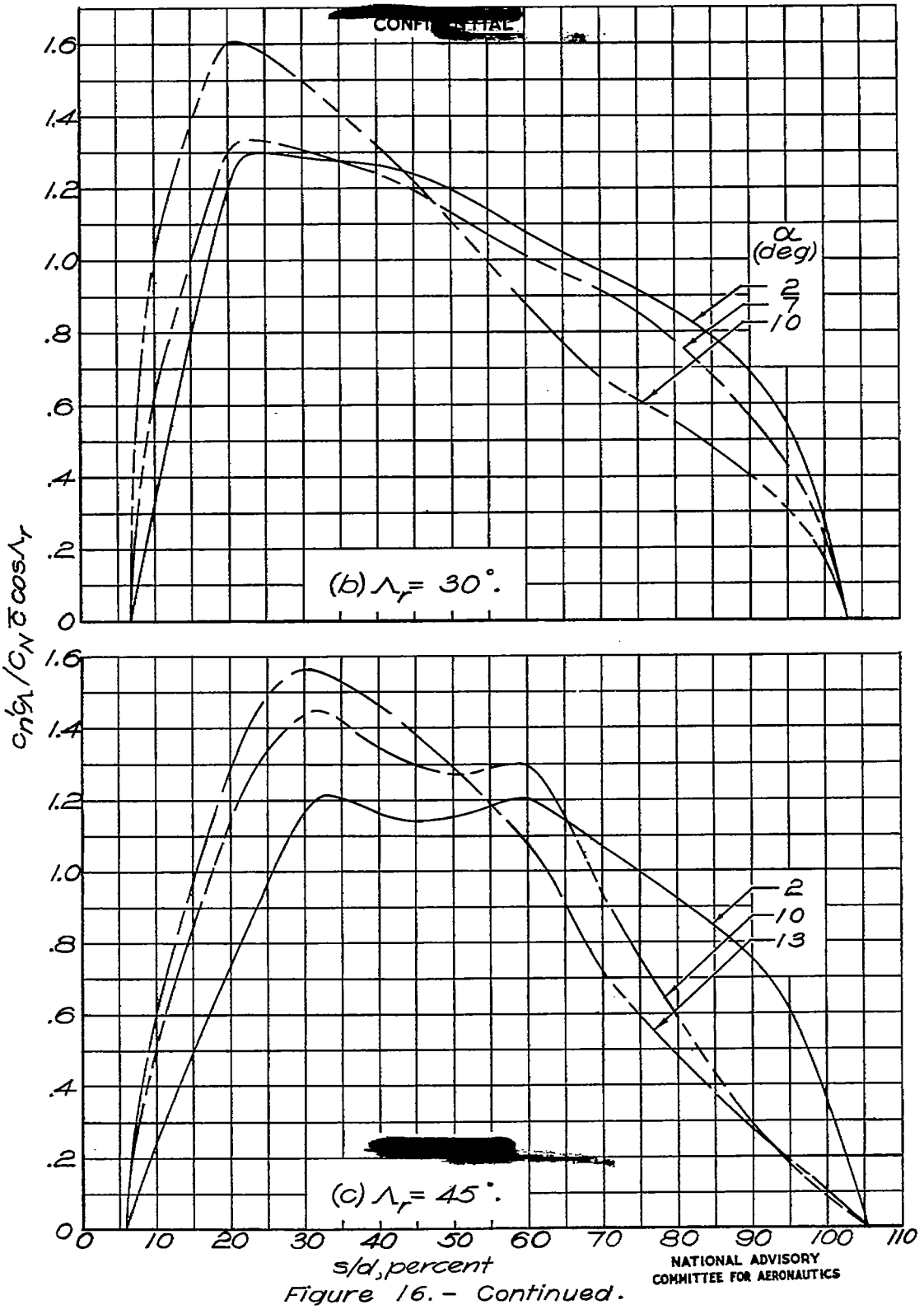

Figure 16. - Continued.

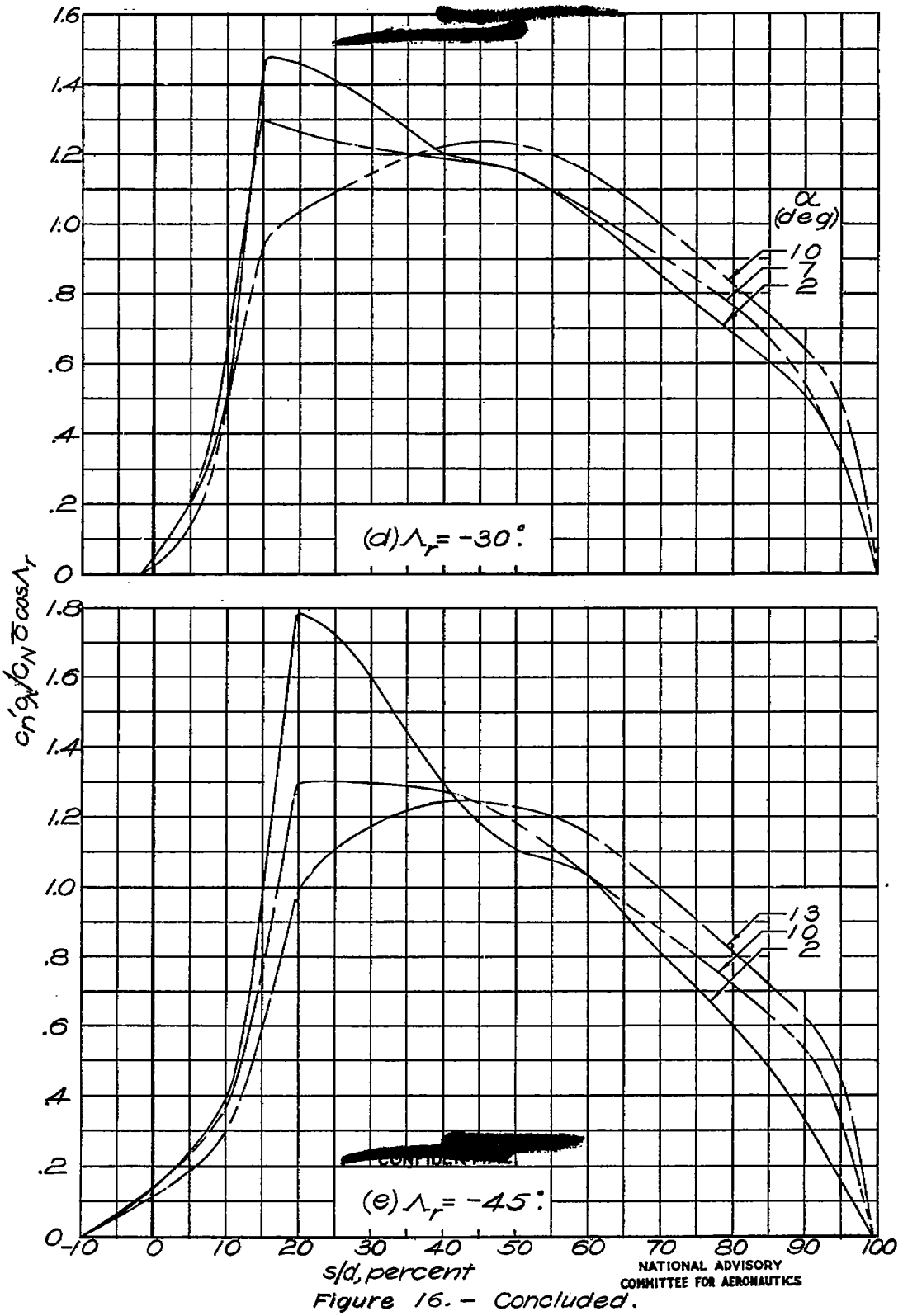

Figure 16. – Concluded.

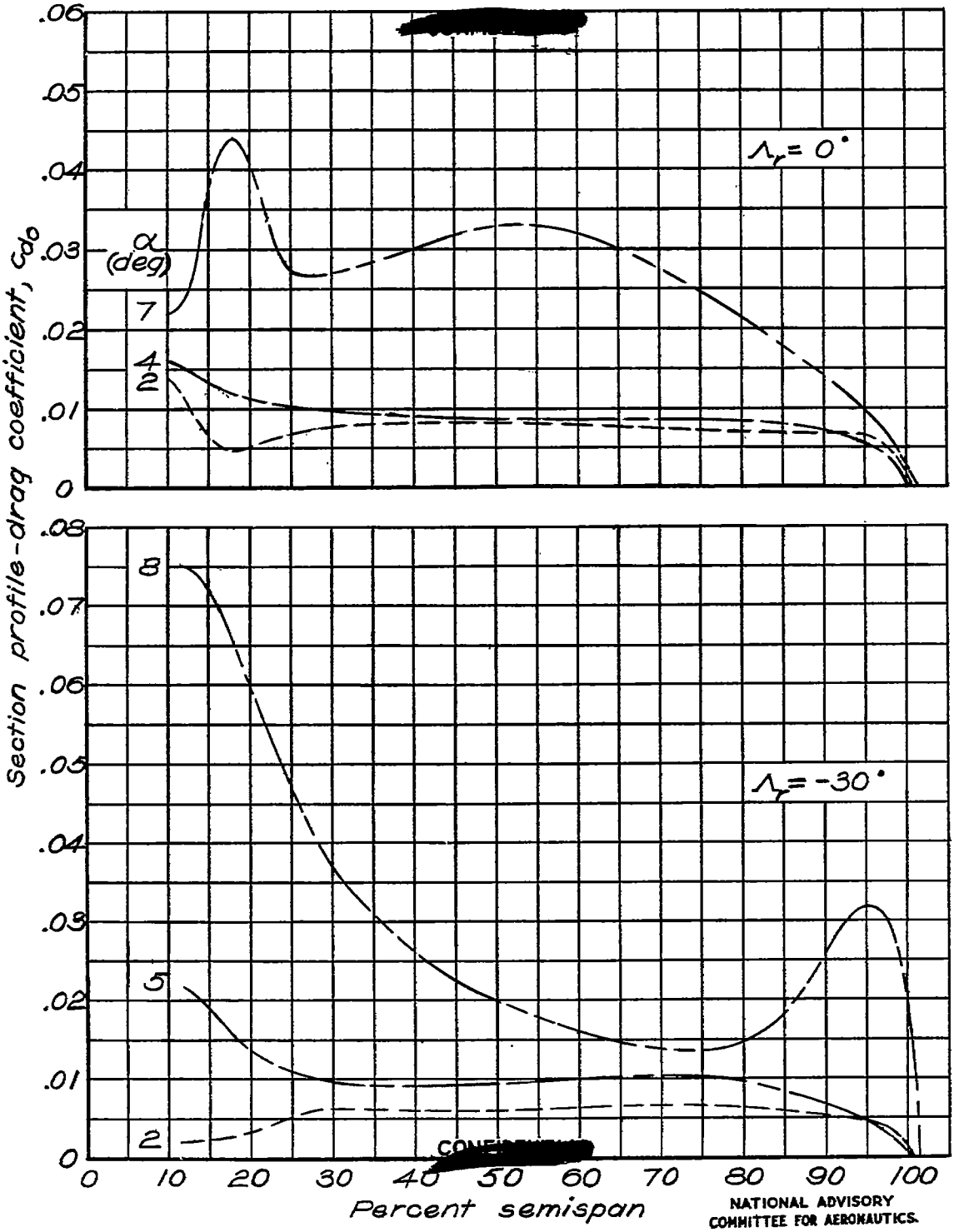

Figure 17 .- Effect of angle of attack on spanwise variation of section profile-drag coefficient. $M = 0.600$.

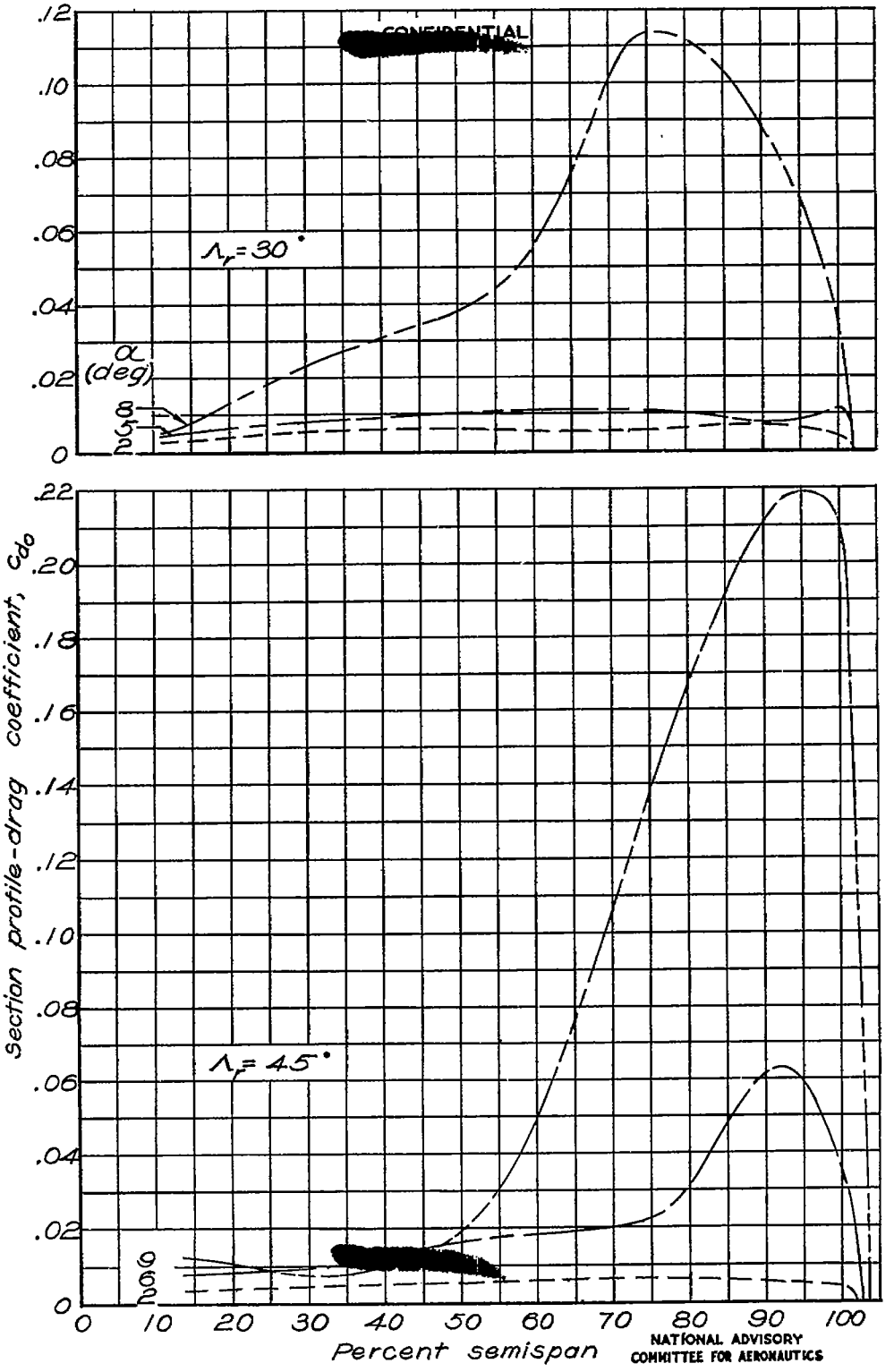

Figure 17 .- Concluded.

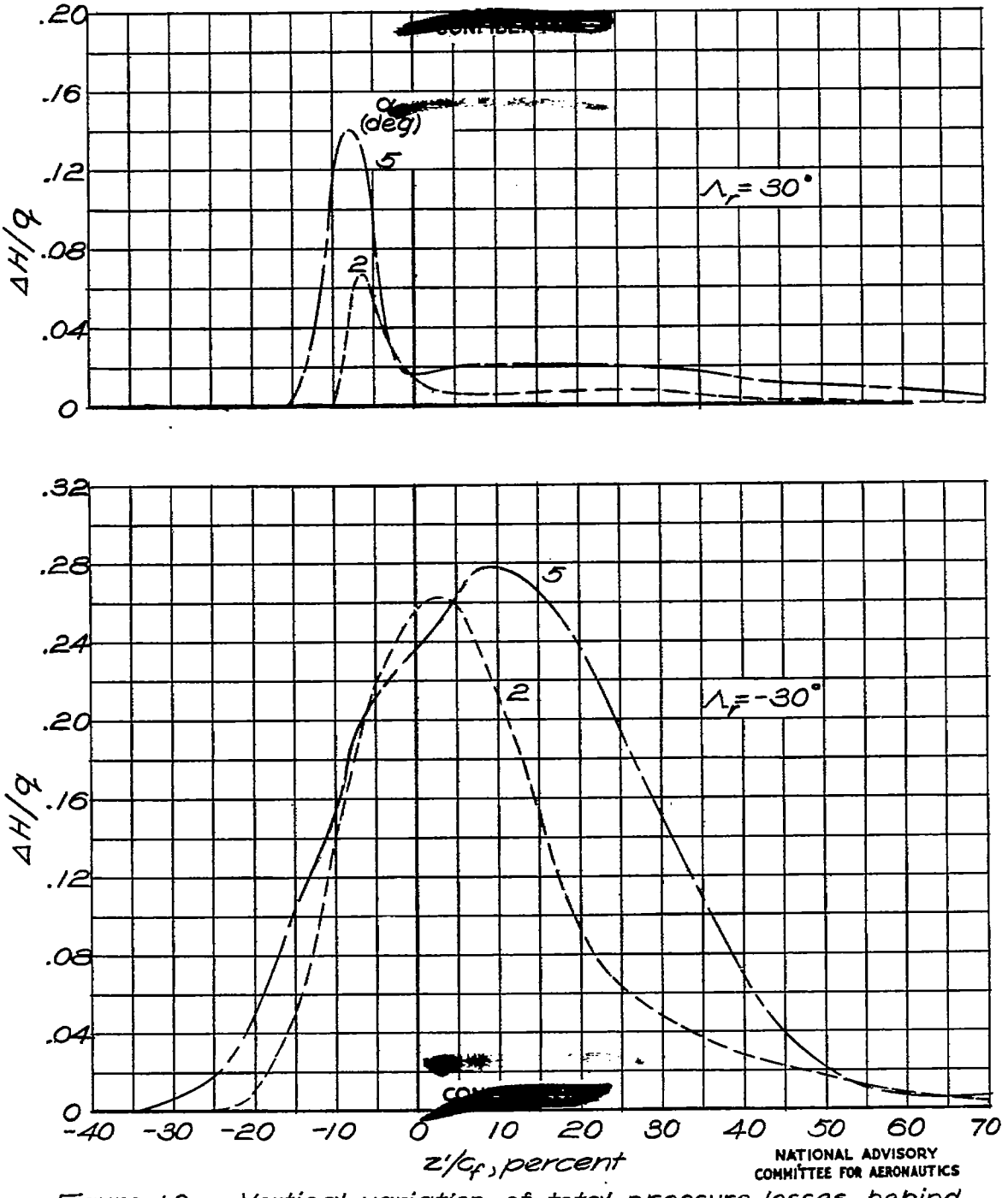

Figure 18.— Vertical variation of total pressure losses behind swept wings. $M = 0.890$.

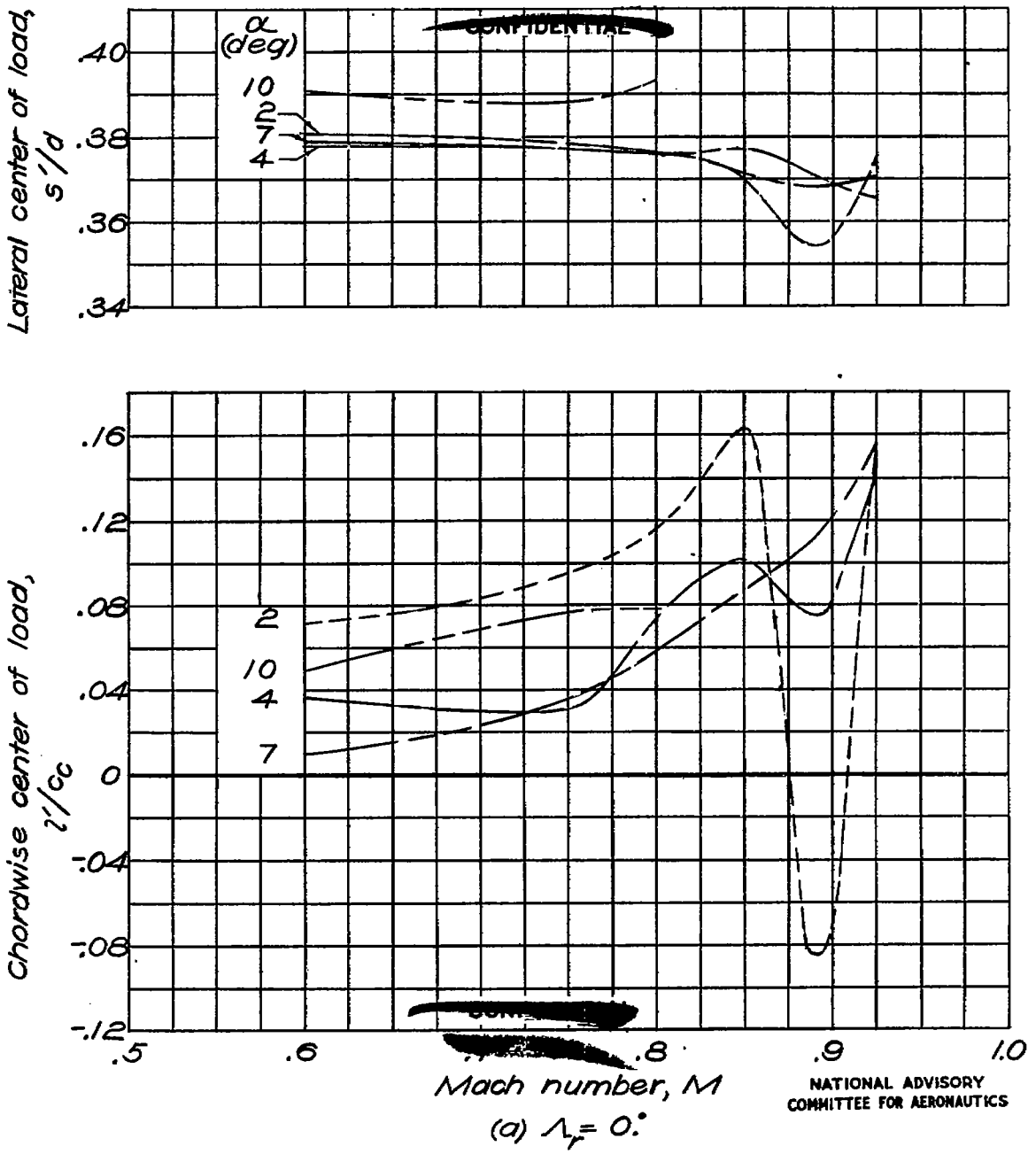

(a) $\Lambda_r = 0°$

Figure 19.– Variation of load distribution with Mach number.

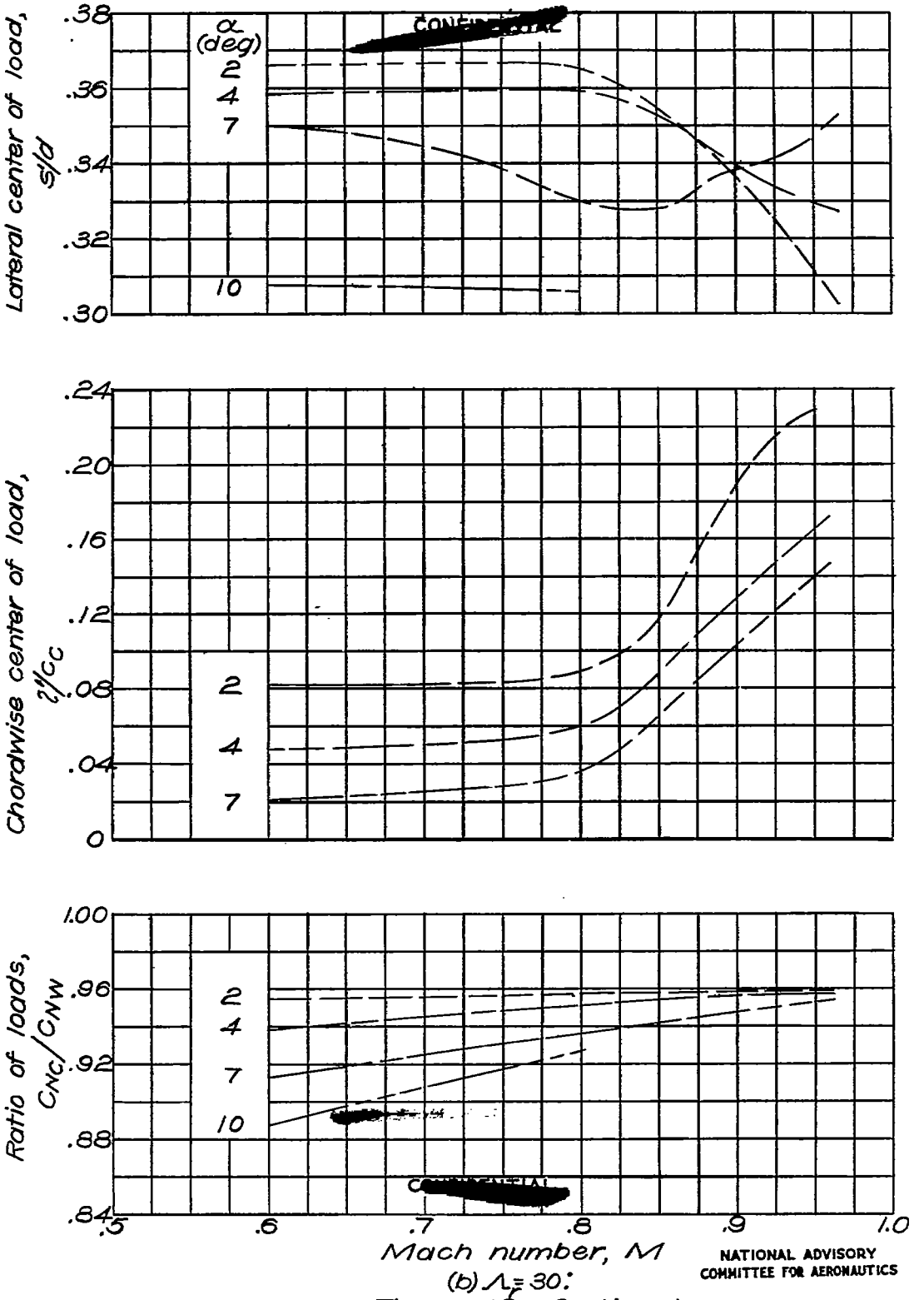

(b) $\Lambda_c = 30°$

Figure 19.– Continued.

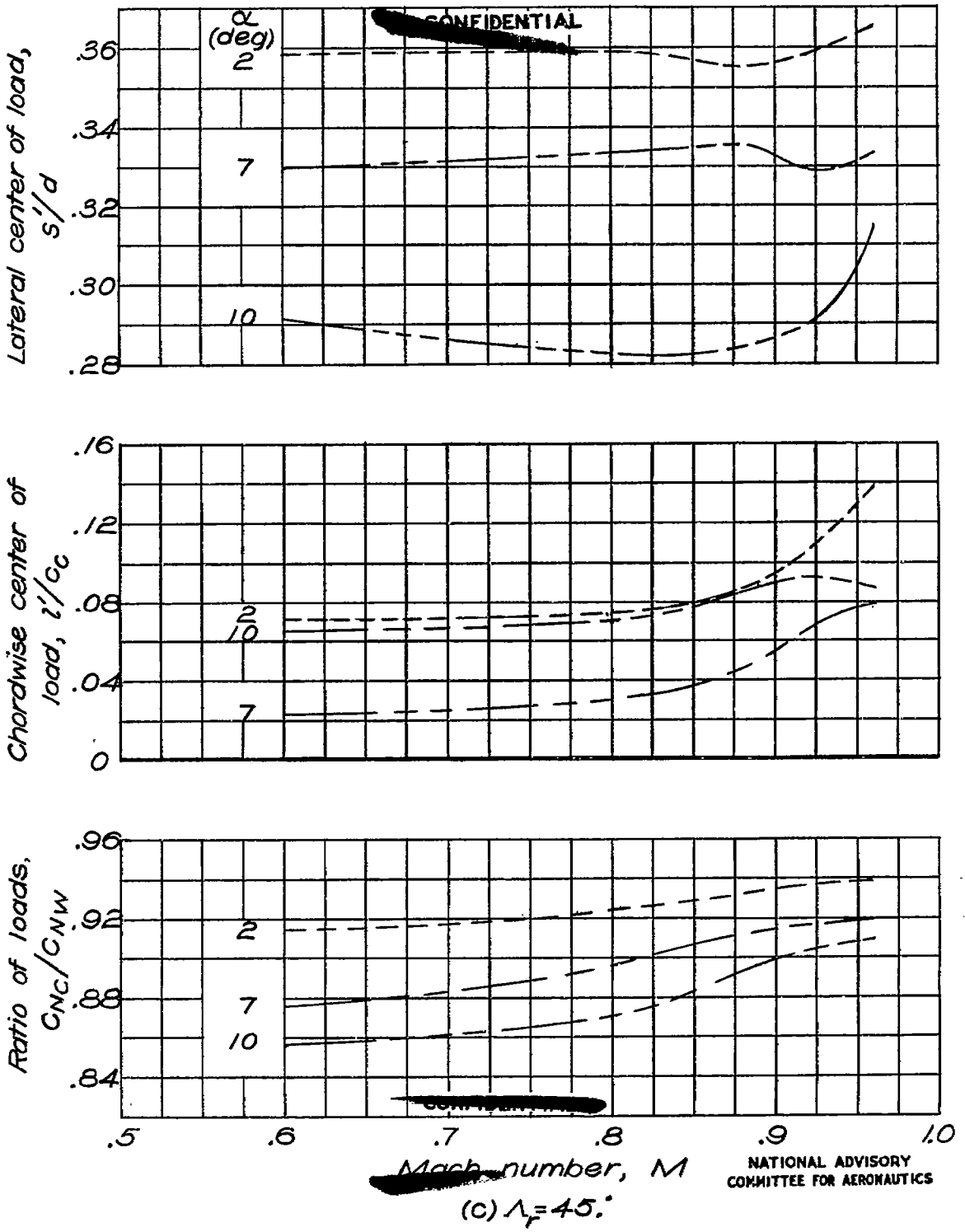

(c) $\Lambda_r = 45°$

Figure 19.- Continued.

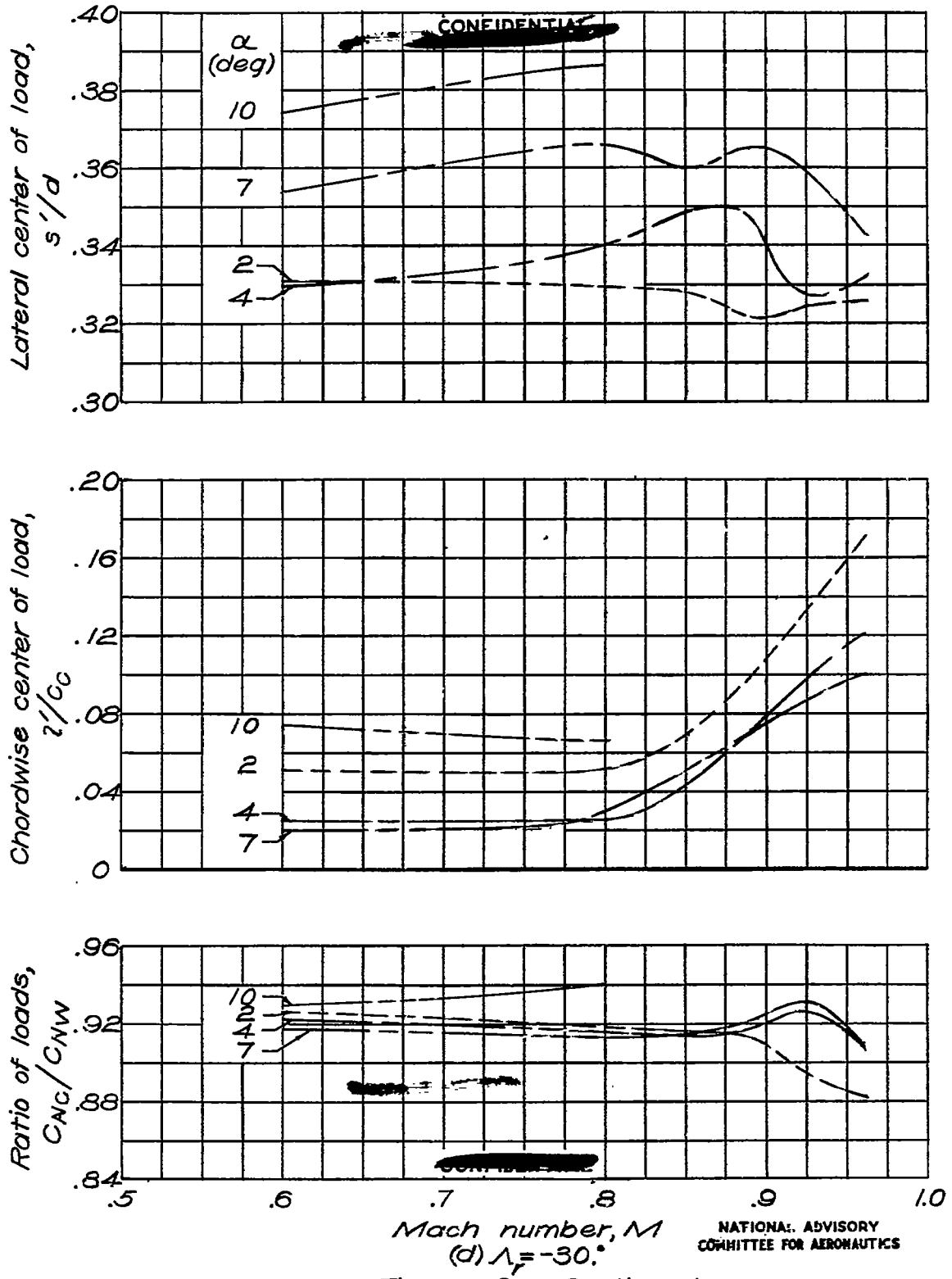

(d) $\Lambda_r = -30°$.

Figure 19.- Continued.

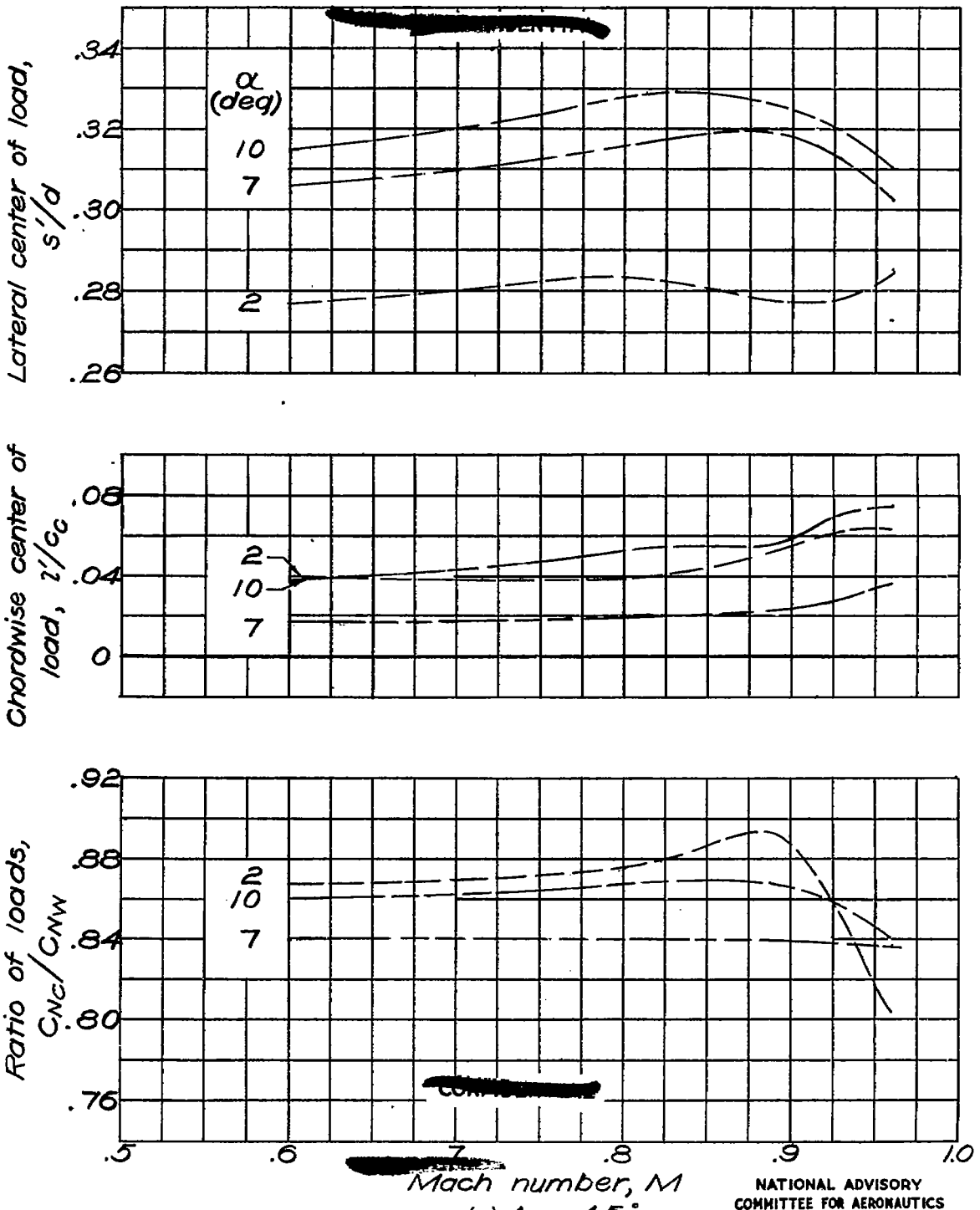

(e) $\Lambda = -45°$

Figure 19.- Concluded.

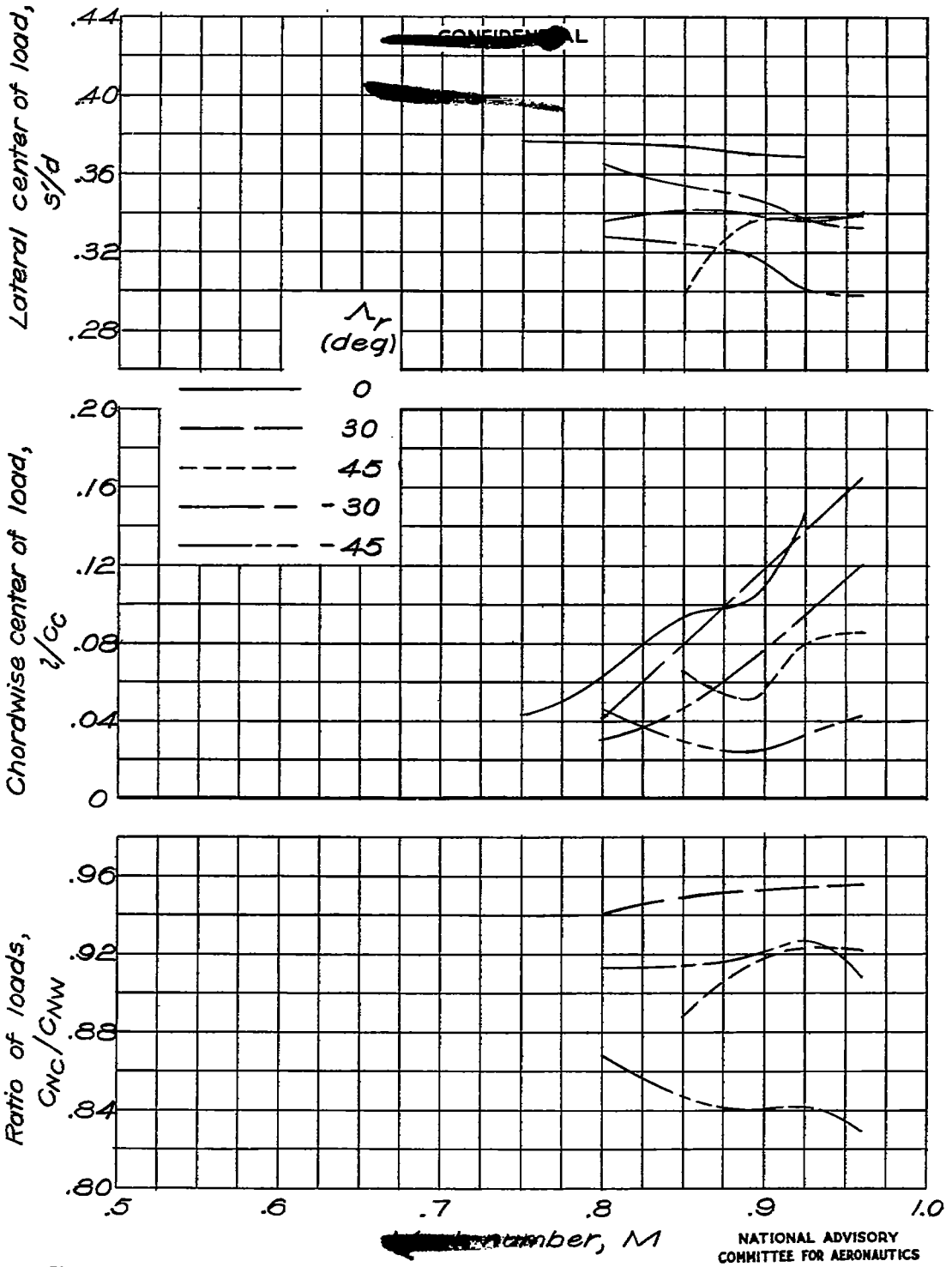

Figure 20.- Variation of load distribution with Mach number for a wing loading of 200 pounds per square foot at an altitude of 30,000 feet.

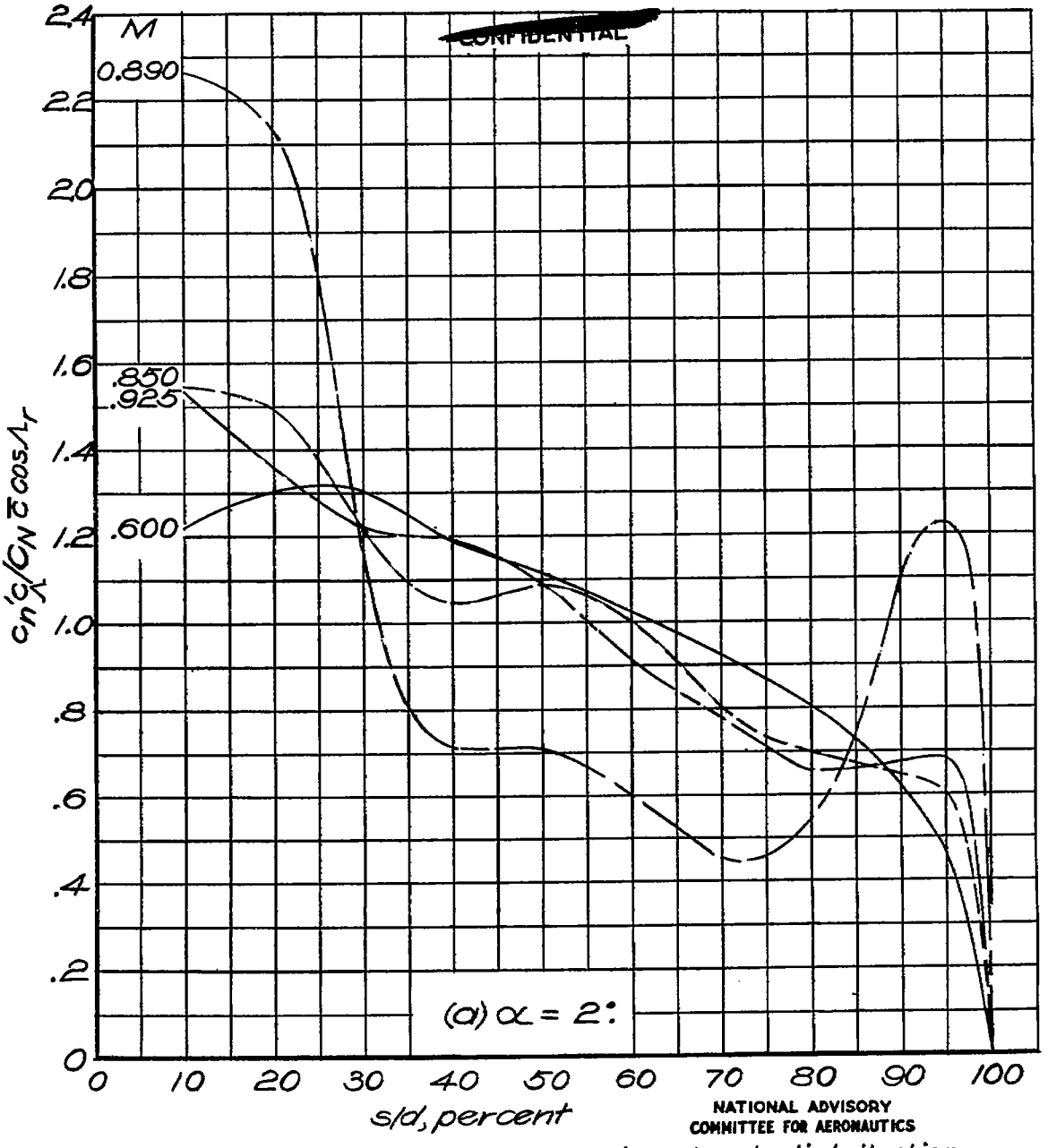

Figure 21.– Variation of spanwise load distribution with Mach number. $\Lambda_r = 0°$.

NACA RM No. L6J01a

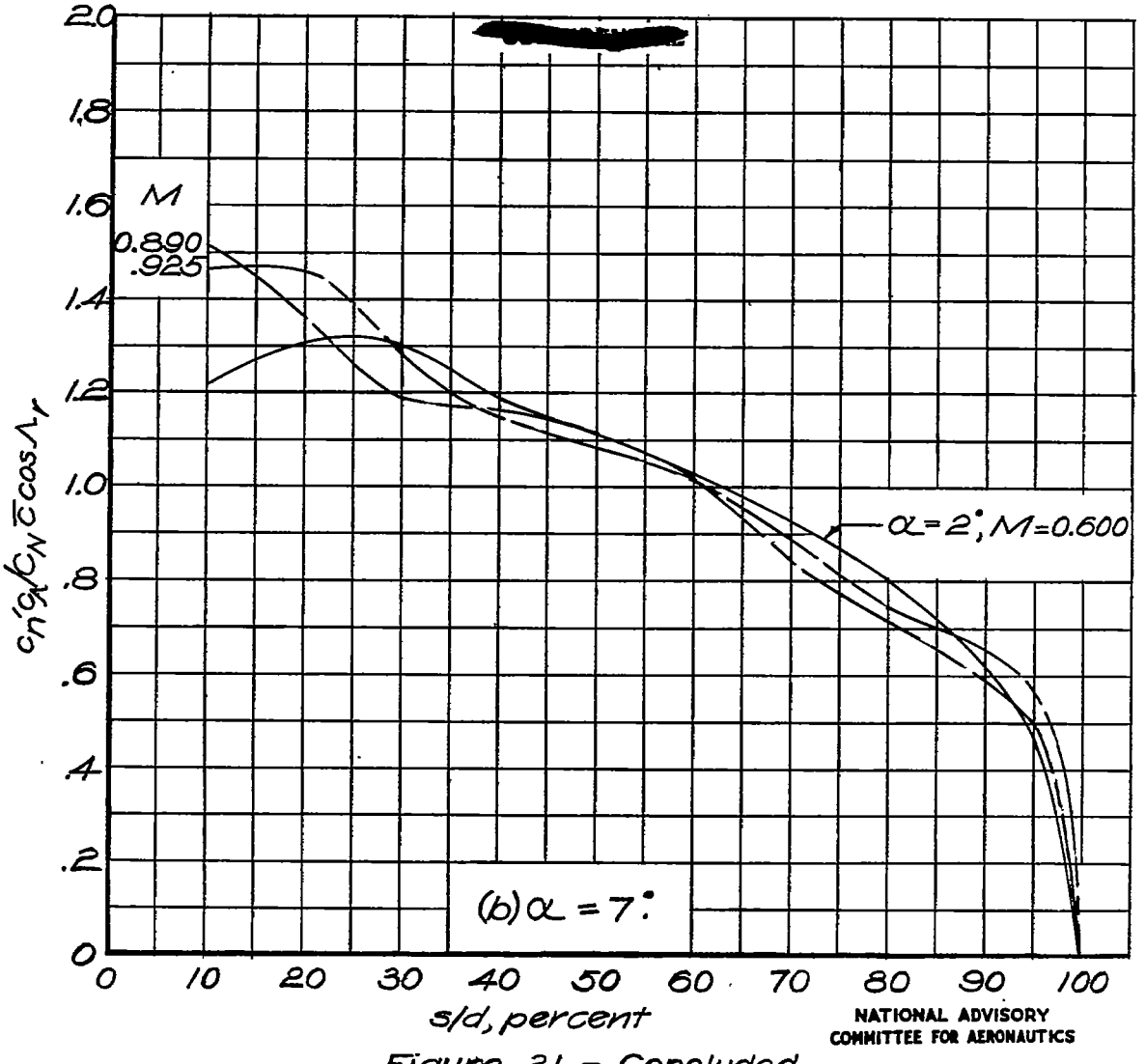

Figure 21.- Concluded.

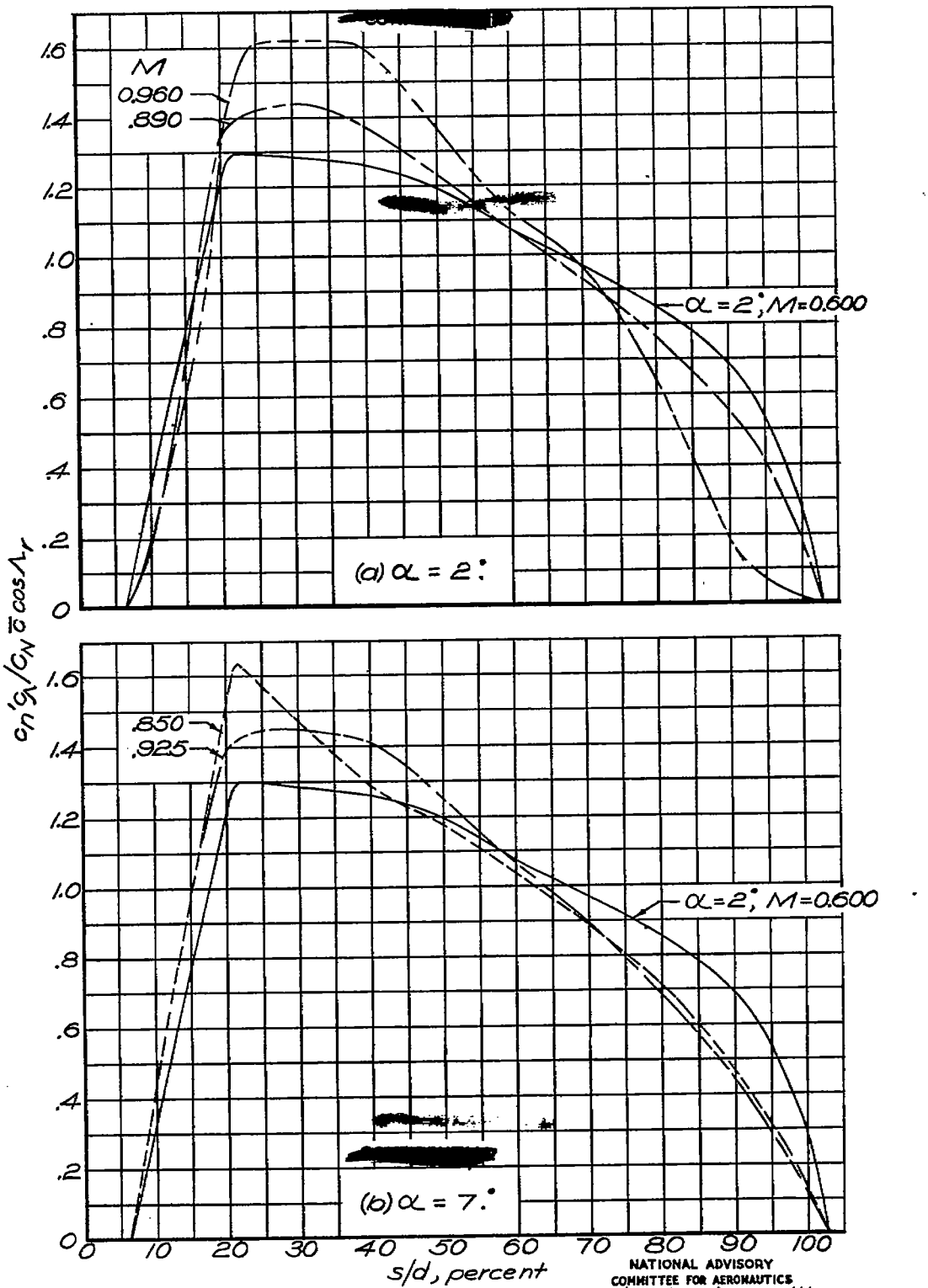

Figure 22.- Variation of spanwise load distribution with Mach number. $\Lambda_r = 30°$.

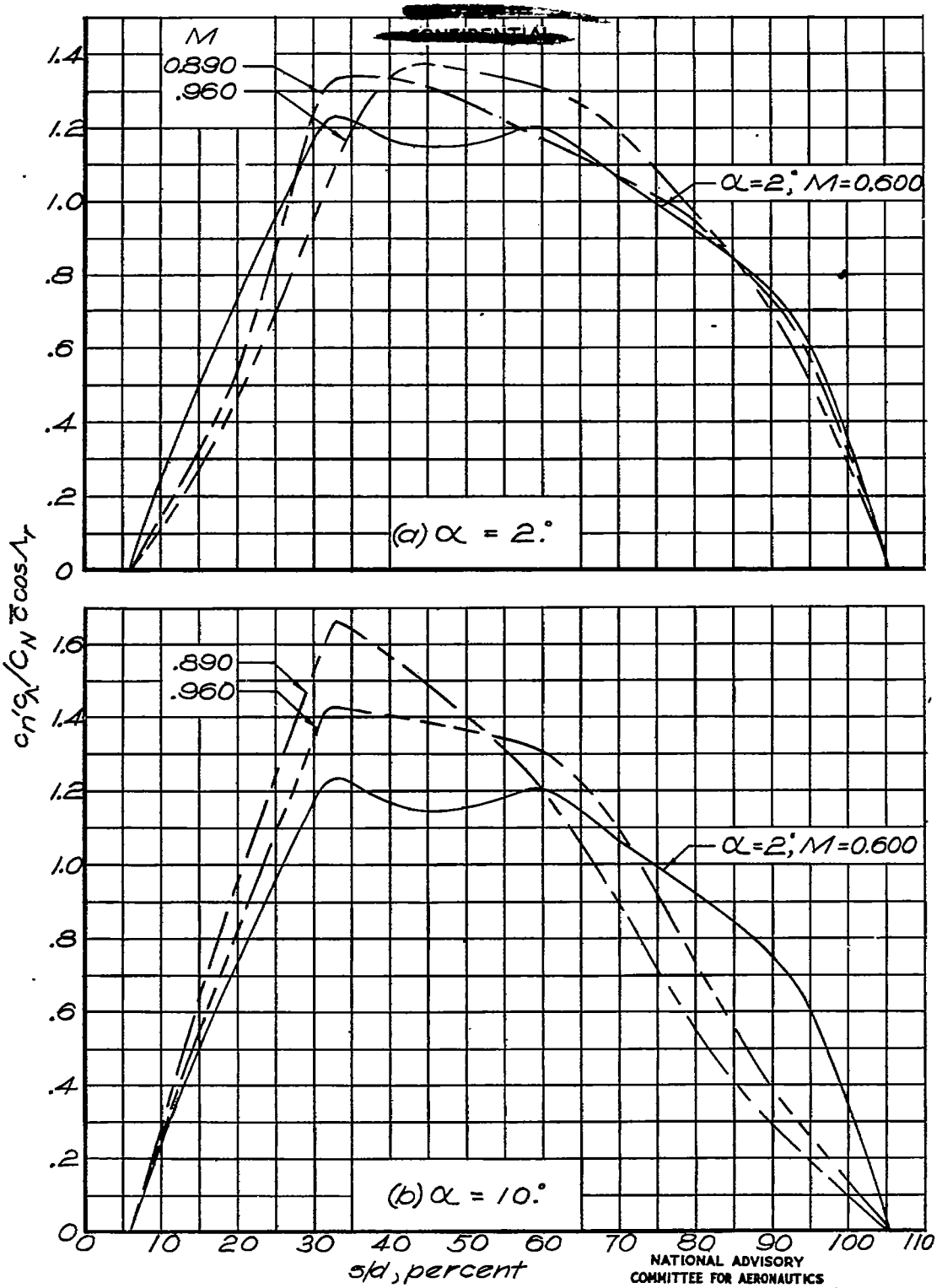

Figure 23.- Variation of spanwise load distribution with Mach [redacted] number. $\Lambda_r = 45.°$

CONFIDENTIAL

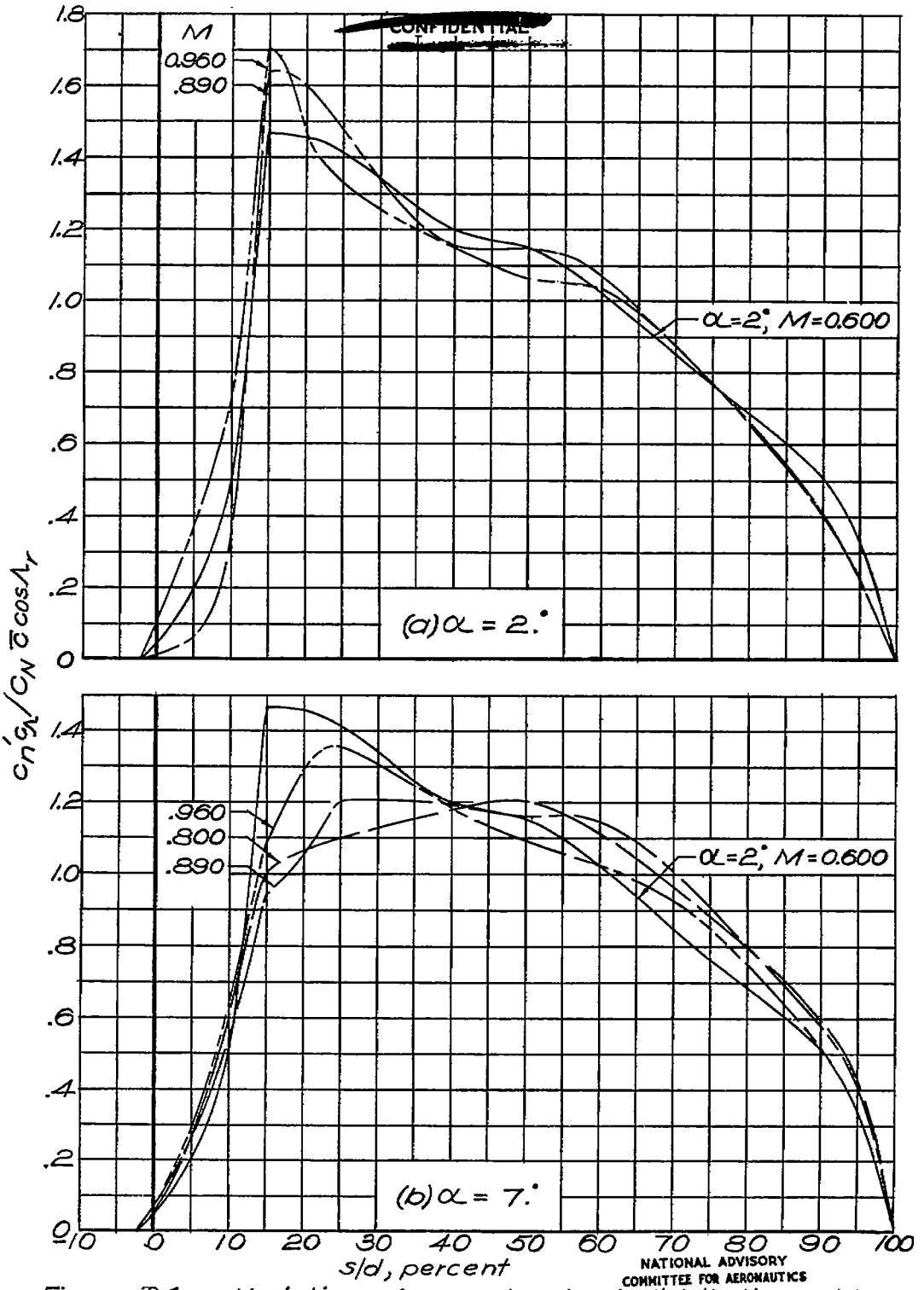

Figure 24.— Variation of spanwise load distribution with Mach number. $\Lambda_r = -30°$.

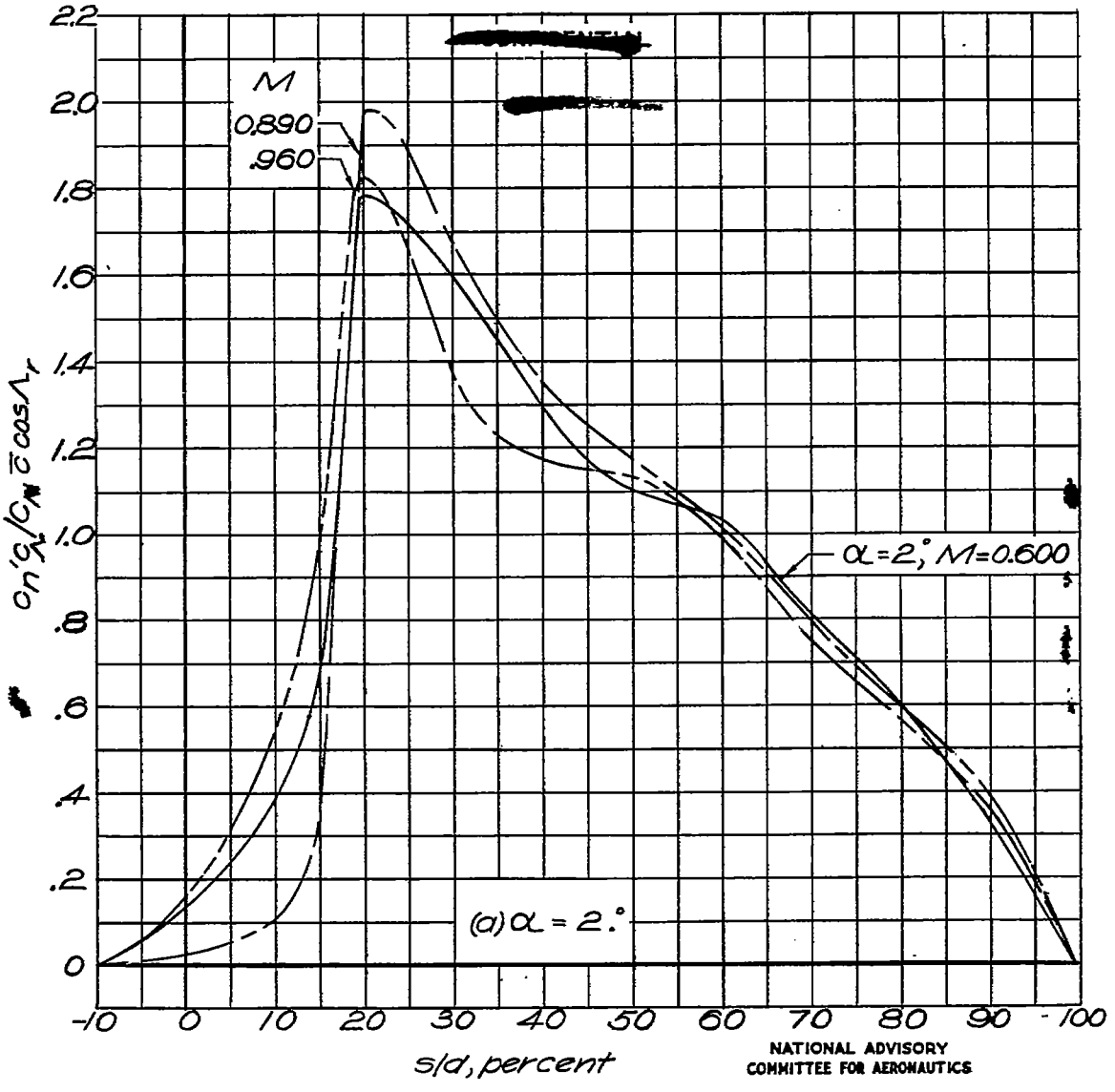

Figure 25.— Variation of spanwise load distribution with Mach number. Λ_r=45.

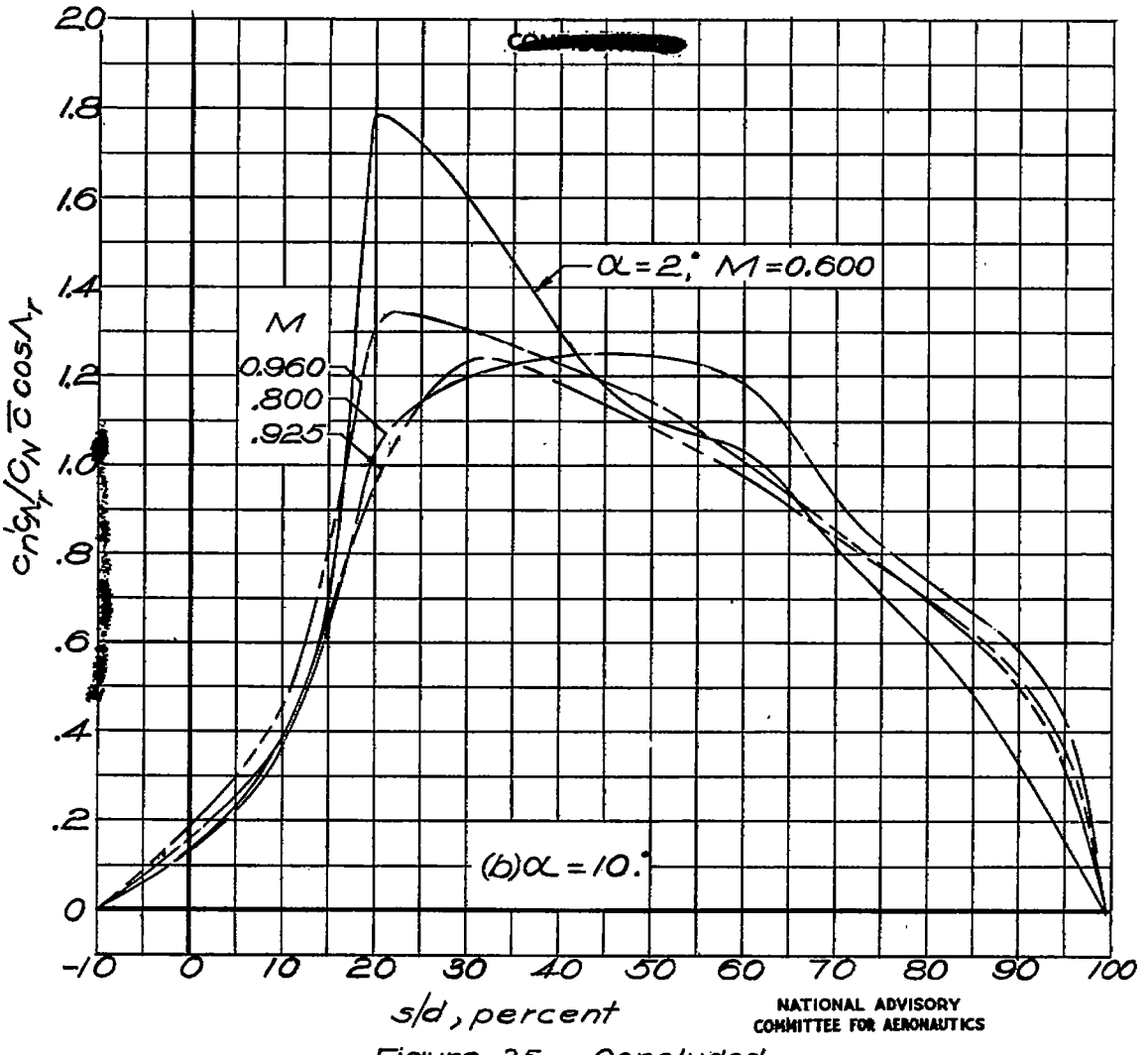

Figure 25.- Concluded.

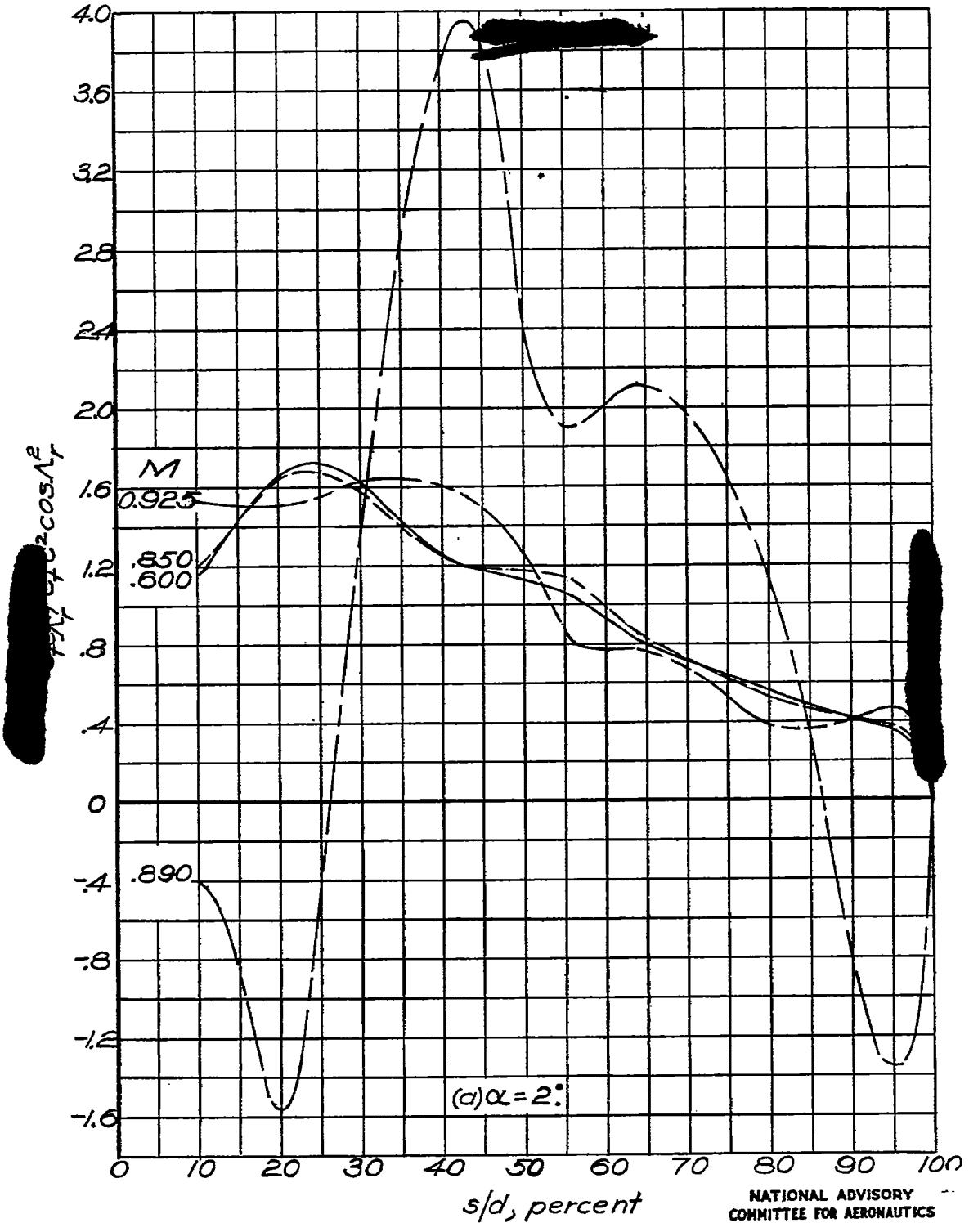

Figure 26.— Variation of spanwise twisting-moment distribution with Mach number. $\Lambda_T = 0°$.

[redacted]

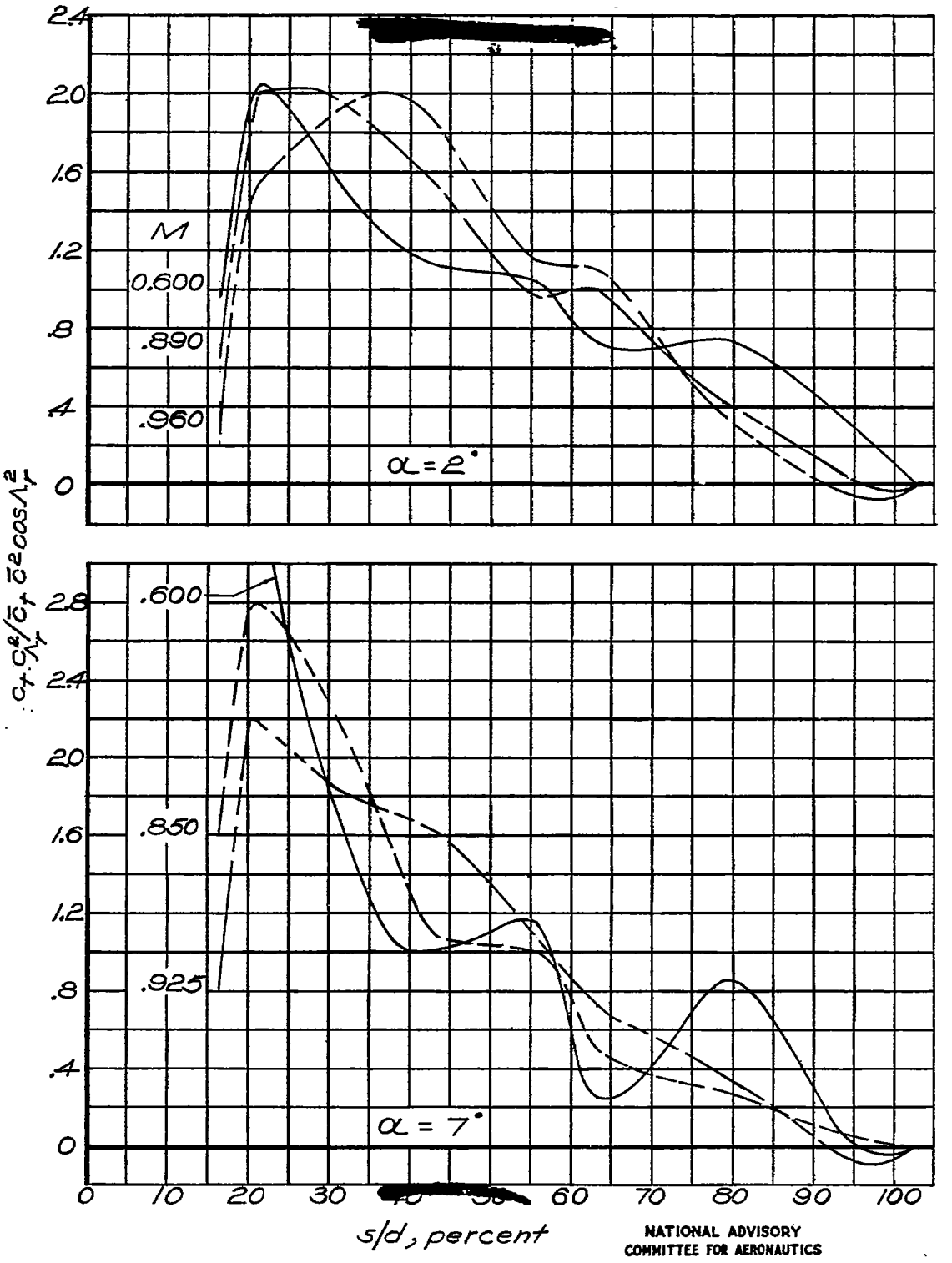

Figure 27.— Variation of spanwise twisting-moment distribution with Mach number. $\Lambda_r = 30°$.

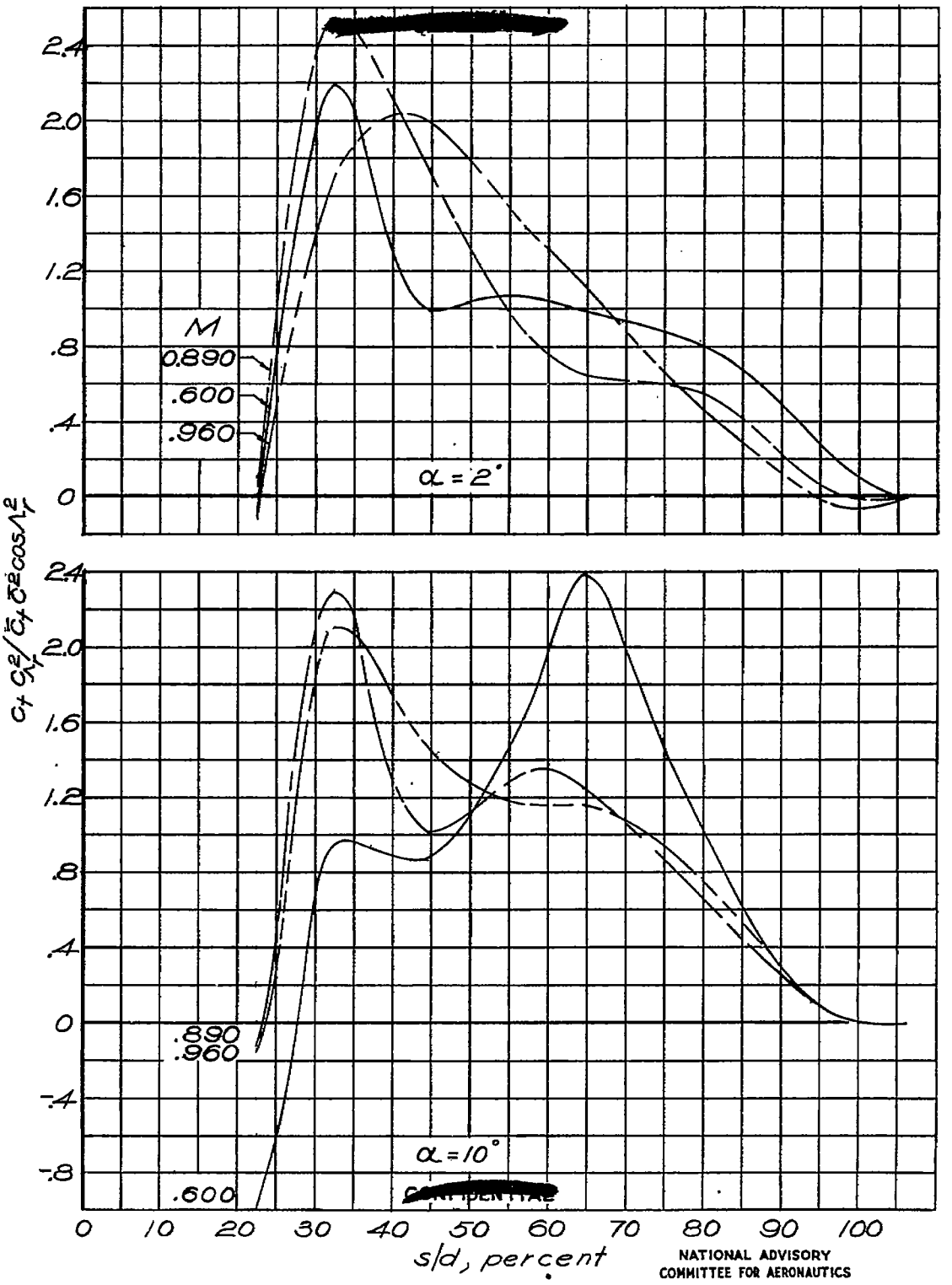

Figure 28. — Variation of spanwise twisting-moment distribution with Mach number. $\Lambda_r = 45°$.

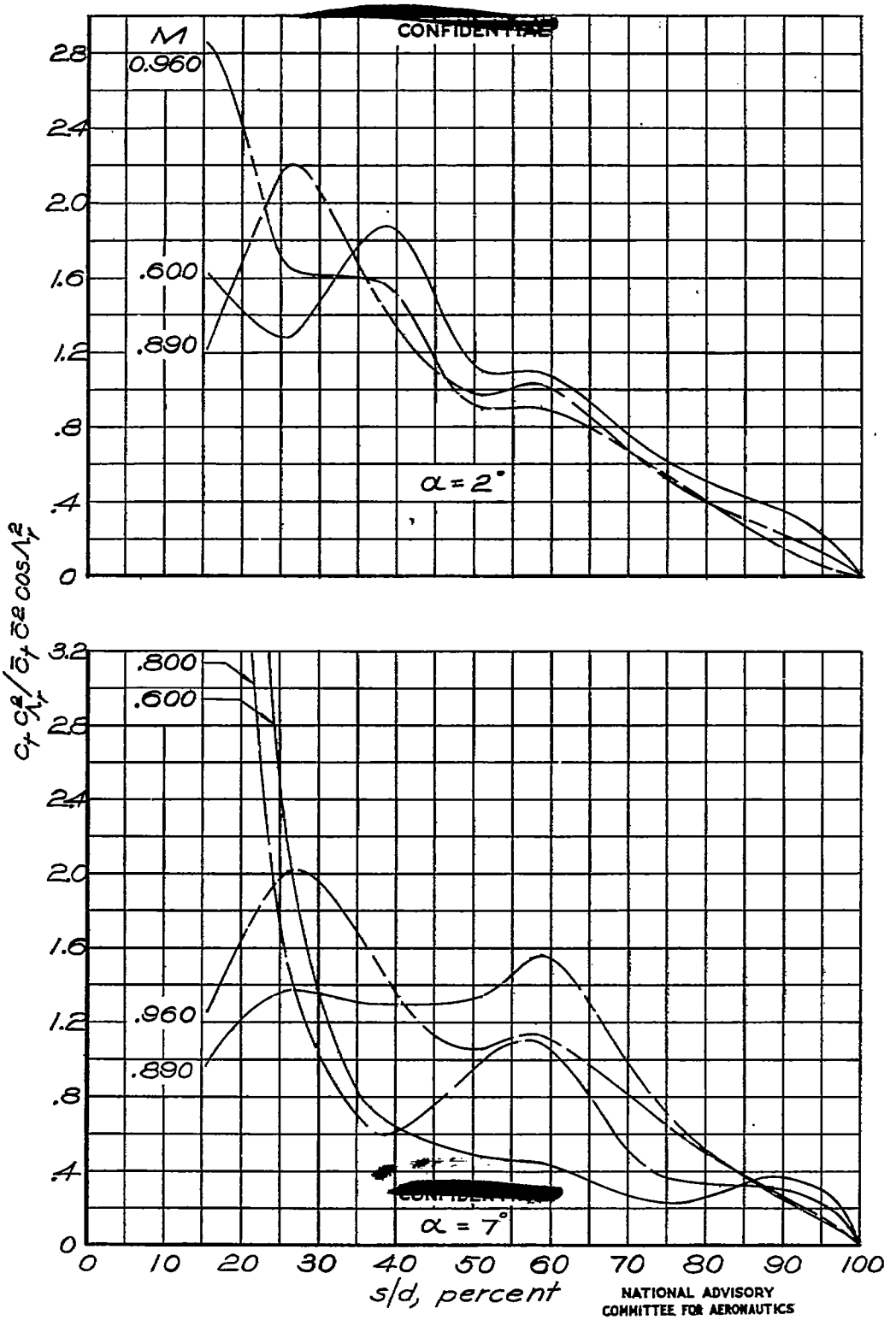

Figure 29.– Variation of spanwise twisting-moment distribution with Mach number. $\Lambda_r = -30.°$

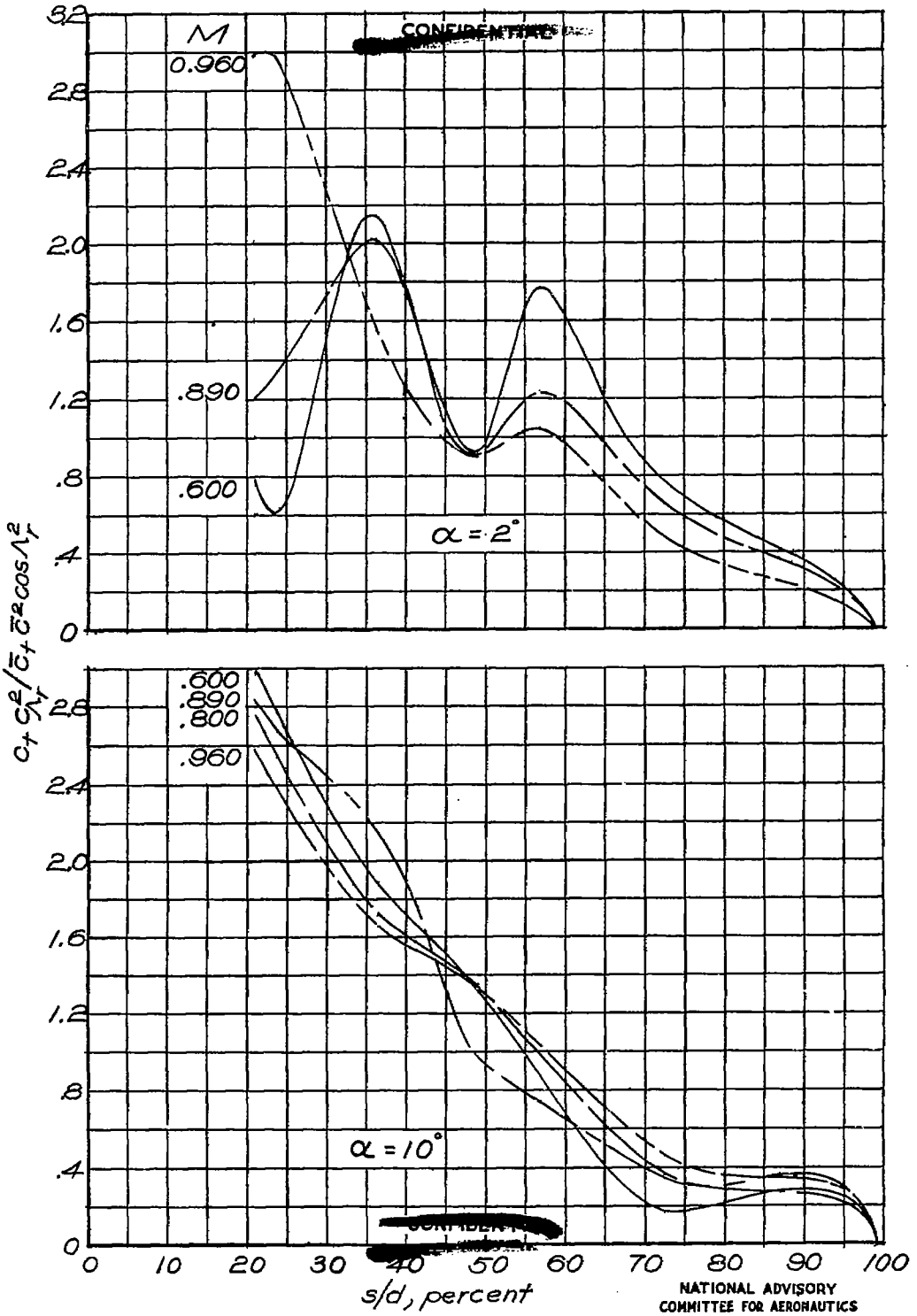

Figure 30.– Variation of spanwise twisting-moment distribution with Mach number. $\Lambda_r = -45°$.

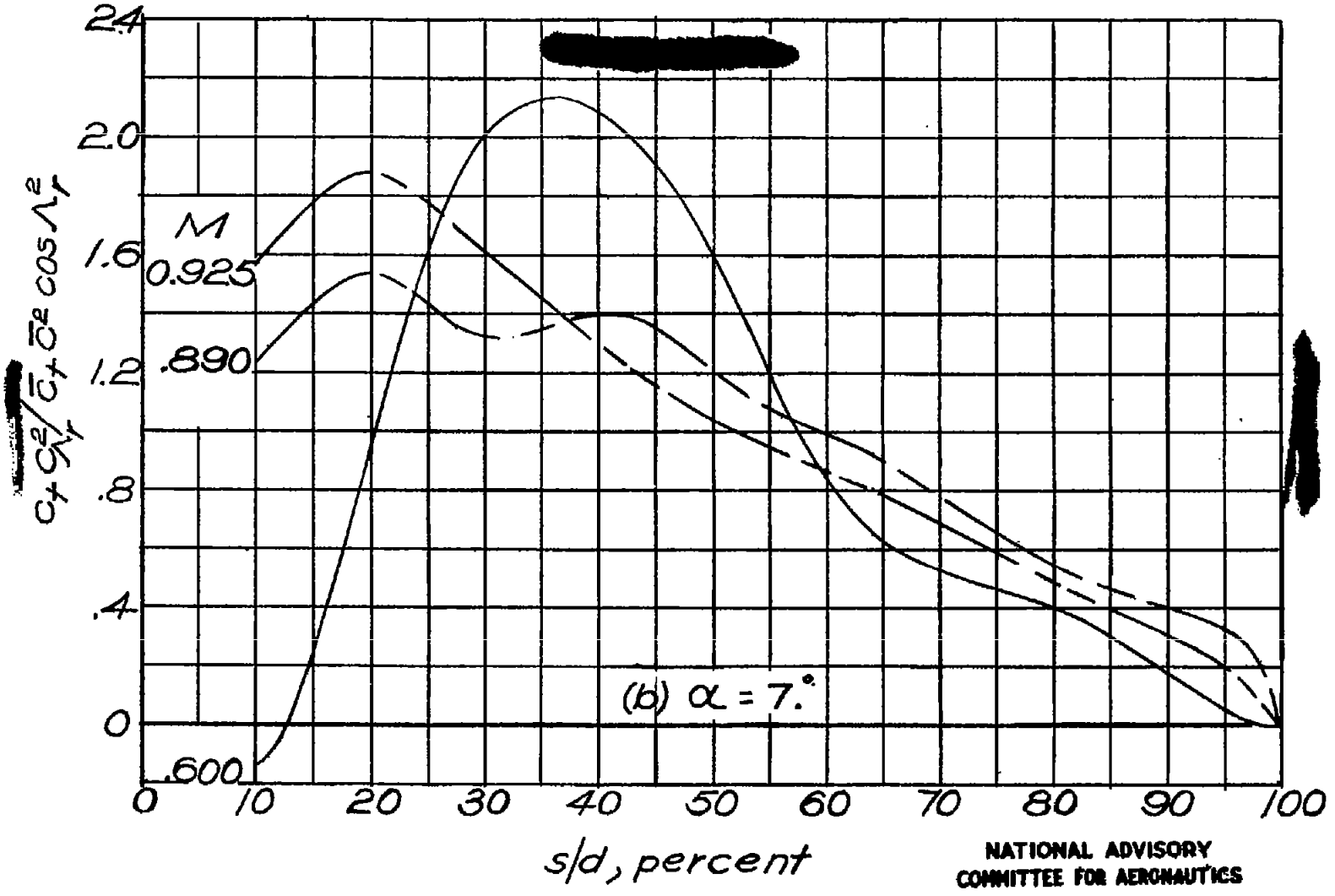

Figure 26.– Concluded.

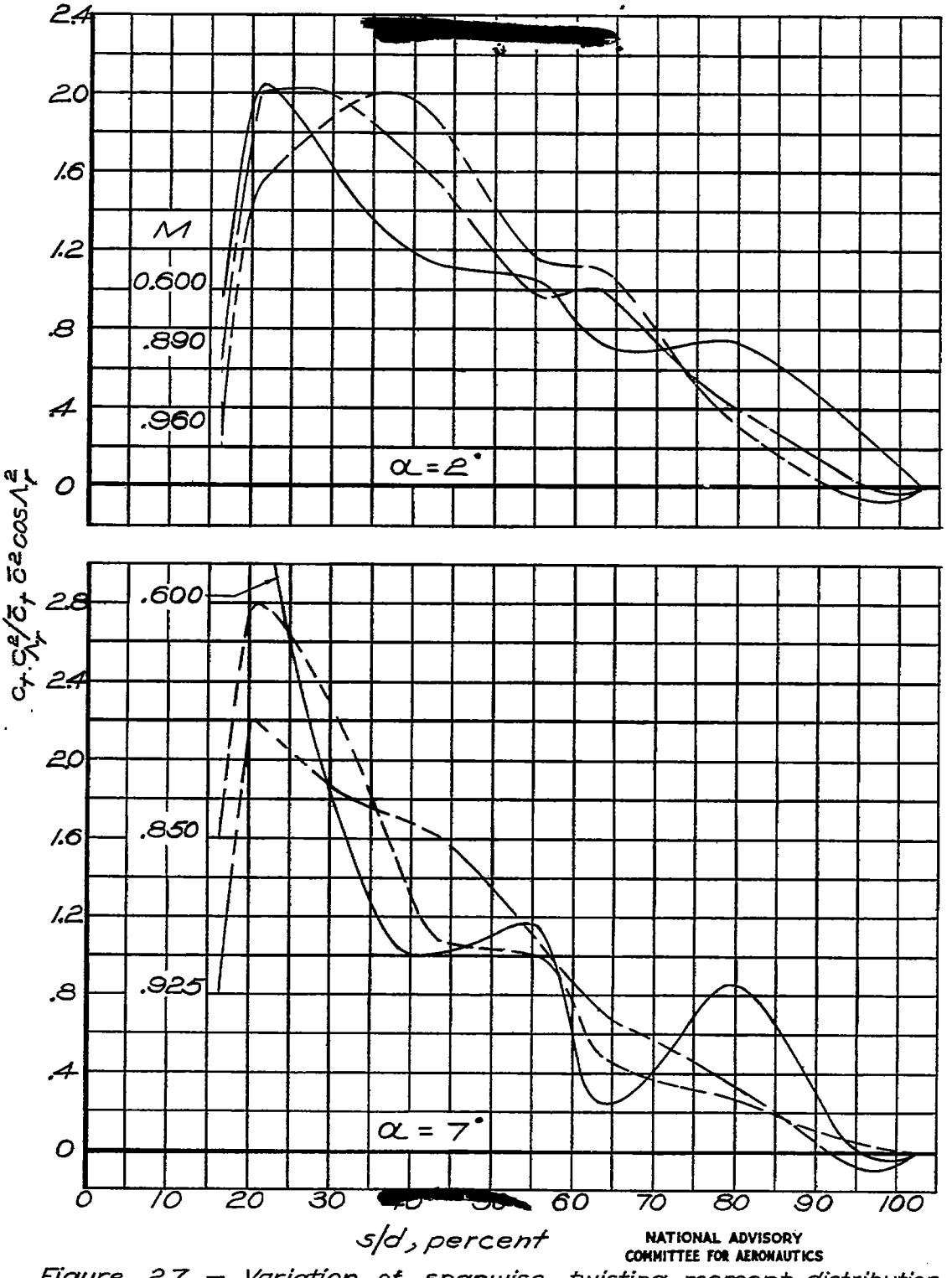

Figure 27.— Variation of spanwise twisting-moment distribution with Mach number. $\Lambda_r = 30°$.

[redacted]

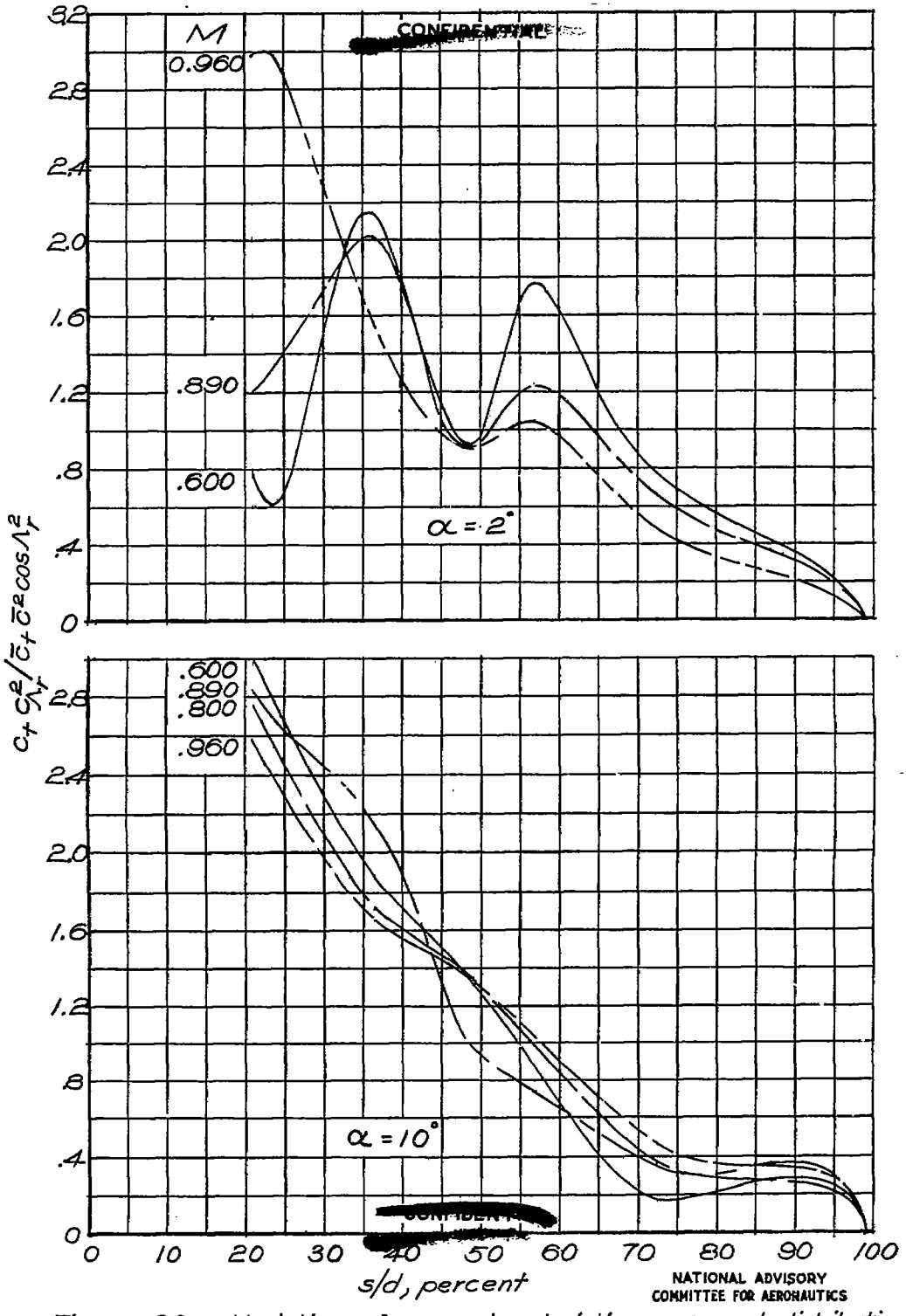

Figure 30.– Variation of spanwise twisting-moment distribution with Mach number. $\Lambda_r = -45°$.